AD-A035 245 ARGONNE NATIONAL LAB ILL ENGINEERING DIV F/G 10/2
EXPERIMENTAL TWO-PHASE LIQUID-METAL MAGNETOHYDRODYNAMIC GENERAT--ETC(U)
NOV 76 M PETRICK, G FABRIS, R COLE, R HANTMAN NAONR-16-76
UNCLASSIFIED ANL/ENG-76-04 NL

1 OF 2
ADA035245

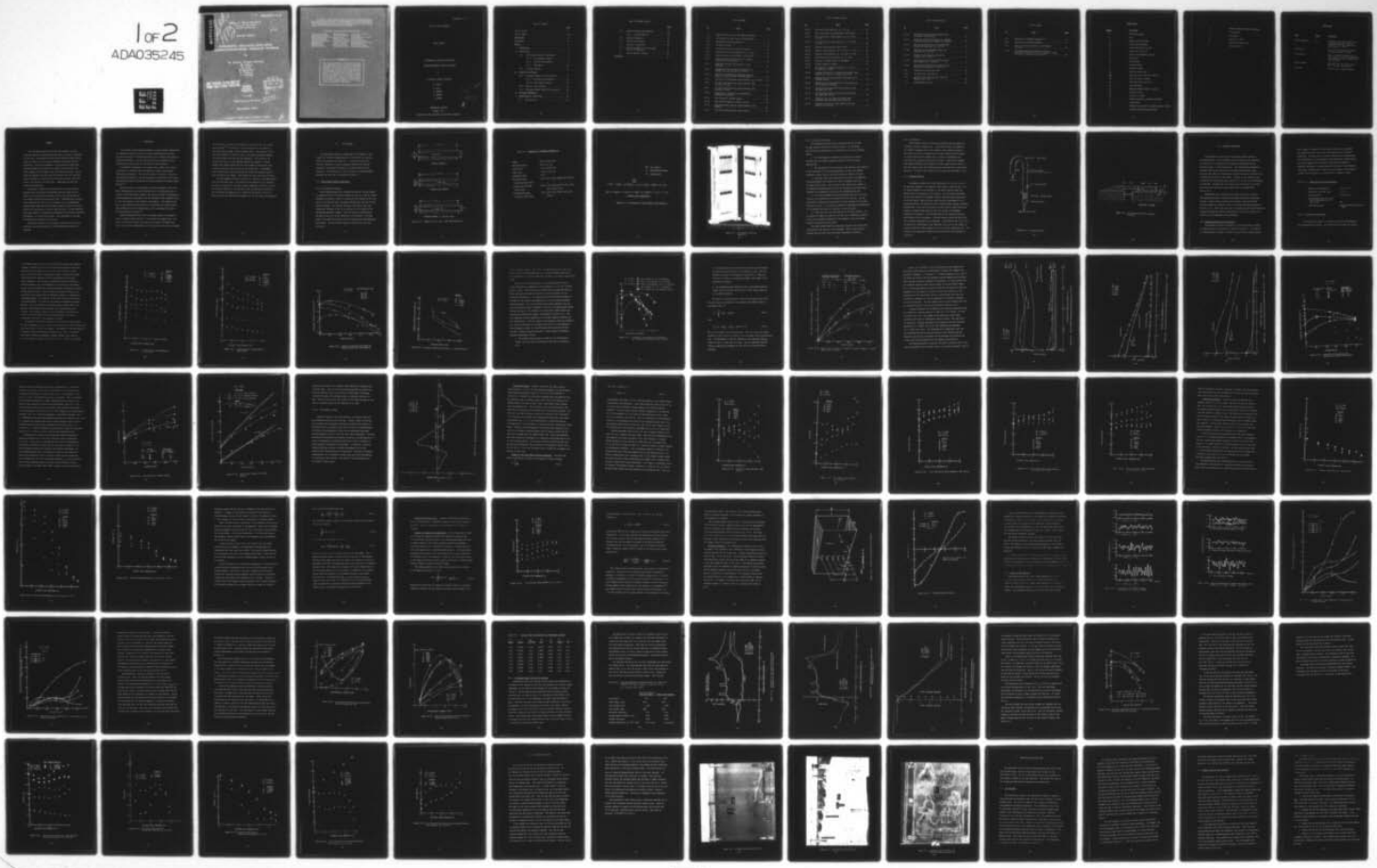

ANL/ENG-76-04

Office of Naval Research
Contract No. NAonr-16-76
Task No. NR 099-404

Annual Report

EXPERIMENTAL TWO-PHASE LIQUID-METAL MAGNETOHYDRODYNAMIC GENERATOR PROGRAM

by

M. Petrick, Project Scientist
G. Fabris
R. Cole
R. Hantman
E. Pierson
J. Cutting

ARGONNE NATIONAL LABORATORY
UofC-AUA-USERDA

Engineering Division

November 1976

The facilities of Argonne National Laboratory are owned by the United States Government. Under the terms of a contract (W-31-109-Eng-38) between the U. S. Energy Research and Development Administration, Argonne Universities Association and The University of Chicago, the University employs the staff and operates the Laboratory in accordance with policies and programs formulated, approved and reviewed by the Association.

MEMBERS OF ARGONNE UNIVERSITIES ASSOCIATION

The University of Arizona
Carnegie-Mellon University
Case Western Reserve University
The University of Chicago
University of Cincinnati
Illinois Institute of Technology
University of Illinois
Indiana University
Iowa State University
The University of Iowa
Kansas State University
The University of Kansas
Loyola University
Marquette University
Michigan State University
The University of Michigan
University of Minnesota
University of Missouri
Northwestern University
University of Notre Dame
The Ohio State University
Ohio University
The Pennsylvania State University
Purdue University
Saint Louis University
Southern Illinois University
The University of Texas at Austin
Washington University
Wayne State University
The University of Wisconsin

ANL/ENG-76 - 04

OFFICE OF NAVAL RESEARCH

ANNUAL REPORT

EXPERIMENTAL TWO-PHASE LIQUID-METAL MAGNETOHYDRODYNAMIC GENERATOR PROGRAM

by

M. PETRICK, PROJECT SCIENTIST

G. FABRIS

R. COLE

R. HANTMAN

E. PIERSON

J. CUTTING

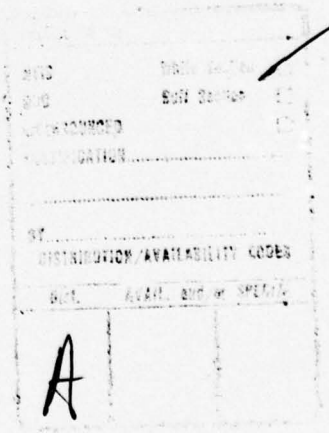

ENGINEERING DIVISION

November 1976

TABLE OF CONTENTS

TABLE OF CONTENTS (Contd.)

LIST OF FIGURES

LIST OF FIGURES (Contd.)

LIST OF FIGURES (Contd.)

LIST OF TABLES

NOMENCLATURE

SYMBOL	DEFINITION
a	Electrode spacing
A	Area
B	Magnetic field strength
C_d'	Local bubble parameter
F	Local load factor, $V_L/u_\ell aB$
F_S	Slip force, Eq. III.2
g	Length of non-magnetic air gap
I_e	End current
I_L	Load current
J	Current density
L	Generator length
$\dot{m}_g$	Mass flow rate of gas
$\dot{m}_{gi}$	Mass flow rate of gas per injector
$\dot{m}_\ell$	Mass flow rate of liquid
P_S	Slip power loss, Eq. III.1
R_L	Load resistance
R_m	Magnetic Reynolds number, $\mu\sigma u_\ell Lw/g$
u_g	Velocity of gas
u_ℓ	Velocity of liquid
V	Voltage relative to negative electrode
V_L	Load voltage
w	Channel width parallel to applied magnetic field
x	Distance measured along generator

z	Distance measured between electrodes
α	Void fraction
μ	Permeability
ρ_{ℓ}	Density of liquid
σ	Electrical conductivity
X	Mixture quality

DEFINITIONS

NAME	SYMBOL	DEFINITION
Bubble Parameter	C_d'	Empirical 'drag coefficient', based on experimental data, used to calculate slip force between gas and liquid, Eq. III.2.
Load Factor	F	Ratio of load (electrode) voltage to induced voltage, $V_L/u_\ell aB$.
Void Fraction	α	Ratio of volume occupied by gas to total volume, or flow cross-sectional area occupied by gas to total cross-sectional area.
Mixture Quality	χ	Ratio gas mass flow rate to total mass flow rate, $\dot{m}_g / (\dot{m}_g + \dot{m}_\ell)$
Slip Ratio		Ratio of gas to liquid velocity.

SUMMARY

A new diverging-channel liquid-metal MHD generator with gas injection along the insulating walls was built and placed in operation in late 1974. This generator yielded nearly-constant liquid velocity along the channel for near-design conditions, as desired for best performance. Extensive measurements of the generator terminal and internal parameters were made over a range of gas and liquid flow rates, magnetic field strengths, and load resistance values. Data is given for generator efficiency and load voltages, and the variations along the channel of liquid and gas velocities, pressure, local load factor, void fraction, and slip ratio. Comparisons are made with theoretical predictions.

Tests made to evaluate the effectiveness of the gas injection indicated that the generator performance improved slightly as the amount of gas injected was decreased, and that the injected gas was not forming the desired pure-gas wall layer. Following this, air-water tests indicated that this was to be expected, and a one-dimensional computer model indicated that performance should be better without the partial flow obstruction of the gas injection ports. The gas injection ports were removed, and substantial improvement was obtained in generator performance - by far the best to date. Data comparable to that for gas injection is presented for this case.

The future directions of the program, including the role of gas injection, and the modifications to the NaK-nitrogen facility are described.

I. INTRODUCTION

The two-phase liquid-metal MHD generator program combines experimental and analytical studies in an effort to better understand the physical processes occurring in two-phase generators and to establish the limits of generator performance. For the past five years this program has been sponsored by the Power Branch of the Office of Naval Research.

The generator experiments are conducted with a NaK-N_2 test facility consisting of a two-phase mixer, MHD generator, magnet, and required auxiliary loop equipment. This facility, used in all tests to date, has been described elsewhere.[1] Earlier experiments on generators with varying geometries have been performed and the results presented in previous annual reports.[2,3]

Analytical models of the generator have been developed to aid in the basic understanding of the flow characteristics in the generator and to provide a (one-dimensional) computer code which is capable of approximately predicting generator performance from the independent input parameters such as flow rate, magnetic field strength, and geometry. This computer code and the semi-empirical technique used to characterize the churn-turbulent drag parameter used in the determination of the interfacial slip ratio have been reported in detail.[2,4]

Previous experiments used first a diverging channel in an attempt to obtain a constant liquid velocity.[2] The channel was designed for a slip ratio of unity as the actual slip ratio was not known, but higher slip ratios were observed experimentally and the liquid velocity was not constant.

Following this a constant-area channel was tested both with and without gas injection.[2,3] The purpose of the gas injection was to remove an electrical shunt through a liquid boundary layer. The existence of this layer was proposed to account for much of the large discrepancy between the theory without the layer and the experiment. In this report the results from tests of a new diverging channel are reported. The new channel has a smaller angle than the first channel as this should yield a close-to-constant liquid velocity at the design point. Experiments were conducted both with gas injection and without the injector ports to directly observe the changes. Some simple air-water tests were also made.

The test program, described in Section II, consists of the NaK-nitrogen tests and air-water tests. The results of the generator tests, presented in detail in Section III, include a careful comparison of runs for varying gas injector conditions. The air-water tests are described in Section IV. The conclusions and suggestions for future work are given in Section V, along with the loop modifications required for the next series of experiments.

II. TEST PROGRAM

The experimental program is summarized in this section. The program for the NaK-nitrogen generator is in Section II.1, and the results are described in Section III. A simple air-water test facility, developed to observe phenomena connected with the gas injectors, is described in Section II.2, and the results are in Section IV. The facility as it will be rebuilt to operate at higher pressures and flow rates is described in Section V.

II.1 NaK-Nitrogen Generator Experiments

II.1.1 New Generator Geometry

A new diverging channel was completed and tested. The new channel is compared with the two previous channels in Fig. II.1, and the channel dimensions are given in Table II.1 along with the locations of the five pairs of gas injector ports, the eight pressure taps, and the six void-fraction windows. The relative locations of the ports, taps, and windows are indicated in Fig. II.2, and Fig. II.3 is a photo of the disassembled generator channel. Only four pairs of injector ports are seen in Fig. II.3 as the fifth pair is in the mixer. The small holes in the right electrode are used for pressure taps and temperature measurements. The gas injector design is shown in Fig. II.2.D of Reference 3.

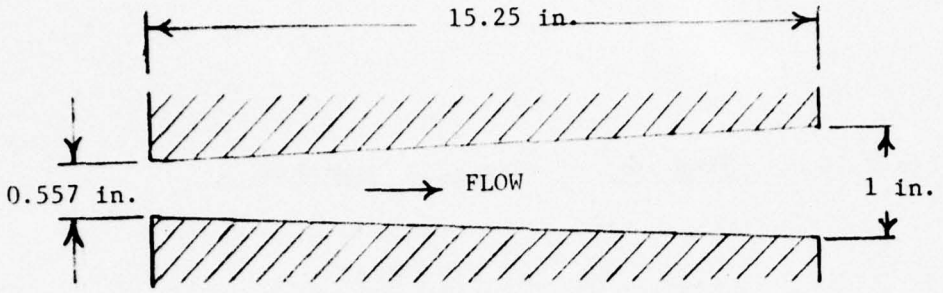

DIVERGING CHANNEL I

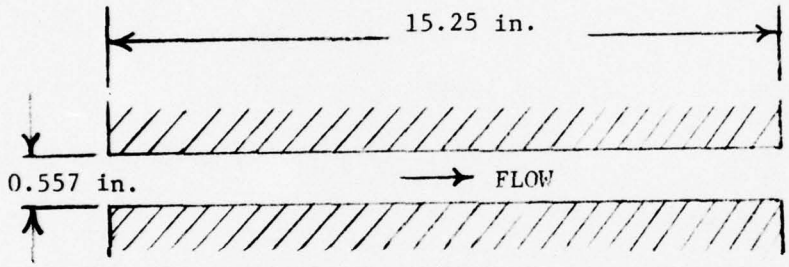

CONSTANT-AREA CHANNEL

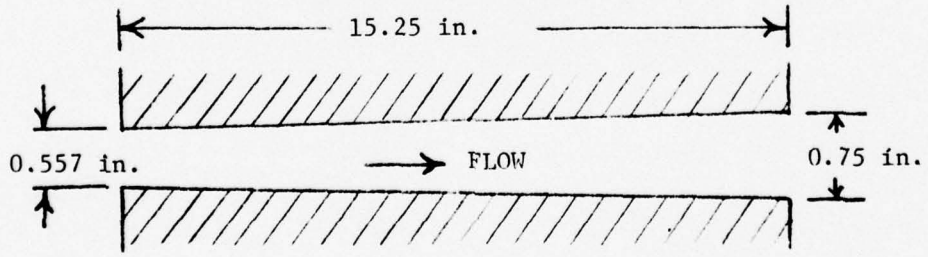

DIVERGING CHANNEL II (present study)

Figure II.1. Channel Contours Used in ANL LMMHD Experiments

Table II.1. Dimensions of Diverging Generator II

Length	38.73 cm (15.25 in)
Electrode spacing	10.16 cm (4 in)
Width, inlet	1.41 cm (0.557 in)
Width, exit	1.90 cm (0.75 in)
Divergence angle	0.73°
Gas-injector-port locations (from inlet)	-4.37, 3.97, 12.84, 28.60, and 37.40 cm
Pressure-tap locations (from inlet)	-8.02, 3.34, 13.18, 20.57, 27.95, 35.33, 42.31, and 46.75 cm
Void-fraction-window locations (from inlet)	0.91, 8.29, 15.67, 23.06, 30.44, and 37.82 cm

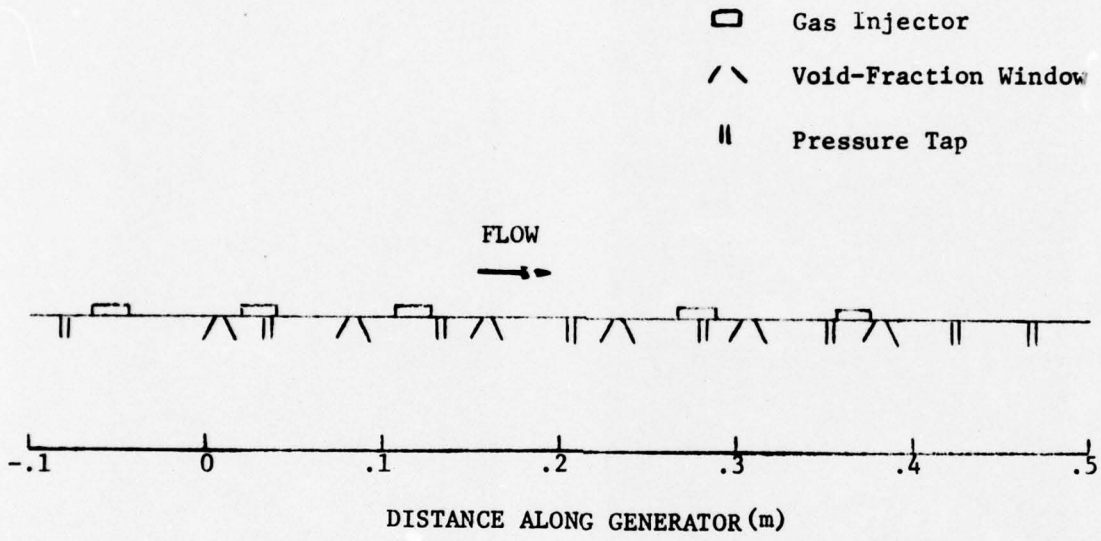

Figure II. 2. Distribution of Ports Along the MHD Generator

Figure II.3. Disassembled Diverging Channel II

II.1.2 Facility Modifications

The experiments described below were performed with the NaK-nitrogen facility described in previous reports. The following modifications were made before the experiments with the new diverging channel:

1. The electromagnetic flowmeter was replaced by a turbine flowmeter which provides an improved accuracy of 1/2% and better repeatability.

2. The new generator has five pairs of gas injection ports instead of the three pairs of the previous generator, so that four nitrogen flowmeters, control valves, and check valves were added to the loop.

3. The single motor and horizontal drive screw of the gamma-ray scanning mechanism were replaced by a pair of stepping motors and horizontal drive screws. The two drive screws improve the rigidity of the gamma-ray scanning mechanism while the stepping motors ensure exact alignment of the gamma-ray source with the photomultiplier tube.

4. The sixty six-gauge wires that connected each end of the load resistor to the generator were replaced with solid bus bars. The bus bars permit a minimum load resistance of 0.09 mΩ instead of the previous minimum of 0.14 mΩ. This reduction permits the experimental determination of the maximum efficiency as a function of load resistance.

5. A new mixer was installed because the old mixer cracked. The two mixers are identical except that the new one is fiberglass instead of lucite, has a different connection to the generator, and has an added pressure tap and gas injection port.

The above modifications have materially improved the accuracy and flexibility of the loop as a test instrument. Most of these will be retained with the major loop modification described in Section V.

II.1.3 Experiments

Three distinct series of tests were conducted, and the results are described in detail in Section III. In the first series, the generator was tested as designed with the gas injector ports operating normally. Since some of this data indicated that the gas injection was not keeping the liquid away from the channel walls, a series of experiments was conducted with varying gas injection flow rates. These tests indicated that higher performance was attained at low gas injection flow rates, so that the injector ports were removed and runs were made with a smooth-wall generator. The latter case yielded the best generator performance to date.

II.2 Air-Water Facility

A plexiglass channel with inside dimensions of 0.1 m x 0.1 m x 2 m was made and connected to the domestic water supply as shown in Fig. II.4. The sudden expansion at the entrance to the square channel causes non-uniform flow with separation in the corners. The perforated plate makes the flow more uniform by providing a uniform relatively-large obstruction to the flow and by creating uniform high turbulence downstream of it to facilitate mixing. The honeycomb, made of packed straws, reduces turbulence perpendicular to the flow and provides a further uniform large obstruction causing a relatively-high pressure drop that reduces the streamwise component of turbulence. The flow downstream of the honeycomb should be very uniform with low turbulence. The wall boundary layers are thin since they originate downstream of the honeycomb. A gas injector port, Fig. II.5, was placed 0.2 m downstream of the honeycomb on one wall of the channel to visually observe the flow patterns due to air injection along that wall. The results of the experiments conducted with this facility are described in Section IV.

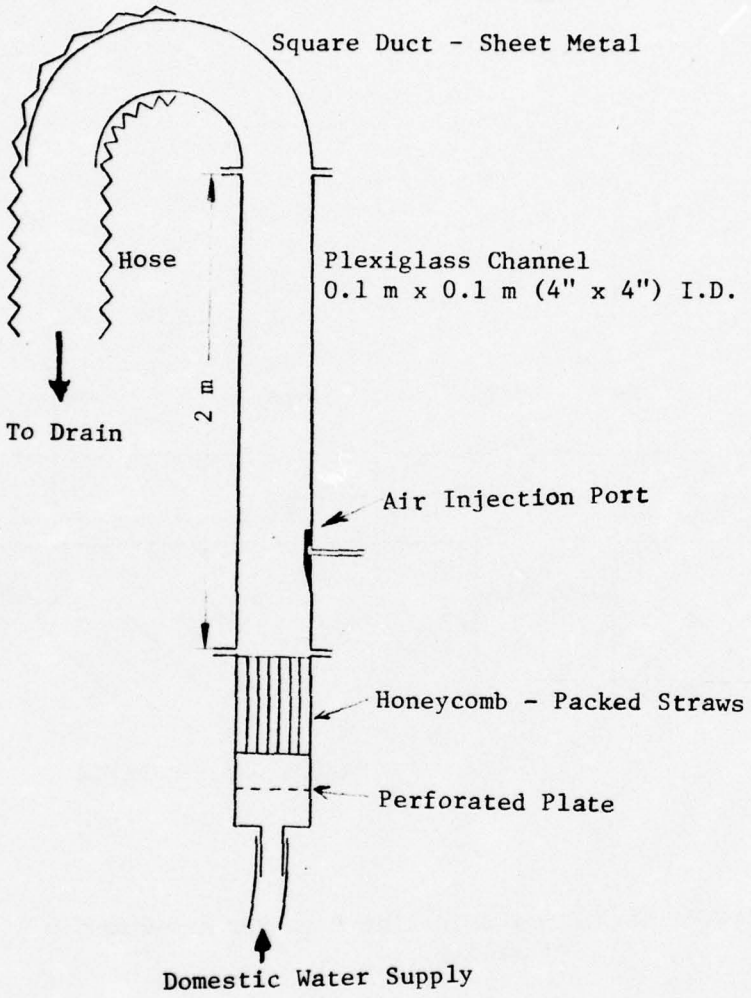

Figure II.4. Air-Water Facility

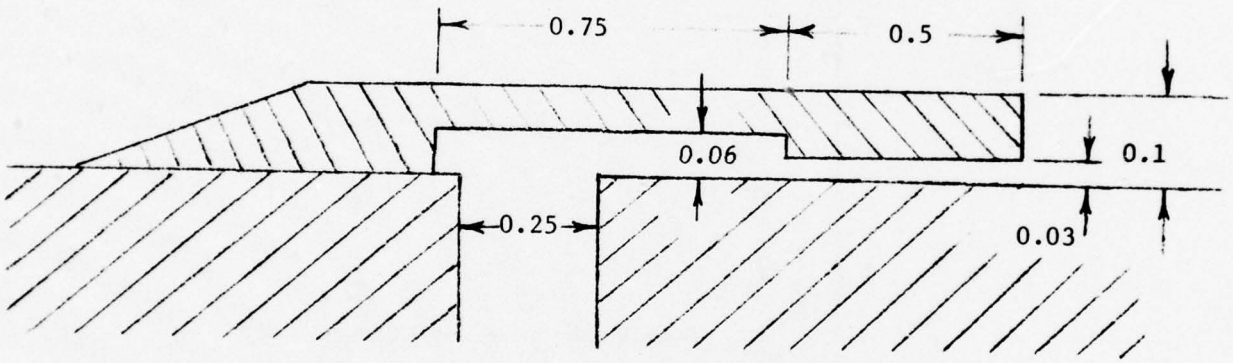

Figure II.5. Air Injection Port For Air-Water Facility

III. GENERATOR PERFORMANCE

The experimental results with the diverging-channel generator are presented here. The measurements with gas injection are summarized in Section III.1, including both the generator performance and the detailed studies of the two-phase flow. The void-fraction measurements indicated that the gas injection was not destroying the shunt layer. Thus data were taken for different gas injection flow rates, Section III.2, to determine the effect on performance. Finally the gas injectors were removed and new measurements made, Section III.3, to see if the performance was improved. Although some of the curves used in Section III.1 include data without gas injection, those results are not discussed until Section III.3.

Measurements made included gas and liquid flow rates, pressures and temperatures along the generator (including upstream and downstream regions), voltage profiles between the electrodes, and void-fraction profiles between the insulator walls at six locations along the generator (see Fig. II.2). These data were used to calculate gas and liquid velocities through the generator, thereby permitting the study of slip effects as a function of the independent system parameters.

III.1 Diverging Channel with Gas Injection

The generator described in Section II.1 was tested under a variety of conditions with gas injection, as listed in Table III.1. The results for this generator, designed to achieve a nearly-constant liquid velocity

over a range of conditions at high mixture qualities, are examined and compared here with the results from generators with different geometries. The main efforts have been concentrated on understanding the relationships of the independent system parameters (liquid and gas flow rates, magnetic field strength, and generator loading) to generator performance, on understanding the principal loss mechanisms (end losses, internal shunt currents, and slip losses), and on gaining insight into the behavior of two-phase flows in magnetic fields.

Table III.1. Experimental Operating Parameters

Magnetic field strength, T	0.6, 0.8, 1.2
Liquid mass flow rate, kg/s	2, 4, 6
Mixture quality	0.0 to 0.015
Gas injection flow rate, total for all injectors as % of mixer flow	8%
Load resistance, mΩ	Variable between 0.09 and 1.0; and ∞

III.1.1 Performance Measurements

First the liquid velocity is observed to see the effectiveness of the constant-velocity design. The liquid velocity through the channel,

as determined using flow-rate and void-fraction data made with gamma-ray scanning, is shown in Fig. III.1 for five mixture qualities and a load resistance of 0.14 mΩ, and in Fig. III.2 for open circuit (no load). Except in the first 20% of the generator length, a relatively-constant liquid velocity was obtained for the loaded generator at non-zero mixture qualities. Some increase in generator efficiency relative to previous generators may be attributable to this result, as the induced voltage $u_\ell aB$ is comparatively constant throughout the generator, thereby minimizing ohmic losses. For zero quality the velocity varies as the reciprocal of the distance from the generator entrance, as expected for a diverging channel. The variation in the liquid velocity for the open-circuited generator is a result of the reduced electromagnetic pressure gradient. Thus, the volume of gas remains almost constant and, as the generator cross-sectional area increases, the liquid velocity must decrease. These examples indicate that the optimum of constant liquid velocity is not achievable for all system parameters, but only for combinations that match to the generator's contour.

The generator isentropic efficiency as a function of mixture quality for load resistances R_L of 0.4, 0.25, 0.14, and 0.10 mΩ is shown in Fig. III.3. (Note that for R_L = 0.10, $\dot{m}_\ell$ is reduced.) The behavior of the efficiency as a function of the load resistance is shown in Fig. III.4. As the load resistance is reduced the generator loading increases, and a peak in efficiency would be expected for some value of R_L. There are not enough

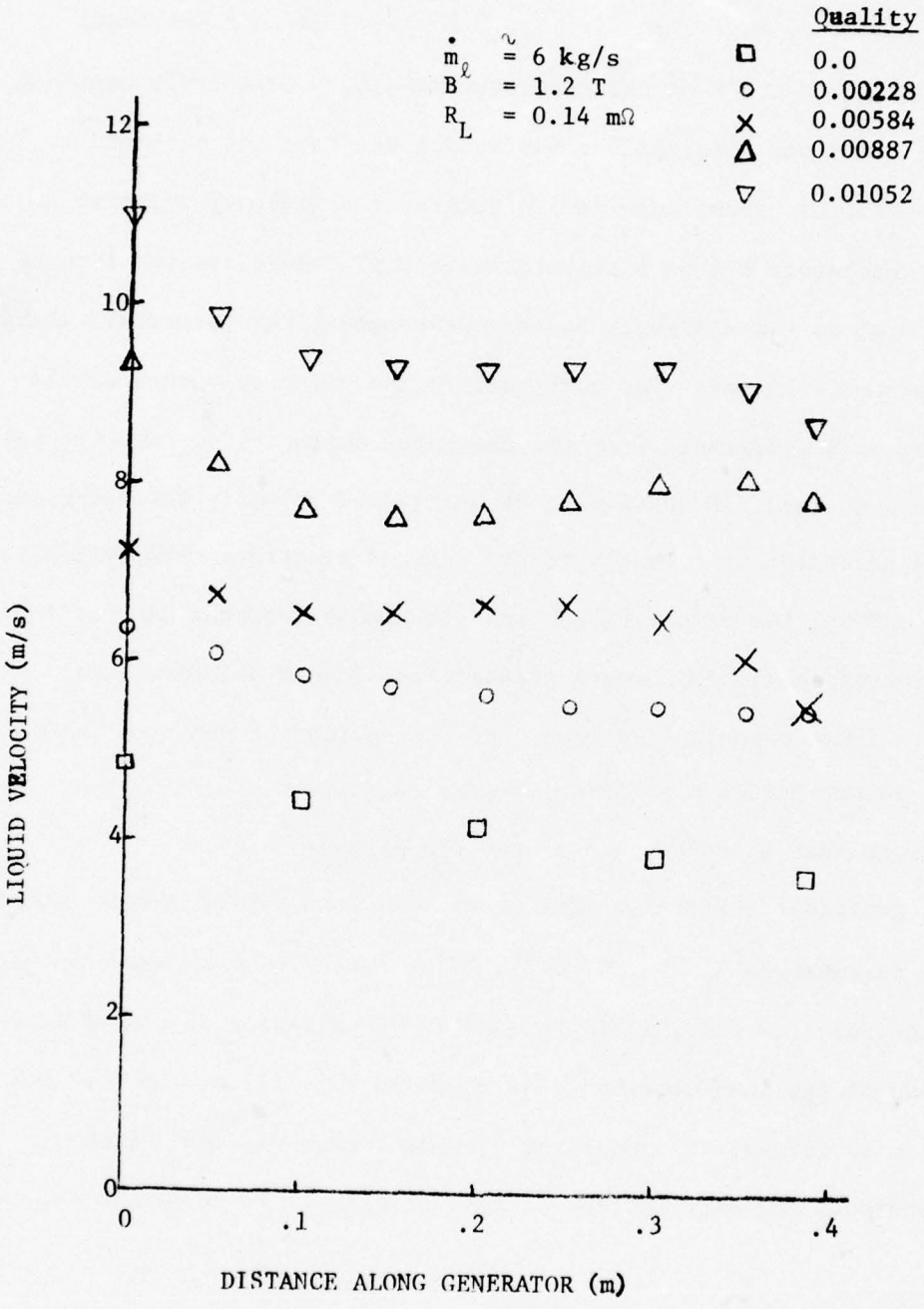

Figure III.1. Liquid Velocity Along Generator, R_L = 0.14 mΩ

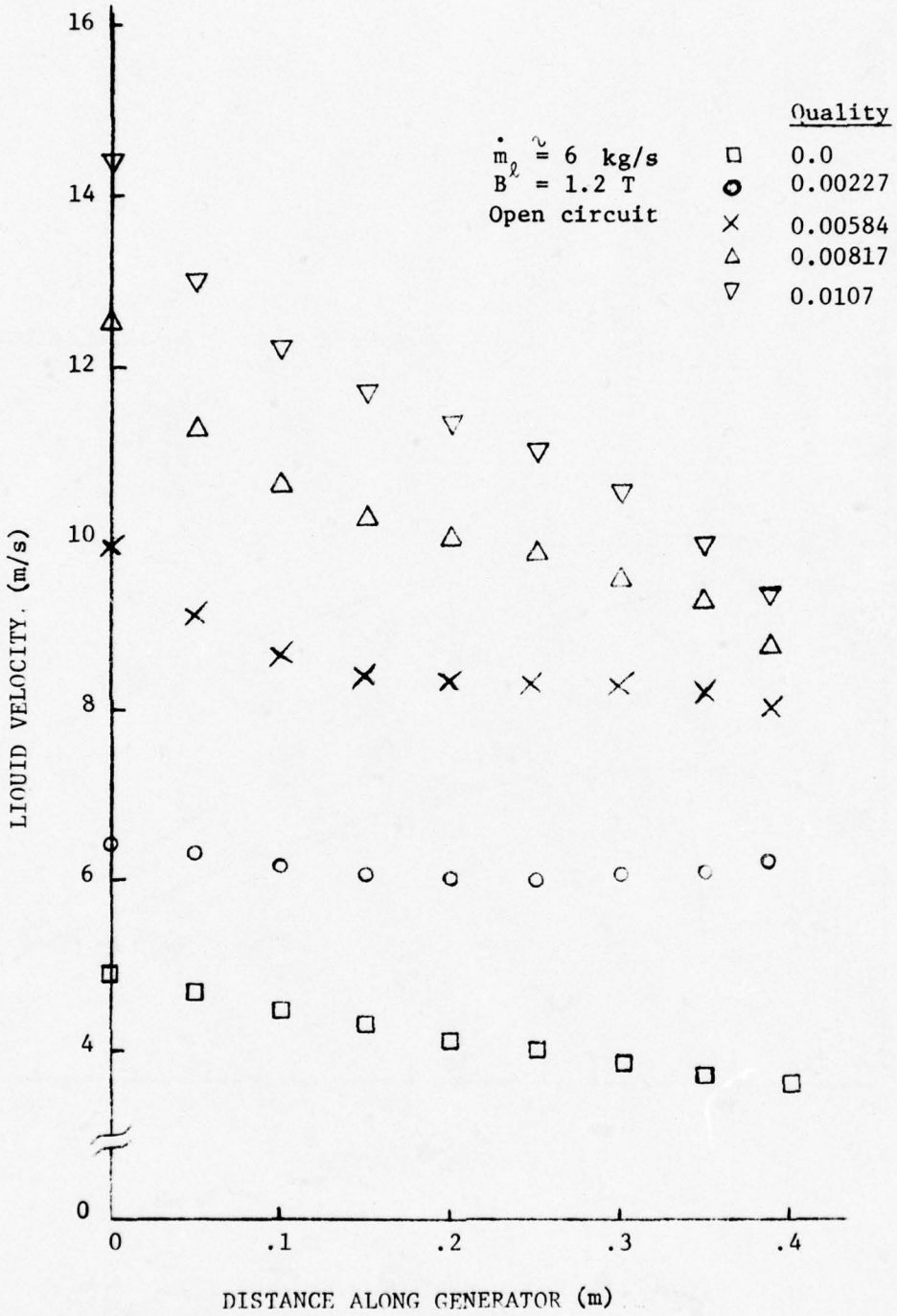

Figure III.2. Liquid Velocity Along Generator, Open Circuit

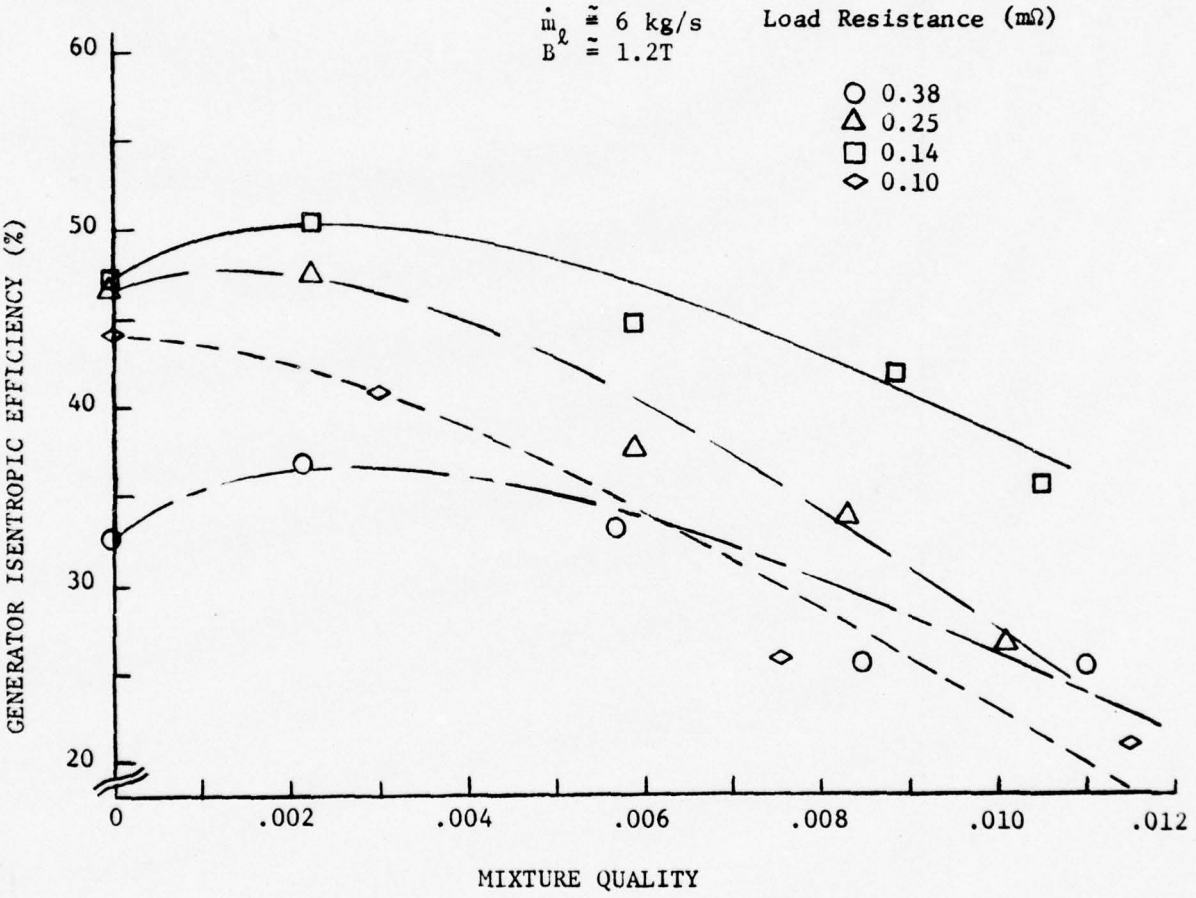

Figure III.3. Generator Isentropic Efficiency Vs. Mixture Quality With Gas Injection

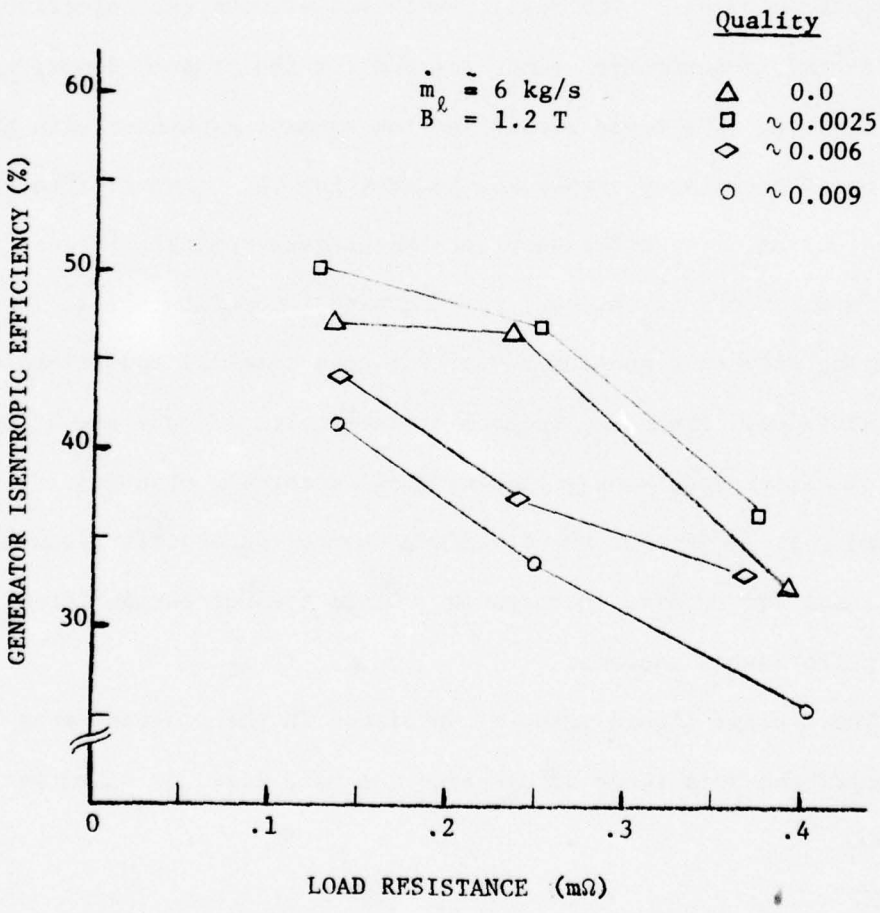

Figure III.4. Generator Isentropic Efficiency vs. Load Resistance

points to locate a peak on Fig. III.4. At high qualities the load factor is low, Fig. III.14 and Section III.1.2, so that it becomes very hard to load the generator to optimum conditions, and there is no sign of approaching a peak.

In Fig. III.5 the efficiencies of the three generators studied at ANL since 1972 are compared for the conditions B = 1.2 T, R_L = 0.25 mΩ, and $\dot{m}_\ell$ = 6 kg/s. (The efficiency is plotted verses average void fraction rather than quality because the former is a better indicator of flow properties and patterns.) The results with and without gas injection are included for the constant-area generator and for the present diverging-channel generator. For these conditions the present generator with gas injection has an efficiency comparable to that for the constant-area channel with gas injection. The efficiency for the present channel without gas injection is substantially higher, as discussed in Section III.3. Note that comparing different generators for the same terminal conditions has very limited value. Since the channel cross-sectional areas are different, R_L = 0.25 mΩ corresponds to a different load factor for each generator. The misloading is larger for the diverging-channel generators because they have a smaller internal resistance. Other reasons for different generator performances include:

1. The average liquid velocity is higher in the constant-area channel, and this tends to decrease the slip loss, as discussed below.

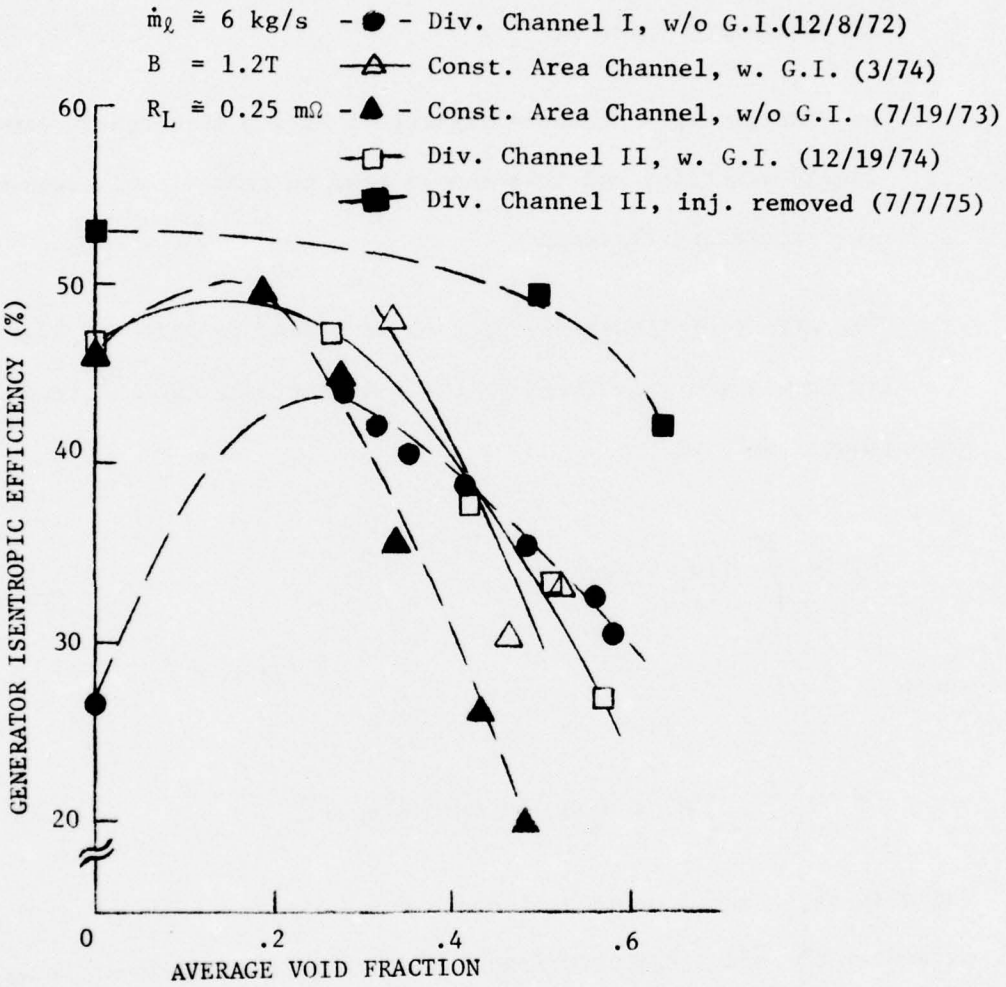

Figure III.5. Comparison Of ANL Generator Efficiencies Vs. Average Void Fraction For $R_L \cong 0.25$ mΩ

2. The gas injector ports protrude from the walls, and each pair restricts the flow area by up to 18% (see Fig. II.3). This may increase the losses, as discussed in Section III.3. There are five pairs of ports on the diverging channel, three pairs on the constant-area channel.

3. The diverging-channel generators have a more-nearly-constant liquid velocity, and this should tend to reduce ohmic losses due to circulating currents.

The effect of liquid velocity on slip loss is shown by Fig. III.6. The slip losses are calculated by the computer code ANLSIS[1] from the experimental data as[2]

$$P_S = \int_0^L A(u_g - u_\ell)F_S dx; \qquad \text{(III.1)}$$

where

$$F_S = \rho_\ell \; C_d' |u_g - u_\ell| (u_g - u_\ell)\alpha(1 - \alpha)^3, \qquad \text{(III.2)}$$

and A is the channel cross-sectional area. The local slip, local bubble parameter C_d', and local void fraction α are calculated from the experimental data. The percentage of slip loss relative to the isentropic enthalpy change is lower at 6 kg/s than at 2 kg/s. This is consistent with the expected reduction in percentage of slip loss as the liquid velocity increases.

B ≅ 1.2T

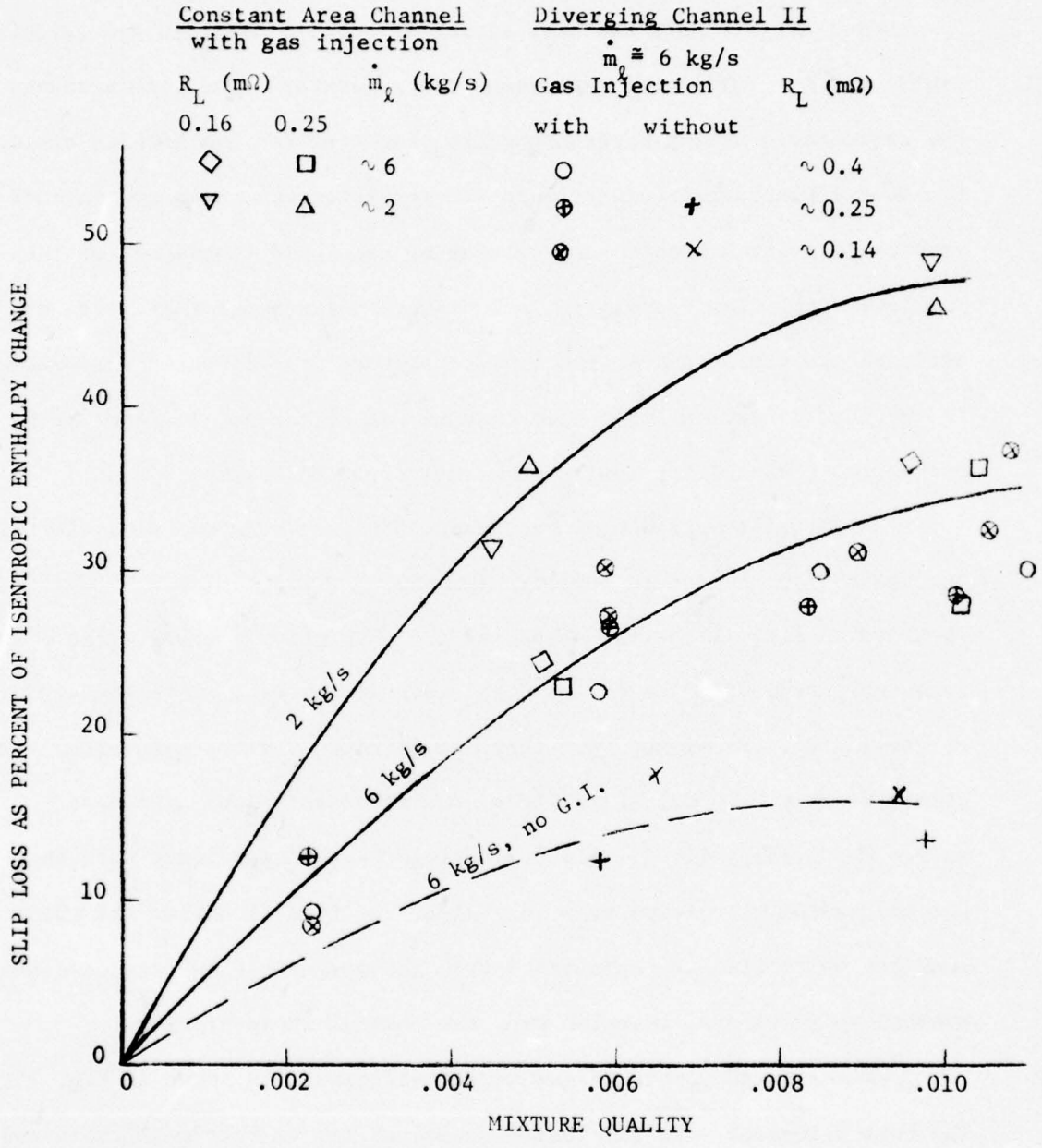

Figure III.6. Slip Loss as a Percent of Isentropic Enthalpy Change vs. Mixture Quality and Flow Rates

In Figs. III.7 through III.12 the measured data are compared with theoretical curves based on the approximate two-phase flow computer code described in Appendix A of Reference 2. A bubble parameter of $C_d' = 100\ m^{-1}$ was chosen as this gave the best agreement between measured and calculated liquid and gas velocities throughout the generator. The code accounts for the decreased coupling between the two phases as the gas bubbles expand due to the pressure gradient along the generator, but does not include the propensity for the bubbles to coalesce at high void fractions, or the possibility of flow transitions such as to semi-annular flow. Also not included are variations in the flow parameters or properties transverse to the flow direction. The area changes due to the gas injector ports are not included except for the one case discussed in Section III.3.

A typical comparison of the measured and calculated velocities along the channel for a mixture quality $\chi = 0.005$, $B = 1.2$ T, and $R_L = 0.25\ m\Omega$ is shown in Fig. III.7. The shapes of the theoretical curves agree reasonably well with the experimental velocity curves. Note the effect of varying C_d'. Excellent agreement was obtained for the open-circuited generator at $\chi = 0.0023$, Fig. III.8, and reasonably-good agreement at $\chi = 0.005$, Fig. III.9. (In evaluating these comparisons, note that the calculated velocities vary only along the flow direction and the measured velocities are calculated from the measured flow rates and the average void fraction measured over the channel cross-section.)

The measured generator isentropic efficiency is shown in Fig. III.10. The best agreement with the theory occurs at low mixture qualities, and the

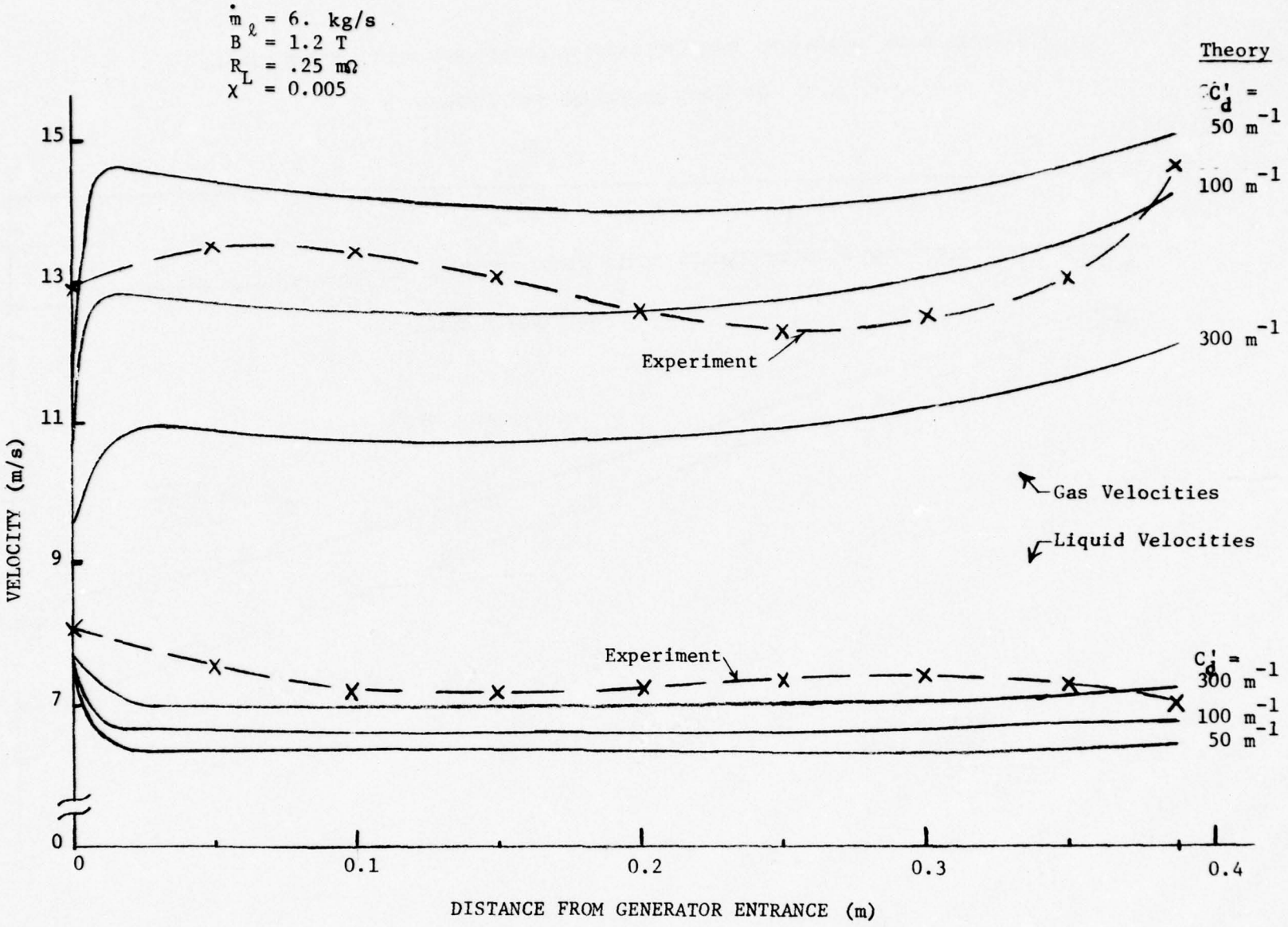

Figure III.7. Gas and Liquid Velocities Along Generator, R_L = 0.25 mΩ

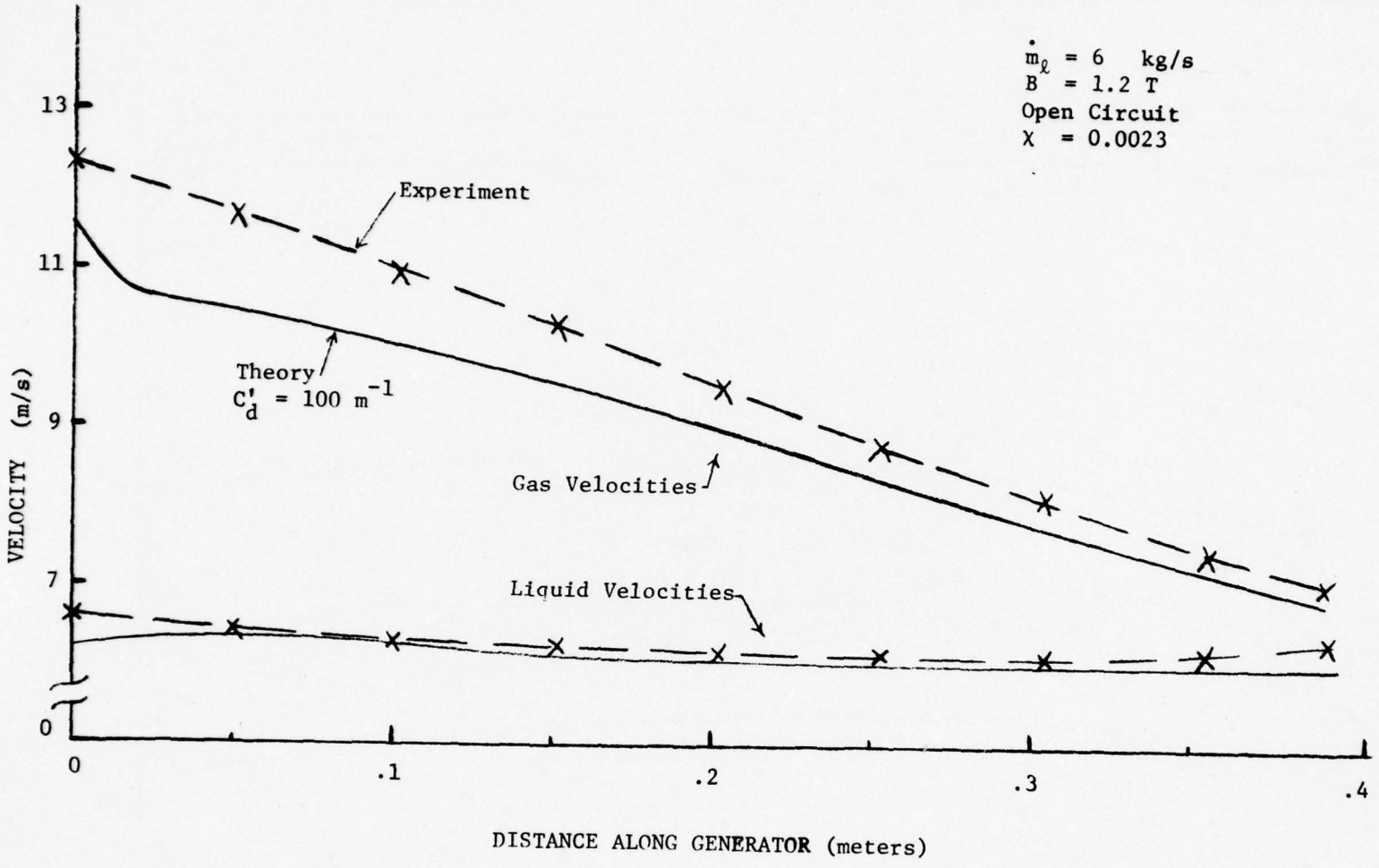

Figure III.8. Gas and Liquid Velocities Along Generator, Open Circuit, χ = 0.0023

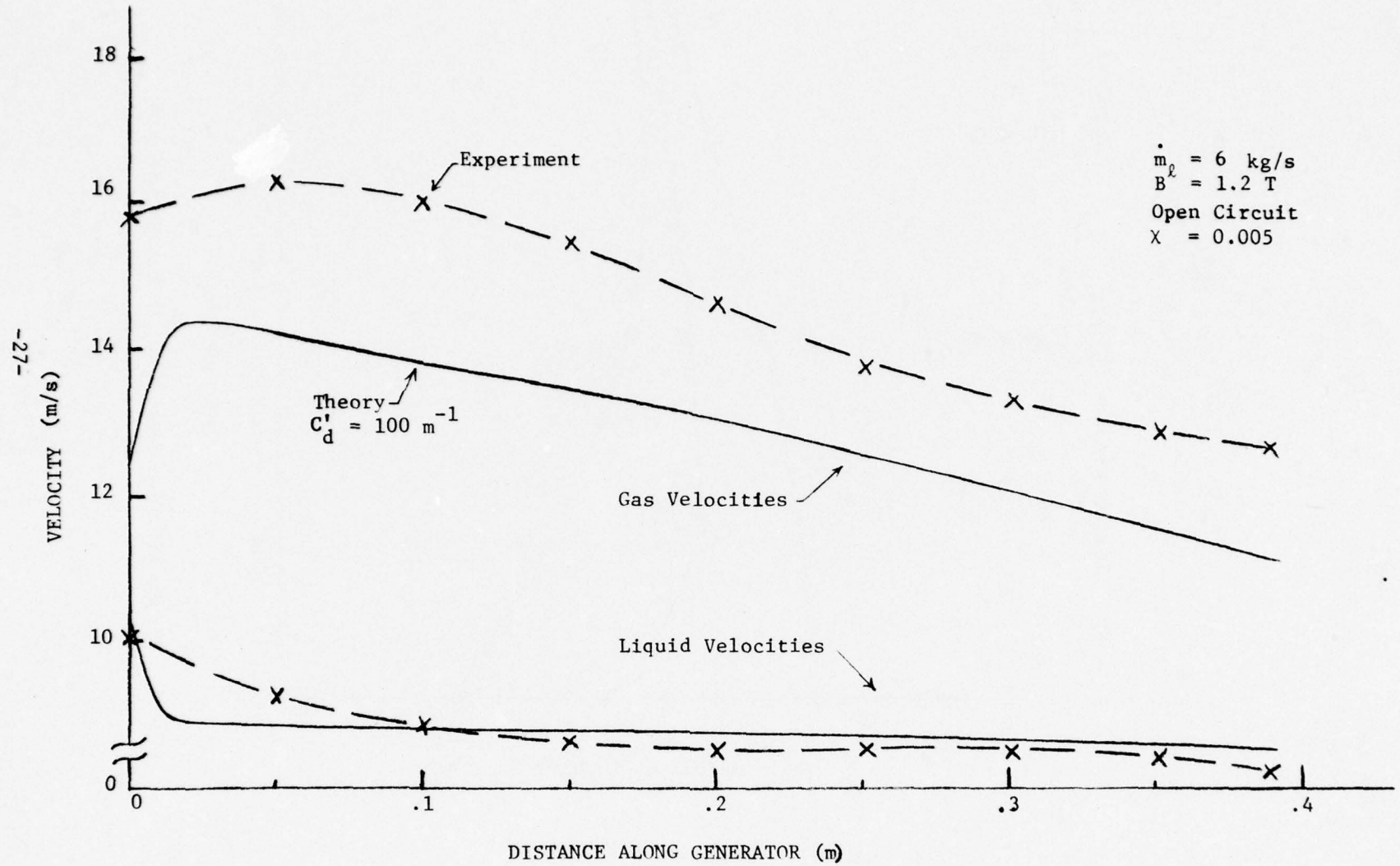

Figure III.9. Gas and Liquid Velocities Along Generator, Open Circuit, χ = 0.005

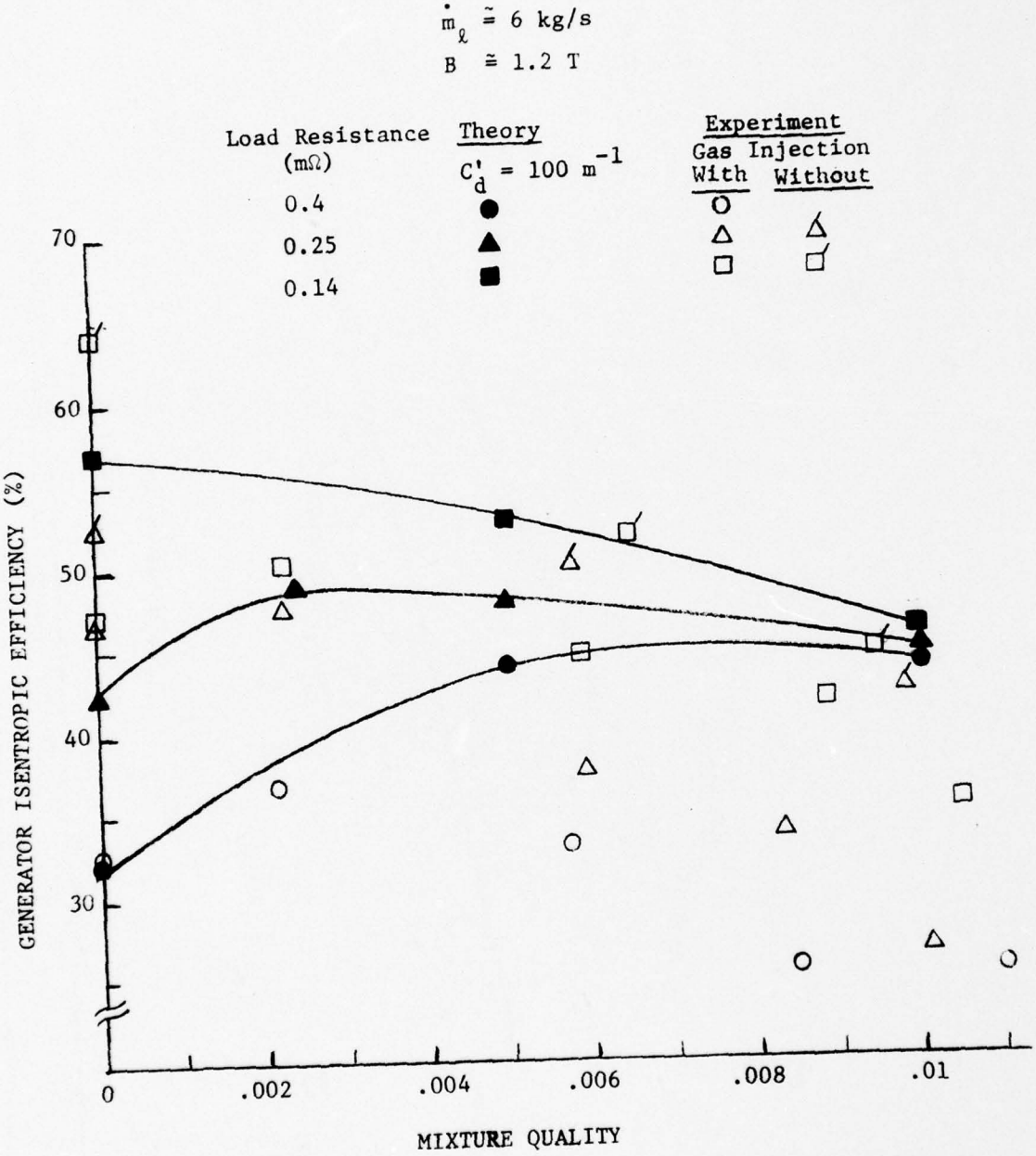

Figure III.10. Comparison Of Theoretical And Experimental Generator Efficiencies

agreement becomes progressively poorer as χ approaches 0.01. (The data without gas injectors are discussed in Section III.3.) The measured and calculated load voltages are shown in Fig. III.11. The agreement is best for R_L = 0.14 mΩ, and becomes worse as R_L is increased. This is consistent with the possible presence of a shunt resistance layer due either to the failure of gas injection to remove the liquid boundary layer or to a non-uniform liquid velocity caused by the abrupt cross-sectional area changes at the gas injectors (see Section III.3). The voltages for an open-circuited generator, Fig. III.12, show good agreement at low mixture qualities, up to χ = 0.0023 which also yielded good agreement between the velocities, Fig. III.8. As χ increases the measured open-circuit voltage increases slower than the calculated value and the velocity agreement is not as good, Fig. III.9. Note that at χ = 0.0023 the measured liquid velocity is above the calculated value but at χ = 0.005 it is below, thus the lower measured voltage.

An excellent fit between the calculated and measured open-circuit voltages is obtained if a 0.5 mΩ shunt resistance layer is postulated, Fig. III.12. This result is consistent with the earlier conclusion that the effects of velocity slip alone are not sufficient to account for the entire difference between the calculated and measured performances, and that shunting effects (end or internal) may account for the difference.[3] (Some of the difference is due to incorrect liquid velocity predictions, see for example Fig. III.9, but the average measured u_ℓ is not sufficiently lower than the calculated value to account for the difference in open-circuit voltage.) The shunt-layer effect is larger for the open-circuited

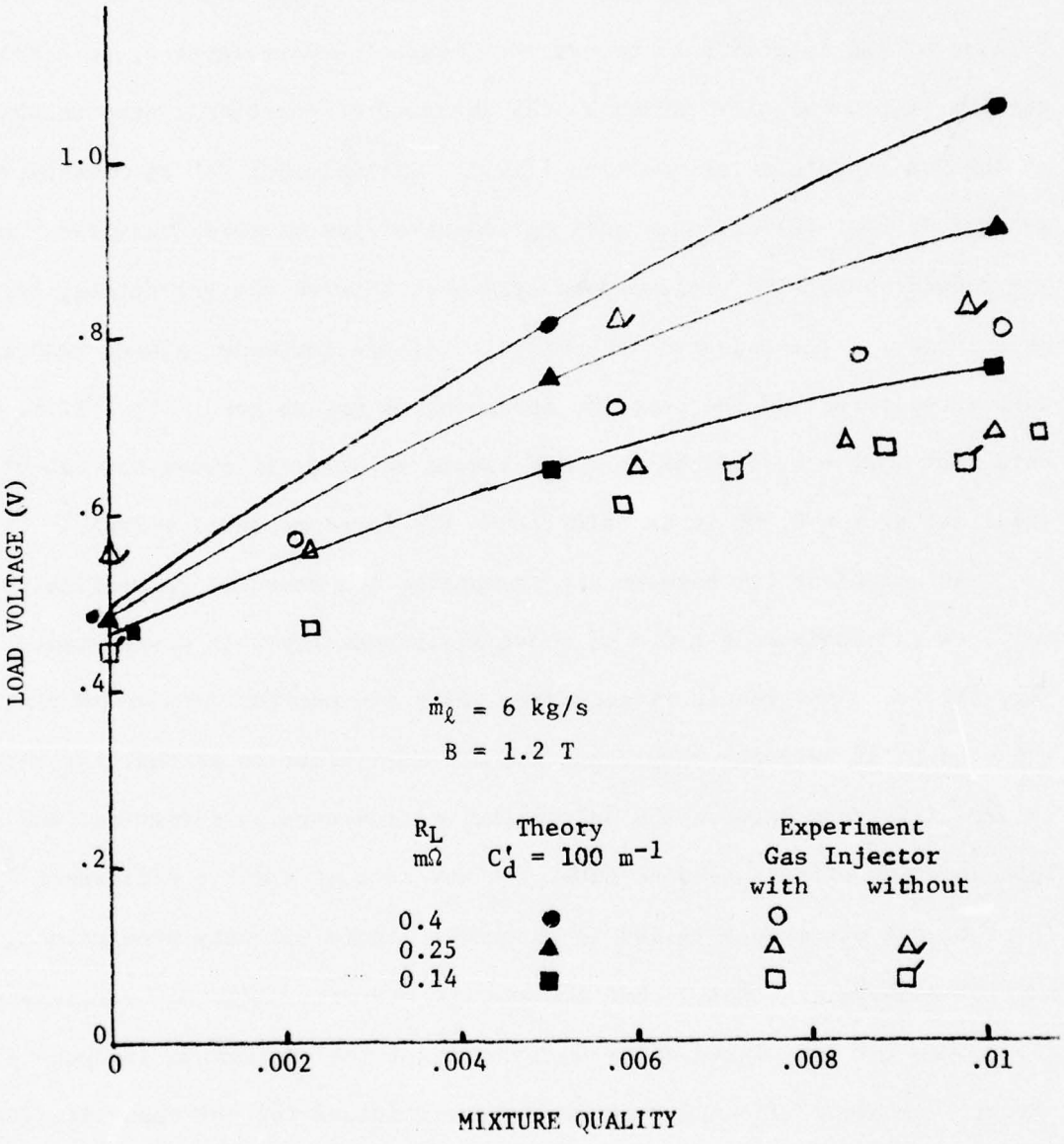

Figure III.11. Load Voltage Vs. Mixture Quality

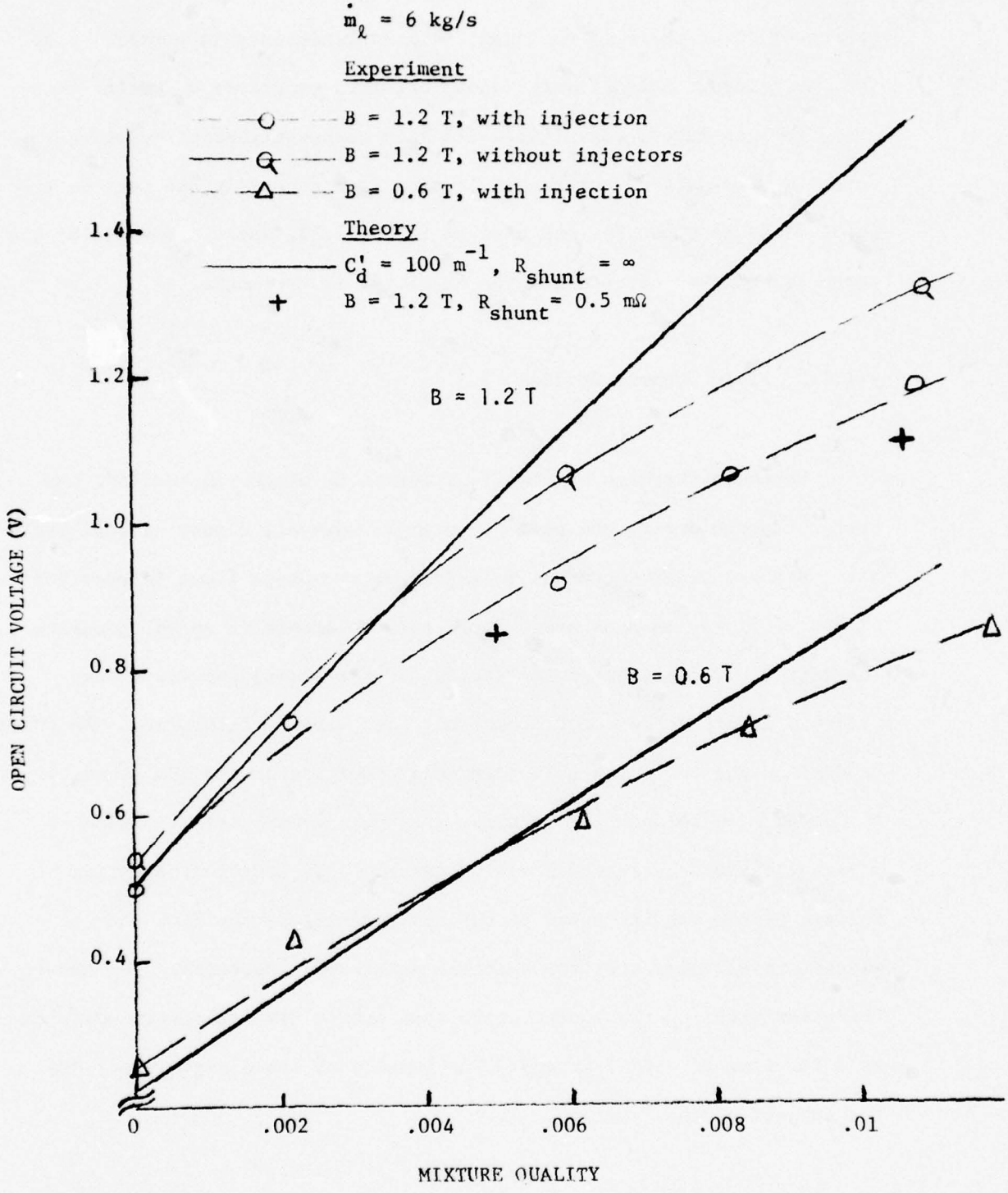

Figure III.12. Open Circuit Voltage Vs. Mixture Quality

generator since there is no (smaller) load resistance in parallel with the shunt layer. Also for the open-circuited generator u_ℓ varies more along the generator, Fig. III.2, and this causes higher circulating currents with part of the machine acting as a generator and part as a pump. This is shown for one case in Fig. III.13, where the shape of the curve is believed correct but the magnitude is too high.

III.1.2 Fluid Dynamic Studies

Extensive resarch on the fluid mechanics of two-phase flows has been conducted during the past ten years. However, almost no data has been obtained with electrically-conducting two-phase flows (except for dispersed flows) in a magnetic field such as exists in an MHD generator. The effects of electromagnetic forces and the associated very-large pressure gradients have not, thus far, been clearly determined. To better understand the two-phase-flow phenomena occurring in the MHD generator, a series of measurements to determine interfacial slip as a function of various generator parameters was undertaken. In addition, a series of voltage probes was installed to further investigate the flow and electric-field characteristics in the generator. Recently, the dynamic characteristics of the generator voltage output have also been measured as a function of void fraction. The results of these experiments are the subject of this section.

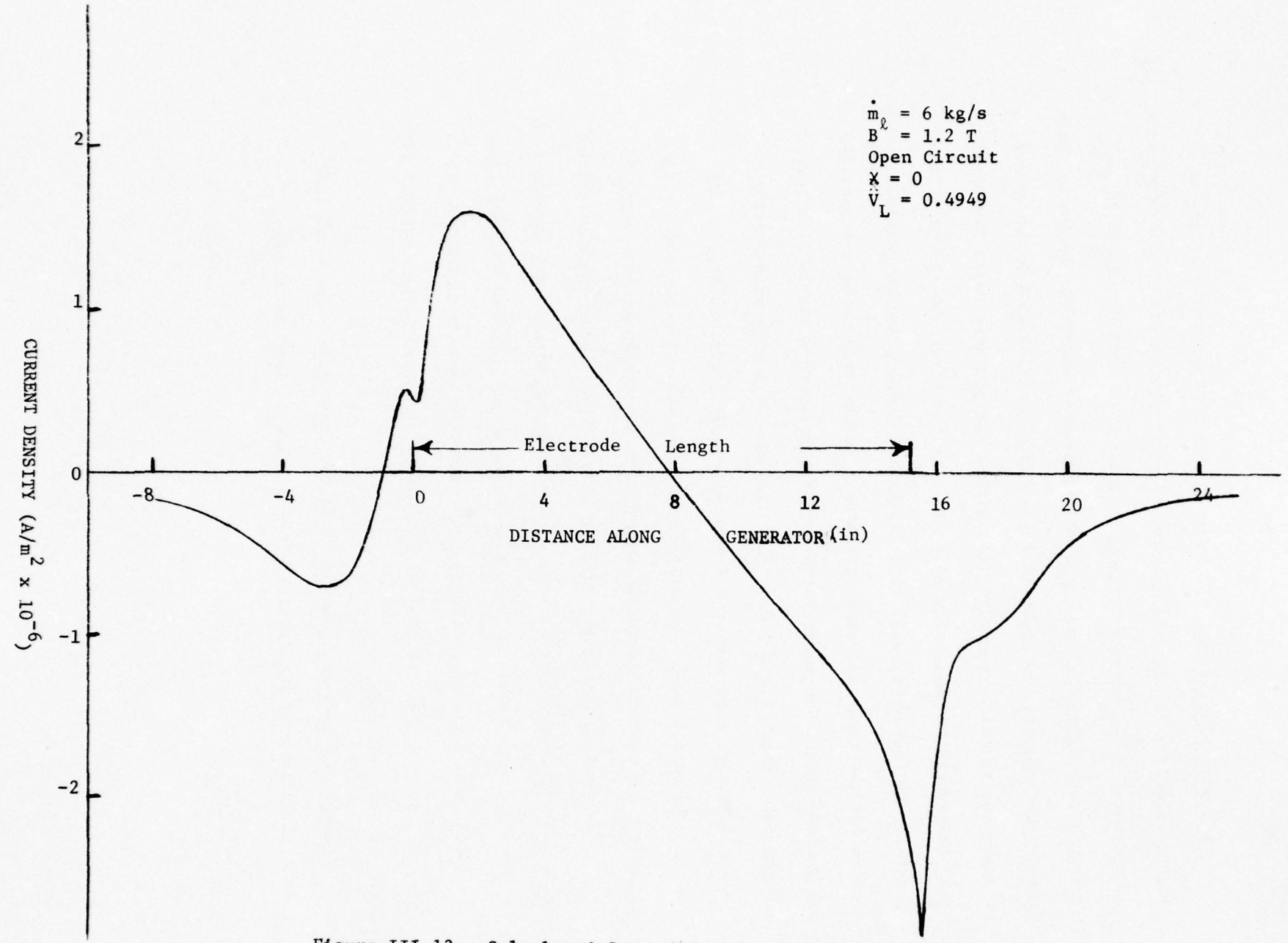

Figure III.13. Calculated Current Density Along Generator, Open Circuit

Velocity Slip Ratio. Velocity slip ratio, the ratio of gas to liquid velocity, is one of the most important parameters in the two-phase liquid-metal MHD generator because it can be the main mechanism of energy loss. Typically the slip ratio increases along the generator with gas injection ports, as shown in Figs. III.14 and III.15 (except at low mixture quality with open circuit), with a particularly rapid increase near the generator exit. The slip ratio in the first two-thirds of the generator is reasonably-well correlated with local pressure gradient. The reason for the rapid increase at the exit is believed to be a transition of the two-phase flow pattern from relatively-uniform bubble flow toward semi-annular flow, i.e., a flow characterized by a high-void-fraction low-conductivity core surrounded by a low-void-fraction slower-moving liquid sheath. Because a large percentage of the bubbles have coalesced at the center of the channel, coupling between the two phases is poorer and the slip ratio is higher than for uniform bubble flow. Other data presented below also indicate the existence of a transition toward semi-annular flow in the flow range studied. With the gas injectors removed the slip ratio was lower and decreased in the last third of the generator, Section III.3 and Fig. III.35. This is an indication that no transition to annular flow occurred for that case.

Change of Local Load Factor Along the Generator. The local load factor is defined as the ratio of load voltage to induced voltage,

$$F = \frac{V_L}{u_\ell aB} \quad . \qquad \text{(III.3)}$$

Ohm's Law in terms of F is

$$J = \sigma u_\ell B(1 - F), \qquad \text{(III.4)}$$

and therefore the local (1 -F) is a relative measure of the current density distribution in the generator. Local load factors are shown in Fig. III.16 for open circuit assuming a constant magnetic flux density along the generator. For zero mixture quality current is generated in the upstream half of the generator ($F < 1.0$) while the downstream half acts as a pump ($F > 1.0$), as shown in Fig. III.13. This is a consequence of the decreasing velocity of the incompressible liquid in the diverging channel, Fig. III.2. The pressure distribution for this case, Fig. III.19, has a slight rise in the last quarter of the generator, confirming that it acts as a pump there.

Another phenomenon shown in Fig. III. 16 is a marked decrease in the value of F for χ greater than about 0.006. When these five experimental runs were repeated, the marked decrease in F was still observed. A similar marked decrease in F was observed for other runs, see for example Figs. III.17 and III.18, though the value of χ where the decrease occurred depended on the generator parameters. Such a phenomenon suggests a transition from uniform bubbly flow toward semi-annular flow at high mixture quality. The region of semi-annular flow contributes less to the terminal voltage because the center core has a lower conductivity even though it has a higher liquid velocity, possibly with liquid entrainment. This higher u_ℓ contributes little or nothing to the terminal voltage. Meanwhile u_ℓ along the wall is reduced, and shunt layer effects are more important for semi-annular flow. Thus, the

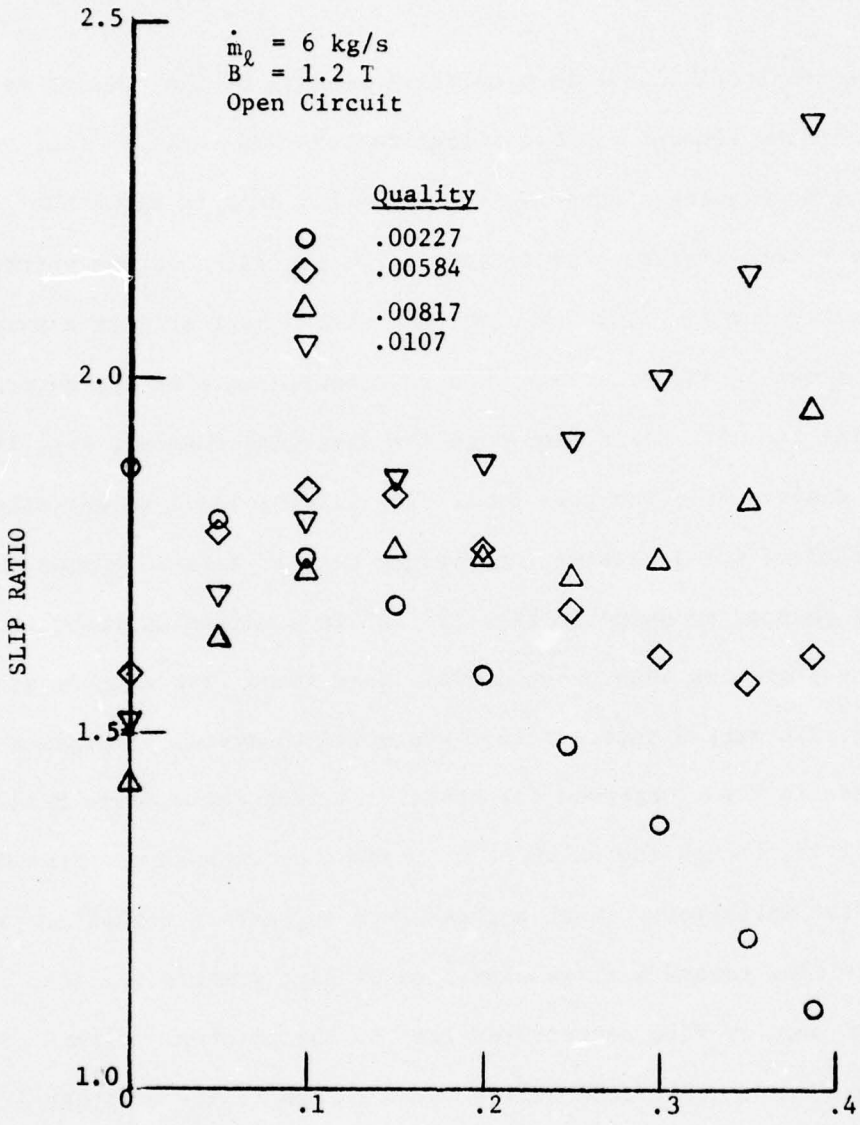

Figure III.14. Slip Ratio Along Generator, Open Circuit

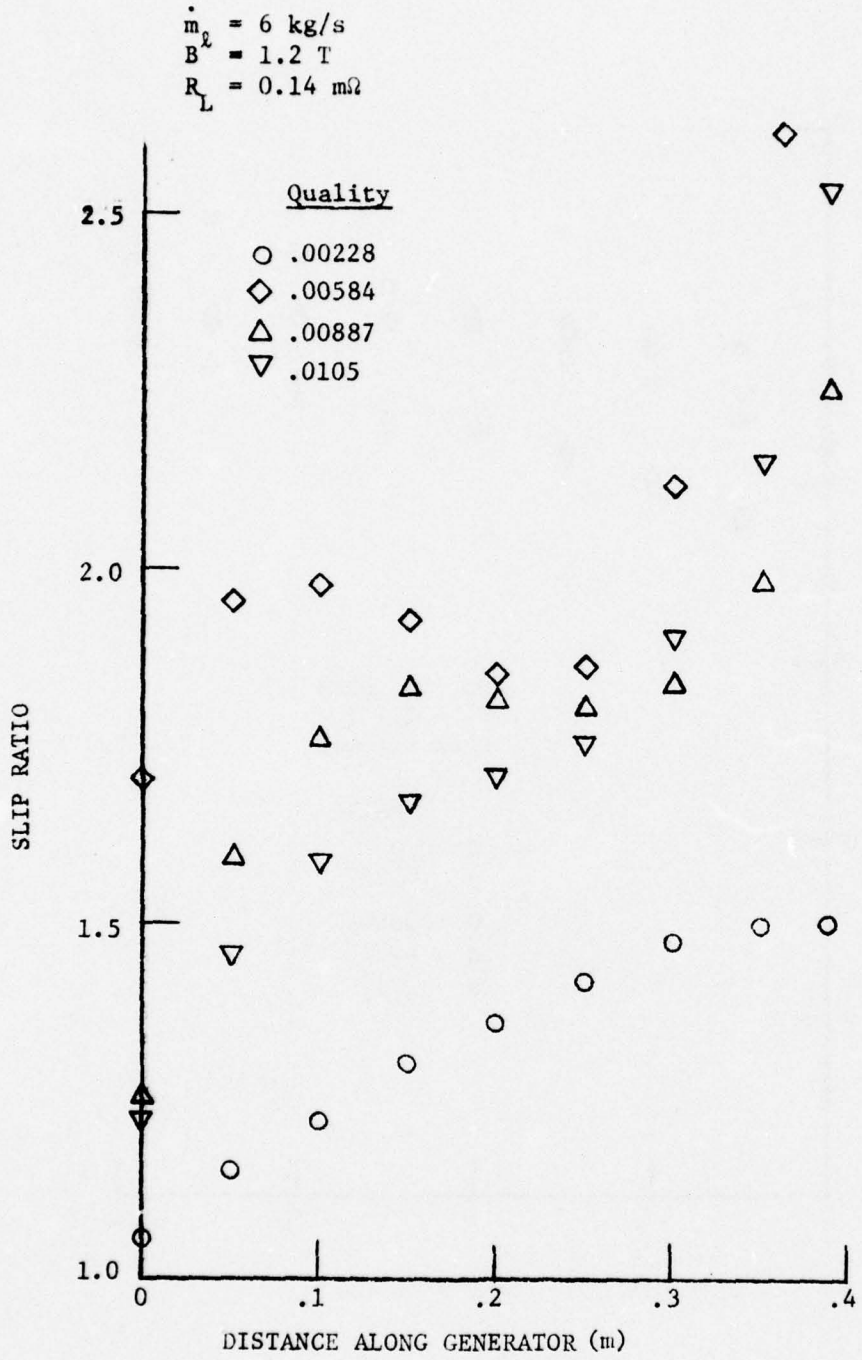

Figure III.15. Slip Ratio Along Generator, R_L = 0.14 mΩ

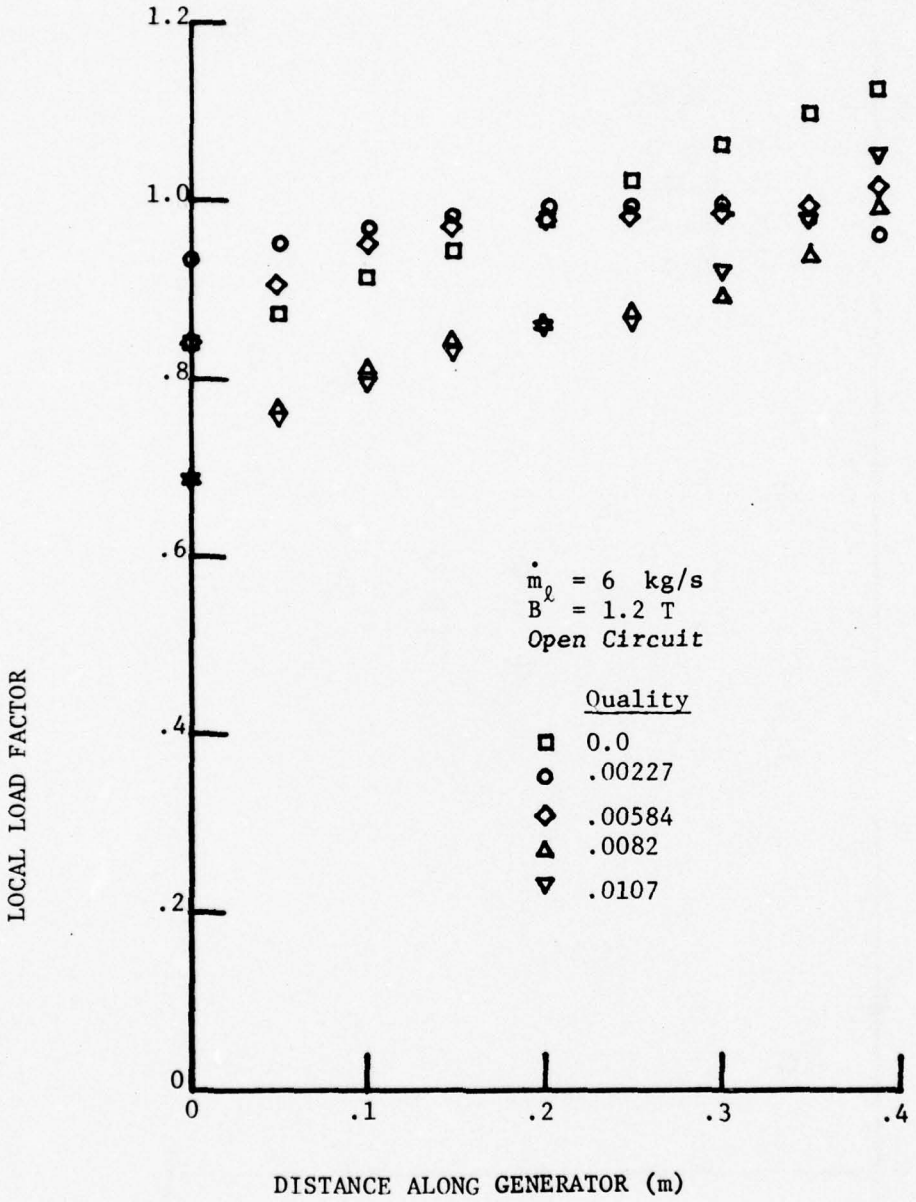

Figure III.16. Local Load Factor Along Generator, Open Circuit

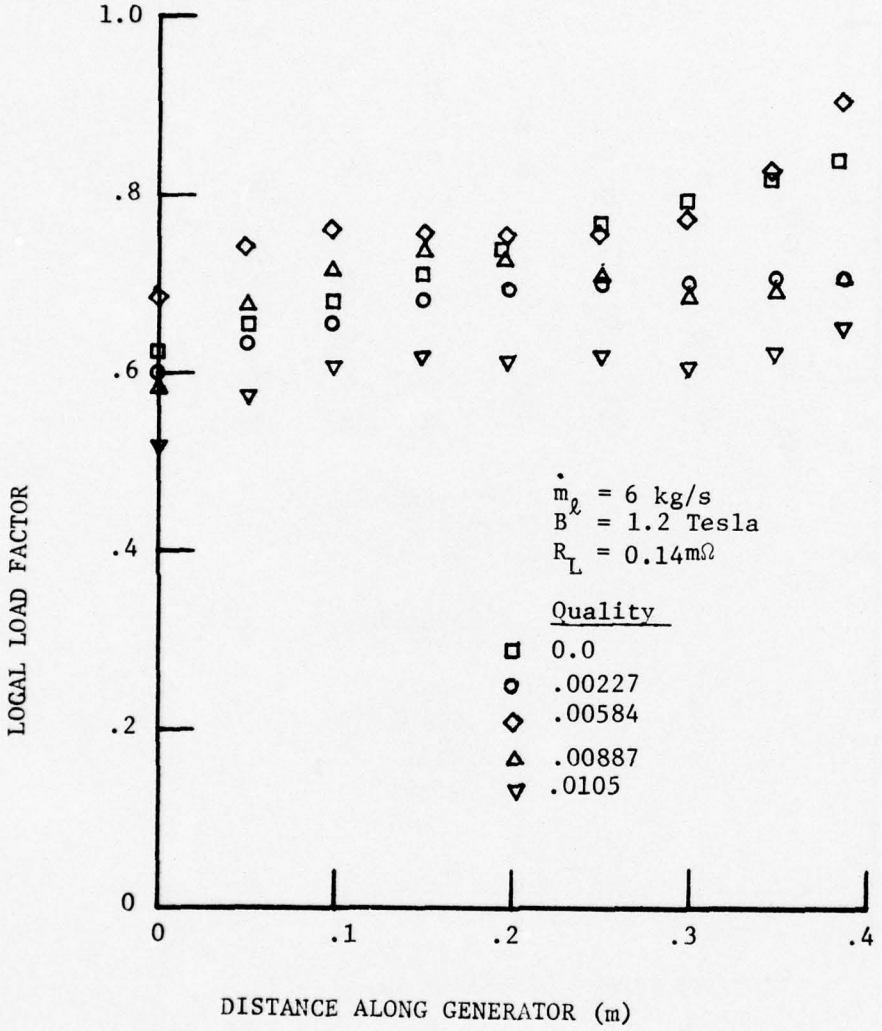

Figure III.17. Local Load Factor Along Generator, R_L = 0.14 mΩ, B = 1.2T

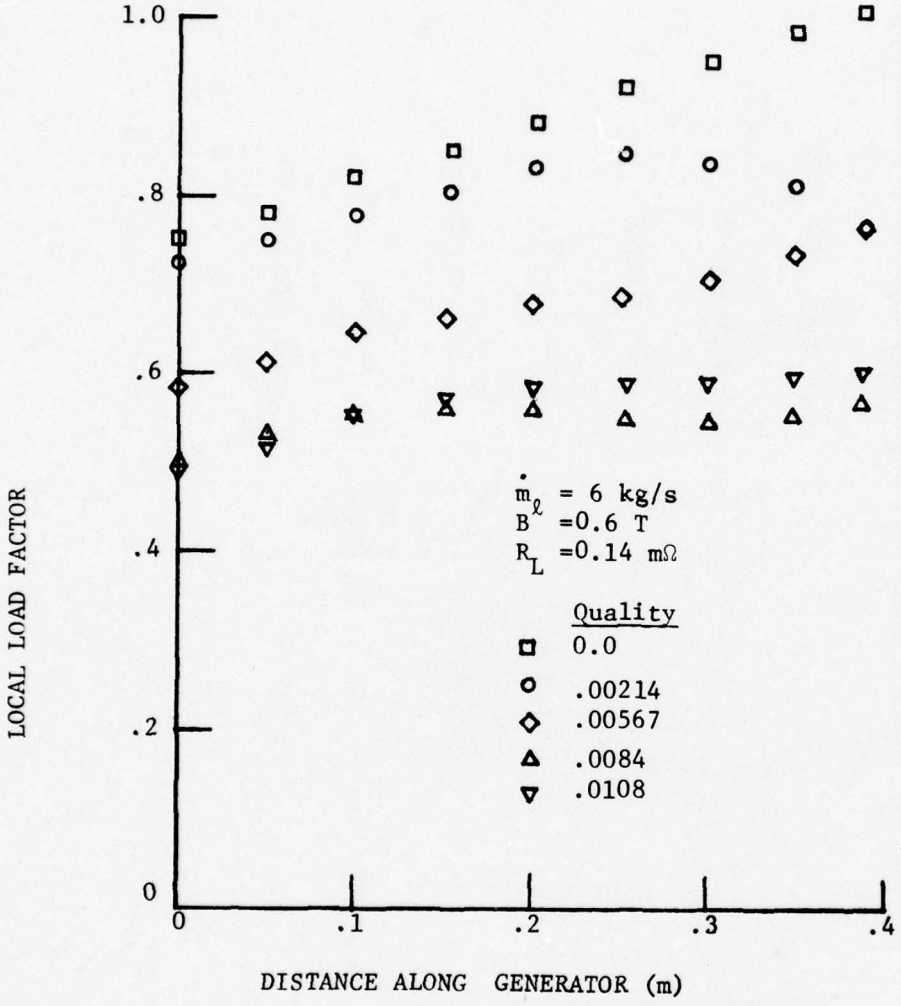

Figure III.18. Local Load Factor Along Generator, R_L = 0.14 mΩ, B = 0.6T

terminal voltage for the entire generator is reduced, and the calculated local load factors are lower because much of the actual liquid flow rate makes little or no useful contribution.

Pressure Distribution. Typical pressure distributions for a magnetic field of 1.2 T and a liquid flow rate of 6 kg/s are shown in Figs. III.19 and III.20. For zero mixture quality and open circuit the largest pressure gradient is at the generator entrance, as expected since the velocity is highest there. The large pressure gradient in the inlet end region (typical of all runs but particularly pronounced for open circuit) is an indication that end losses could be somewhat higher than expected. In some cases, however, part of the end regions are generating regions. For R_L = 0.14 mΩ and χ = 0, Fig. III.20, the high pressure gradient extends to the mid-point of the generator.

For all non-zero-quality non-open-circuit runs with a magnetic field of 1.2 T, pressure gradients in the middle third of the generator were two to three times larger than those in the first third of the generator. A gradual decrease in pressure gradient over the last third of the generator is typical of the data. At zero mixture quality and 1.2 T this pressure distribution was observed only for the lowest load resistance, 0.1 mΩ, but at 0.6 T it was observed for all mixture qualities including zero, Fig. III.21.

The gradual decrease in pressure gradient in the last third of the generator is more evidence of a possible transition from uniform bubbly flow to semi-annular flow, particularly since the liquid velocity

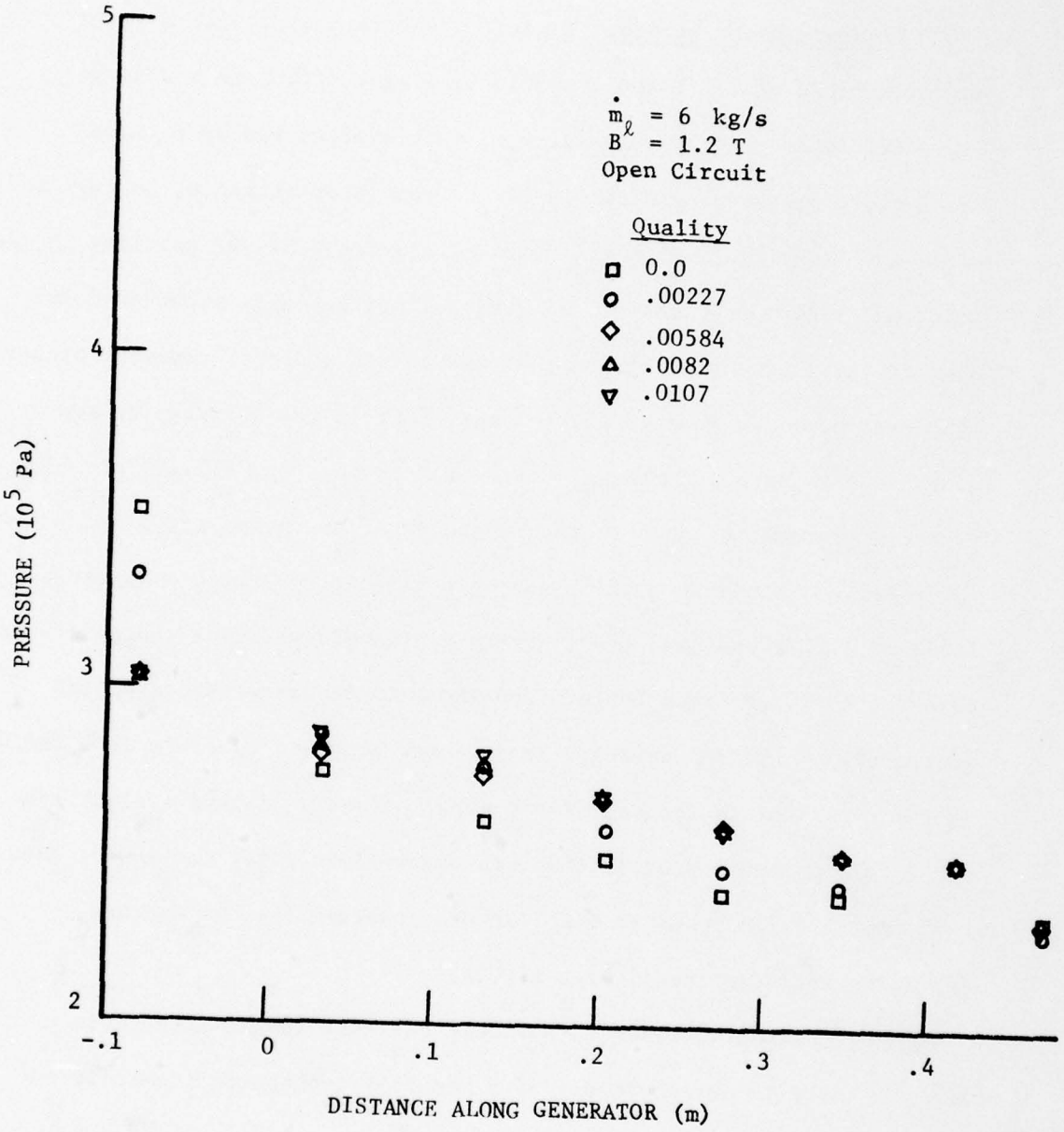

Figure III.19. Pressure Along Generator, Open Circuit

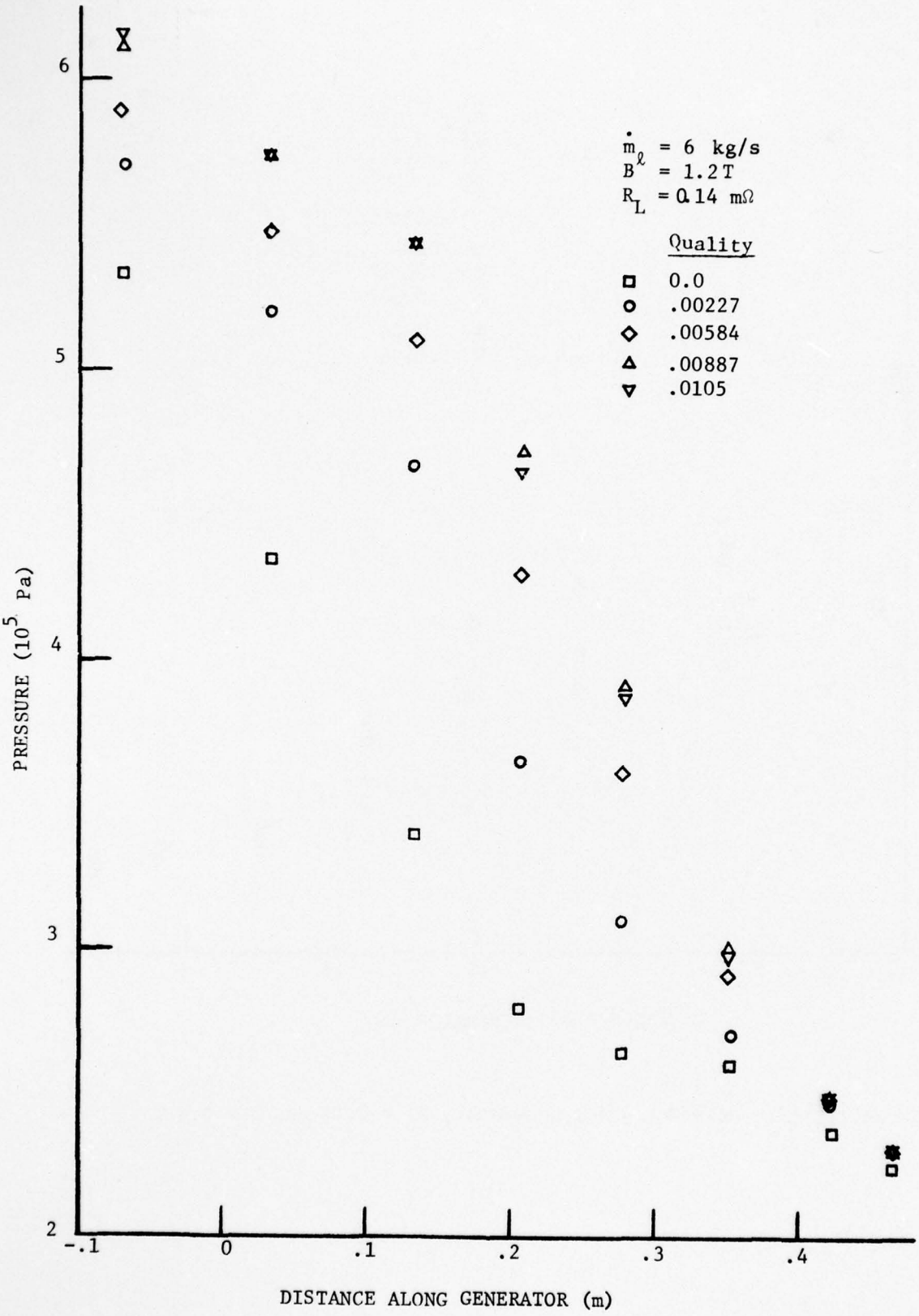

Figure III.20. Pressure Along Generator, R_L = 0.14 mΩ, B = 1.2 T

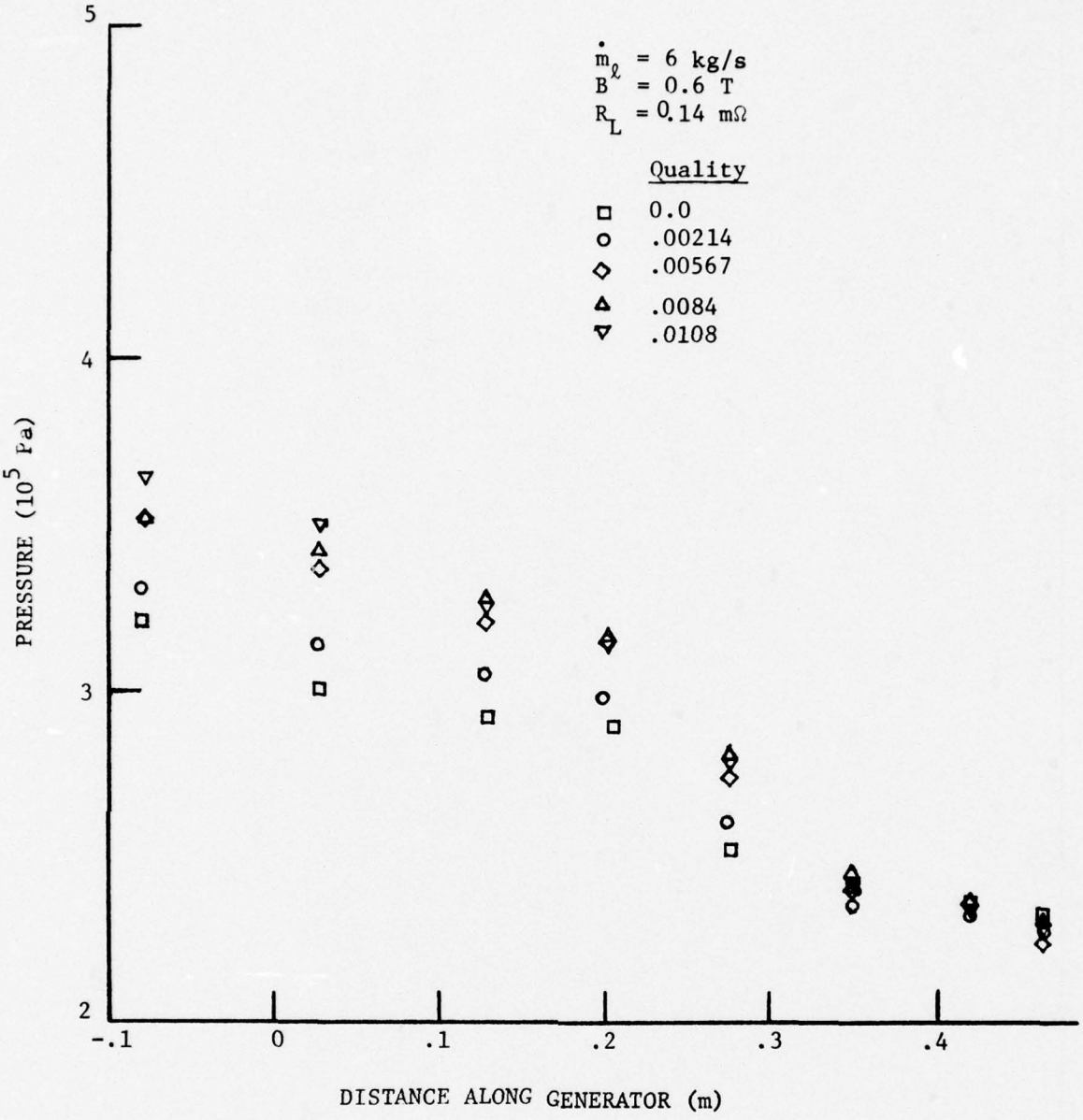

Figure III.21. Pressure Along Generator, R_L = 0.14 mΩ, B = 0.6 T

decreases slightly and the slip ratio increases in the last third of the generator. A change of flow pattern as postulated could reduce the coupling between the gas and the liquid to allow the simultaneous increase in slip, decrease in liquid velocity, and decrease in pressure gradient.

There are three possible explanations for the behavior of the pressure gradient in the first two-thirds of the generator. First, due to fringing, the applied magnetic field is about 11% less at the ends of the electrodes than in the middle. If the local load factor F is 0.8 at the center of the generator, then the Lorentz force at the entrance can be approximately 40% of that in the middle.

Second, as shown in Figs. III.1, III.17, and III.18, the liquid velocity tends to be highest in the beginning of the generator and consequently the local load factor lowest. This leads to larger currents in the beginning, Eq. III.4, and a higher Lorentz force. This effect is about the same magnitude as for the fringing magnetic field, and the two are additive.

Third, the generator is not perfectly compensated. The load current passes through the compensation bars, but not the end currents in the fringing regions. The effect of imperfect compensation can be easily derived for a constant-velocity generator with the product of electrical conductivity and channel width (parallel to B) a constant. Taking the integral form of the magnetic induction equation over a contour extending the distance g between the iron magnet poles and a length dx, applying

Ohm's Law, and differentiating yields

$$\frac{dB}{dx} = \frac{\mu\sigma u_\ell wB}{g} - \frac{\mu\sigma wV_L}{ga} - \frac{\mu I_L}{gL} \quad . \tag{III.5}$$

Since the total current produced by the generator equals the load current plus the end current,

$$\int_0^L Jwdx = I_L + I_e, \tag{III.6}$$

the solution for the magnetic field is

$$B(x) = \frac{\mu I_e}{g}\exp(R_m x/L) + \frac{V_L}{u_\ell a} + \frac{I_L}{\sigma u_\ell wL} \quad ; \tag{III.7}$$

where $R_m = \mu\sigma u_\ell Lw/g$ is the constant magnetic Reynolds number. With a magnetic Reynolds number less than unity, end currents of approximately 4000 amp, and a magnet pole gap of 0.1 meter; the increase in B from the beginning to the end of the generator would be less than 7% of the applied magnetic field. This amounts to a change of 43% in the Lorentz force if the local load factor is 0.8 at the center. In addition, if the forward current within the generator is non-uniform relative to the current distribution in the compensation bars, a similar distortion of the magnetic field would occur. The combination of the effects described above is sufficient to double or triple the pressure gradient in the middle third of the generator compared to the first third.

Void-Fraction Distribution. A typical void-fraction distribution, Fig. III.22, indicates no significant change in void fraction along the generator. This is a consequence of the increase in slip along the generator.

Results of Voltage Probe Measurements. Five voltage probes located 10.2 cm from the generator entrance were installed as shown in Fig. III.23 to measure voltage profiles. The voltage measurements were used to deduce features of the velocity profile between the electrodes. Each probe (see Fig. C2 of Reference 3) consists of a copper wire with a 0.15 cm diameter epoxy insulator molded around it. The probe length determines the position of the uninsulated tip of the probe relative to the insulated wall of the generator. Probes V_1, V_3, and V_5 are located on the channel centerline, probes V_2 and V_4 at the wall. A multi-channel digital voltmeter recorded the probe voltages.

The voltage measured by one probe located at position z relative to the negative electrode (z = 0) is

$$V(z) = \int_0^z \left[u_\ell(z')B - \frac{J}{\sigma(z')} \right] dz' \quad . \qquad \text{(III.8)}$$

Equation III.8 shows that the generator internal voltage is a nonlinear function of distance from the negative electrode, and the shape of the

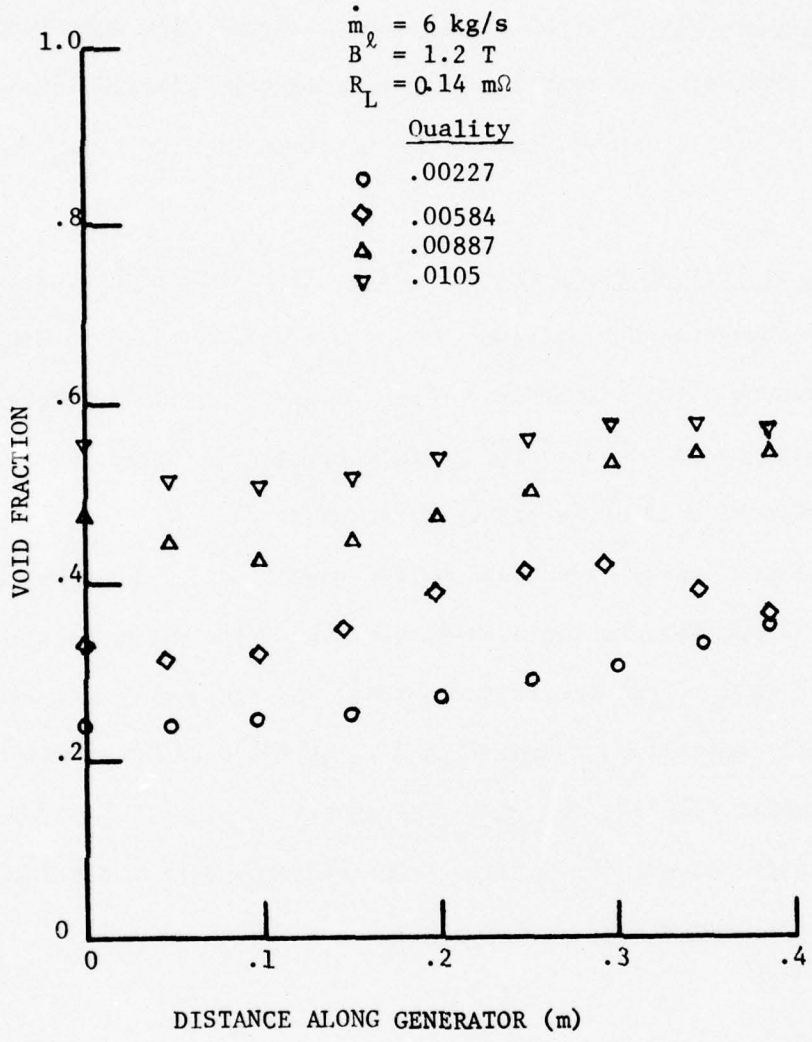

Figure III.22. Void Fraction Along Generator, R_L = 0.14 mΩ

function depends on $u_\ell(z)$ and $\sigma(z)$. At $z = a$, $V(a) = V_L$, the load voltage, or

$$V_L = \overline{u_\ell} aB - Ja(\overline{1/\sigma}) \quad ; \tag{III.9}$$

where $\overline{u_\ell}$ and $(\overline{1/\sigma})$ are the average liquid velocity and average resistivity, respectively. If the liquid velocity and conductivity are both constant over the cross section, then the internally-generated voltage will be a straight line from the negative electrode to the positive electrode. Differentiating Eq. III.8 and using Eq. III.9 to eliminate the current density yields the liquid velocity in terms of the slope of the voltage-probes data as

$$\frac{u_\ell(z)}{\overline{u_\ell}} = \frac{d\ (V/\overline{u_\ell} aB)}{d\ (z/a)} + \frac{1/\sigma(z)}{(\overline{1/\sigma})}\ (1-F). \tag{III.10}$$

The voltage profile was measured under a wide variety of experimental conditions. The results for the constant-area channel, presented in Appendix C of Reference 3, showed an S-shaped voltage profile. The ratio $u_\ell(z)/\overline{u_\ell}$ is approximately 1.75 near the electrodes for pure liquid, $\chi = 0$. This M-shaped velocity profile is probably caused by vorticity created by fringing magnetic-field gradients near the entrance to the generator,[5,6] even though the peak velocity ratio increases along the generator. For $\chi \neq 0$ the curvature of the voltage profile is less pronounced, but retains

the same general shape. The velocity of the non-zero-quality data cannot be computed using Eq. III.10 because the spatial variation of the conductivity is unknown.

The diverging-channel data even show a reversal in the orientation of the S-curve as mixture quality increases from zero to approximately 0.01 due to reduced core conductivity and increased core velocity. Typical diverging-channel data are shown in Fig. III.24. (The right half of the curve for $\chi = 0.0$ is not shown because these probes were not working.) These conclusions at high mixture quality are consistent with the tendency toward semi-annular flow.

Voltage Fluctuations. The instantaneous voltages on both of the electrodes, their difference (the terminal or load voltage), and their sum were observed with an oscilloscope. Typical instantaneous traces are shown in Figs. III.25 and III.26. For zero mixture quality no voltage fluctuations were present, but as gas was added an AC component appeared in the load voltage as shown in Fig. III.25. The average peak-to-peak amplitude of this AC component is roughly proportional to mixture quality, and the dominant frequency varies from about 100 Hz at low mixture quality to about 60 Hz at high quality. The frequency variation and the average velocity in the channel give a rough estimate of relative bubble size. For example, the bubble size indicated by Fig. III.25 increased roughly by a factor of four as χ increased from 0.0025 to 0.010.

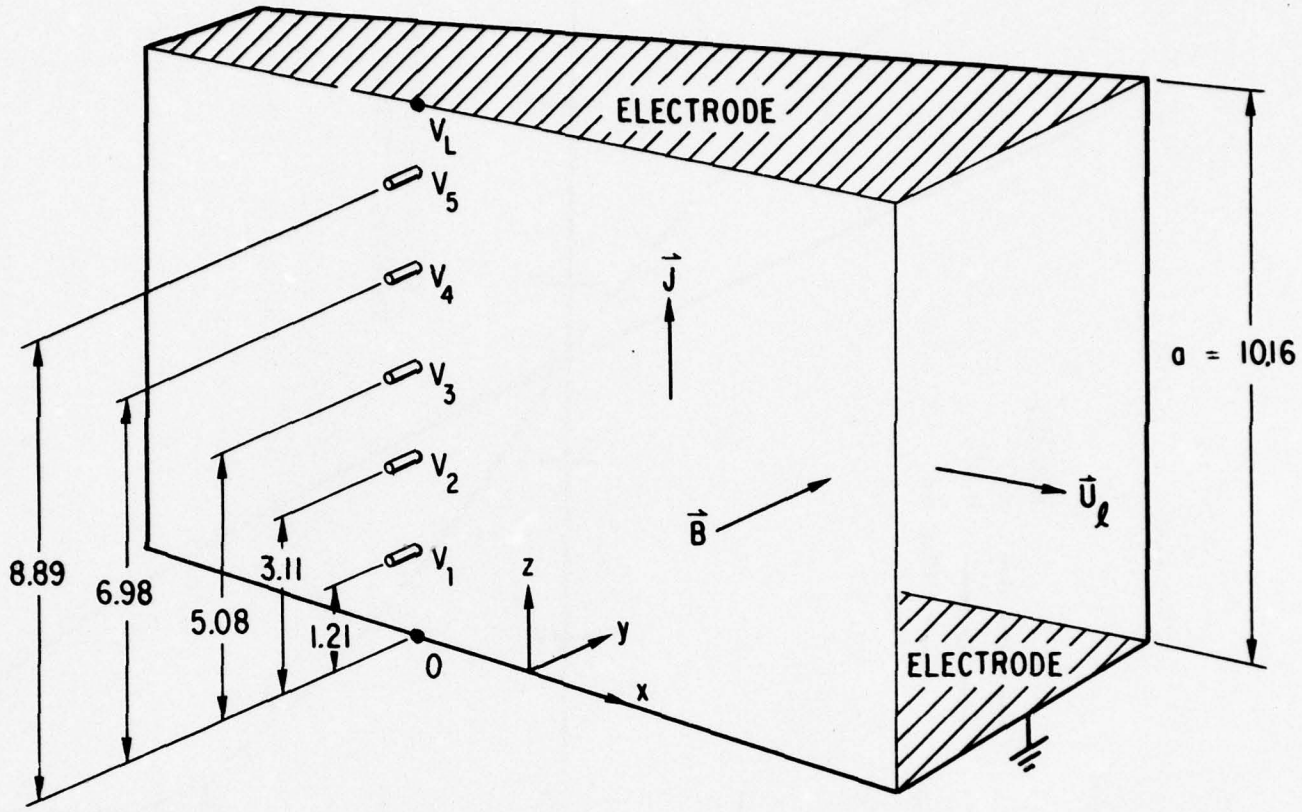

Figure III.23. Position Of Voltage Probes In Generator

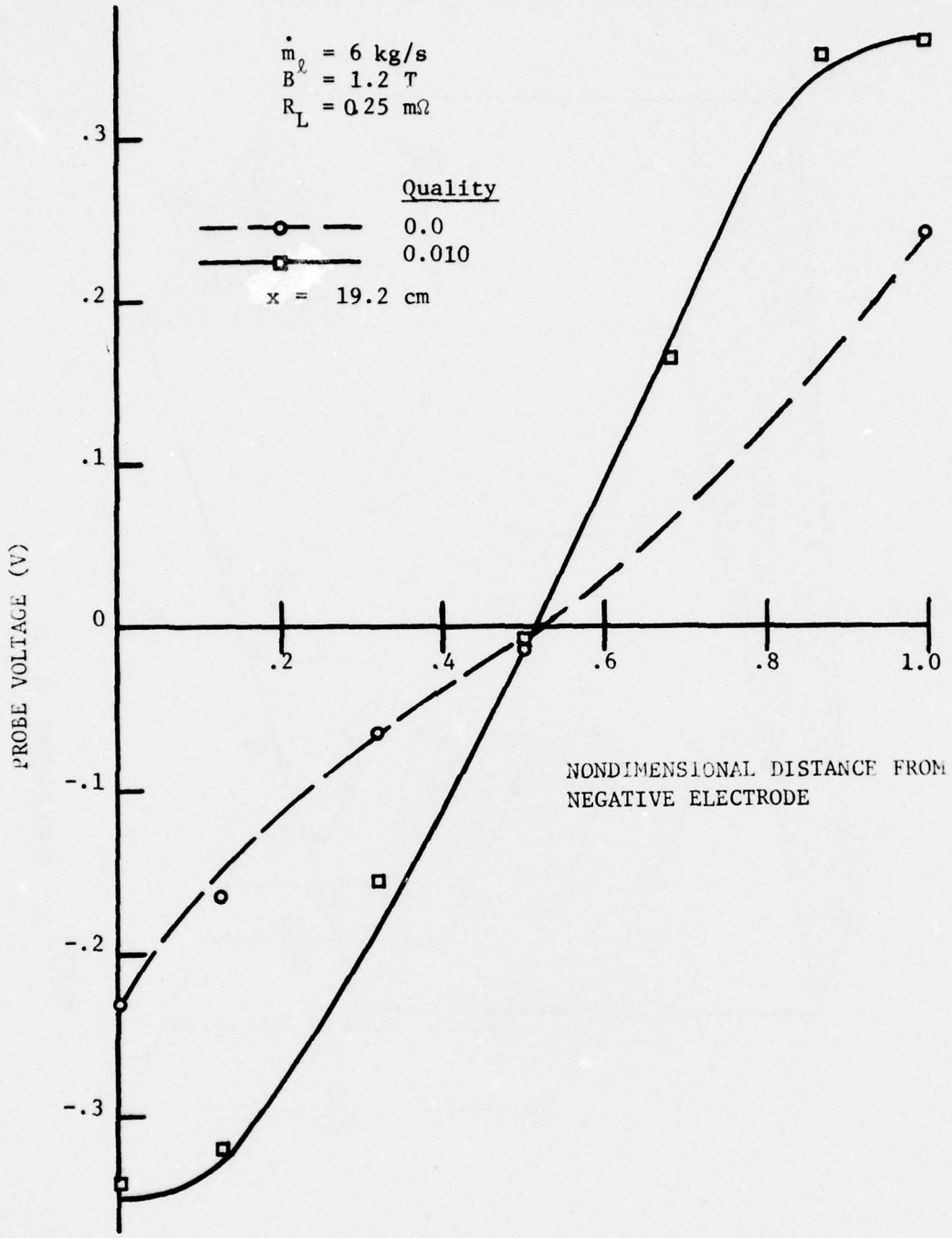

Figure III.24. Voltage Potential Profiles

Figure III.26a indicates that a high degree of correlation exists between the voltage fluctuations of the positive and negative electrodes, both measured relative to the voltage at the centerline of the channel. A typical trace of the sum of the AC components of these voltages, Fig. III.26c, has an amplitude that is two to three times larger than the AC amplitude of the terminal voltage, Fig. III.26b. This confirms the correlation between the voltages.

The voltage correlation may be the result of fluid of nigh void fraction flowing alternately along one electrode and then along the other. The increase in the peak-to-peak fluctuations of the terminal voltage and voltage sum, Figs. III.27 and III.28, tends to support this hypothesis.

It should be noted that the voltage fluctuations were greatly reduced when the gas injection parts were removed. Fluctuations would also become smaller as the generator size is increased, as improved mixers are used, and as more-uniform two-phase mixtures are used in the generator (see Section V.4).

III.2 Effect of Gas Injection

During experimental runs with a loaded generator for $\chi = 0$, $B = 1.2$ T, and with gas injection it was observed that the void fraction profiles (across the channel width parallel to B) were very uniform and approximately equal to zero at the first five void-fraction windows. This indicated that the gas left the walls and was mixed

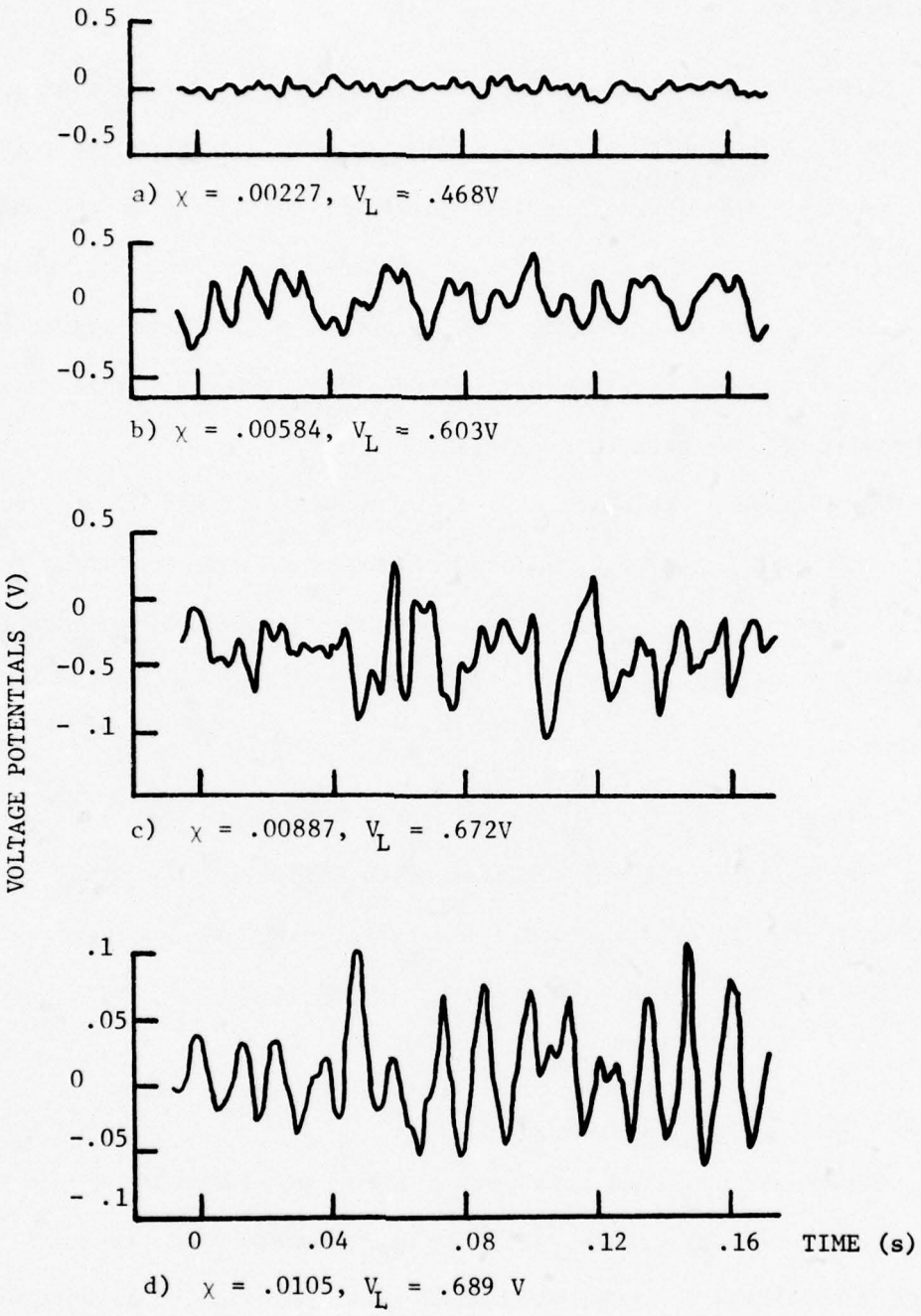

Figure III.25. Fluctuations in Terminal Voltage, R_L = 0.14 mΩ, B = 1.2T, $\dot{m}_\ell$ = 6 kg/s

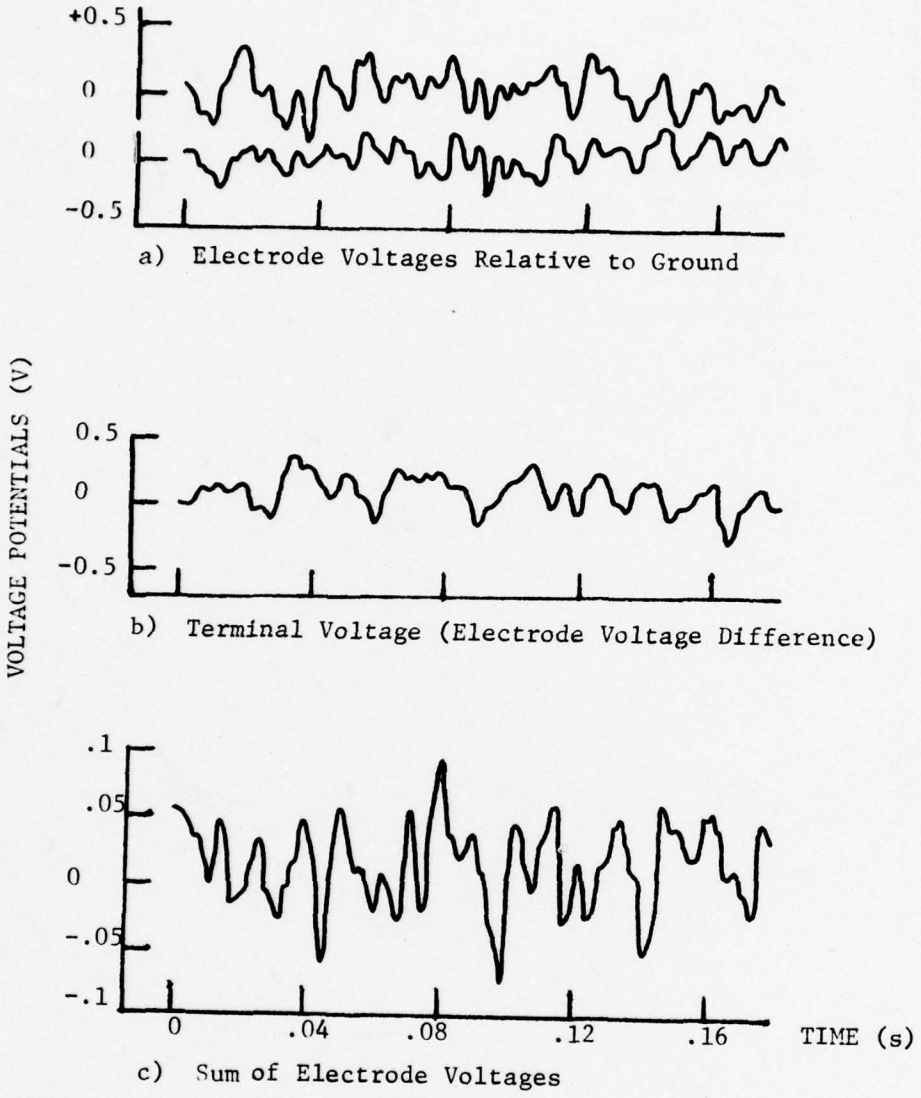

Figure III.26. Different Recordings of Voltage Fluctuations, Open Circuit, B = 1.2T, $\dot{m}_\ell$ = 6 kg/s, V_L = 0.731

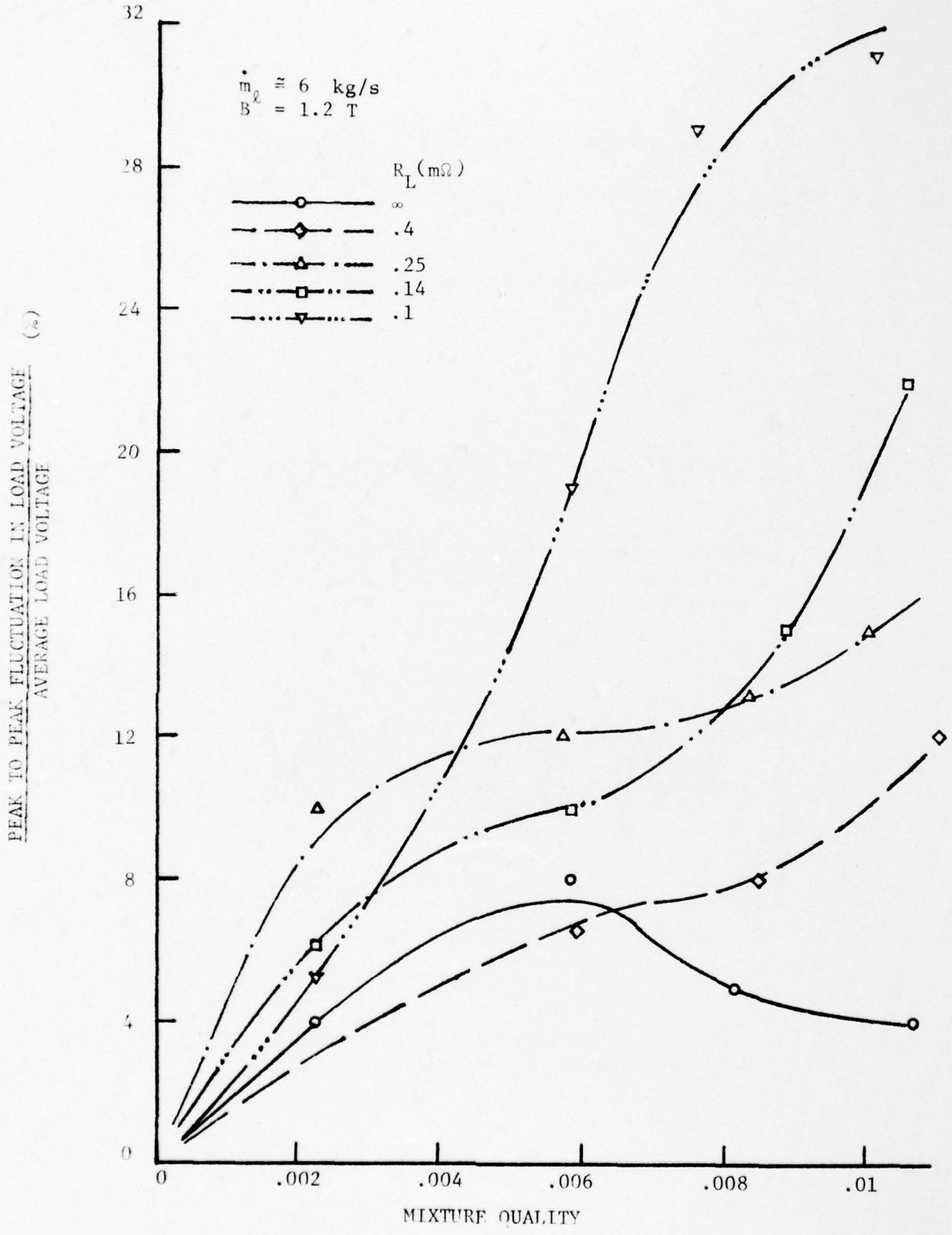

Figure III.27. Average Peak to Peak Amplitude of Fluctuations of Terminal Voltage

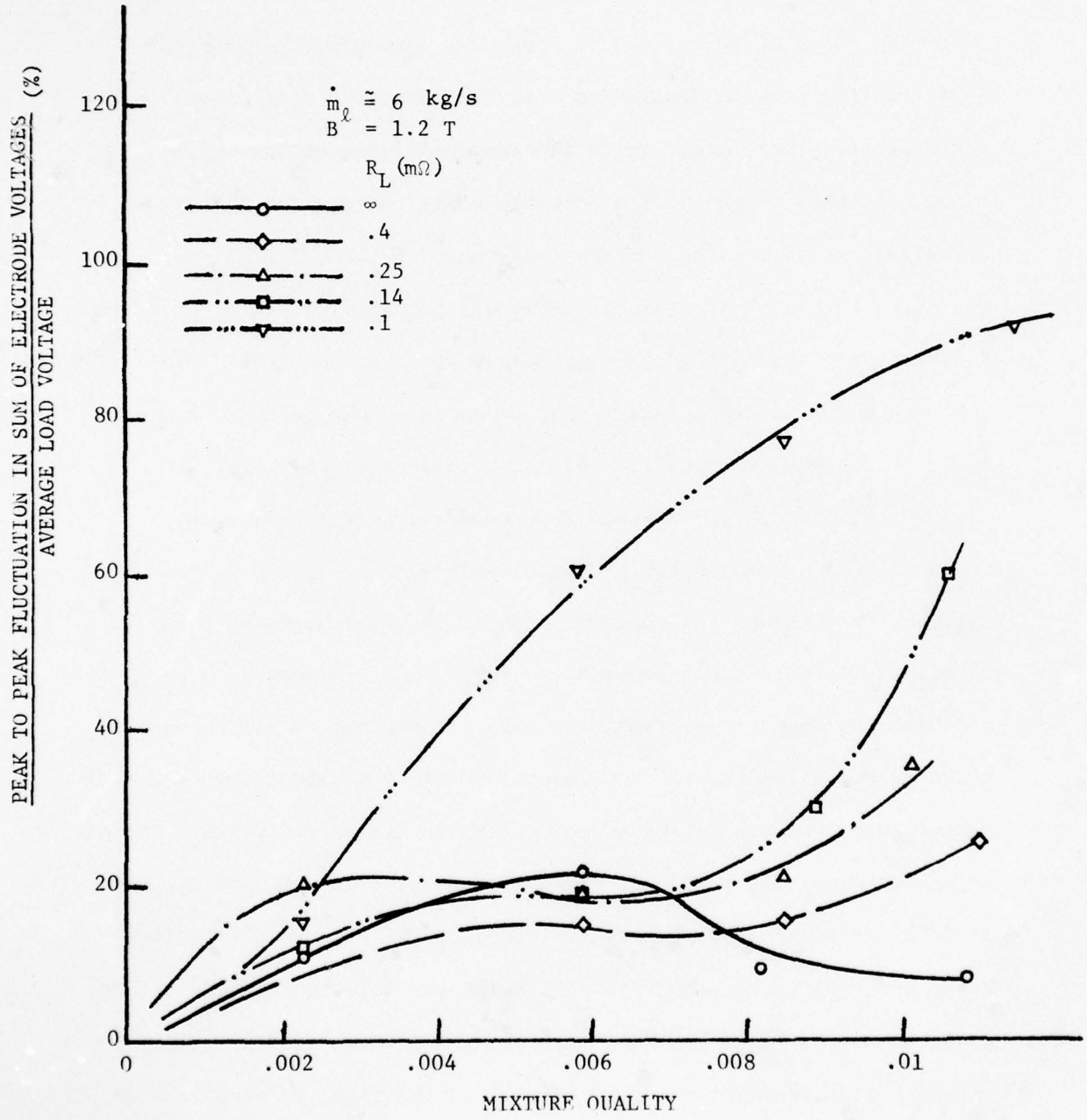

Figure III.28. Average Peak to Peak Amplitude of Fluctuations in Sum of Electrode Voltages

approximately uniformly with the liquid. At the sixth and last window, located just inside the exit end of the generator, the void fraction was low at the center of the channel and high near the walls (see Fig. III.1 of Reference 3). Only the last window showed the void-fraction profile desired to minimize shunt and friction losses. These profiles were practically independent of the amount of gas injected. Examination of the pressure distributions for these runs revealed that high void fraction (gas) next to the walls existed wherever the local pressure gradient was positive, i.e. the pressure differential force pushed the gas bubbles against the liquid flow. For negative pressure gradients, as exists for power generation, no gas could be detected next to the walls (see also Section II.1).

The MHD generator channel is oriented so that the flow is vertically down. Thus, the pressure gradient will have a small positive value along the whole generator with zero magnetic flux density. The void-fraction profiles for B = 0, $\dot{m}_{\ell}$ = 6 kg/s, $\chi_{\text{inlet}} = 0$, and high gas injection through all five ports along the right wall are shown in Fig. III.29. The gas injection rate was higher than the flow-meter range, but was estimated to be roughly 1.5 g/s/injector. The gas injectors along the left wall had only a small flow rate, on the order of 0.01 g/s/injector, to prevent plugging. The high void fractions along the right wall, the wall with large gas injection, show that the injectors are effective. Note that the gas diffuses quite rapidly into the bulk flow, possibly in part because of the high gas flow rate and the

resulting increased interface instability, but the asymmetry between the two walls is clear. The cause of the high void fraction at the left wall for window 3 (0.1568 m) is a small gas pocket that happened to be stable at that location only. (Similar pockets were observed for other runs.) Similar measurements on an air-water flow facility are described in Section IV.

The void-fraction profiles with B = 1.2 T and all other conditions the same except for a somewhat reduced gas injection rate are shown in Figure III.30. In this case the gas mixes more rapidly and the tendency is to create symmetrical void-fraction profiles that are peaked in the center. From this it can be inferred that the gas injectors are not effective in preventing the formation of a liquid layer on the walls. To have a clear demonstration of this it is necessary to measure the void fraction right at the wall, but this is not possible with the present gamma-ray system.

Following the question on the effectiveness of the gas injectors, runs were made under various conditions with high and low gas-injector flow rates. The high and low runs were made one right after the other to be sure that other parameters did not change. Almost always the efficiencies at low injection rates were about 1 1/2 percentage points higher, as shown in Table III.2 for four representative cases (all taken on the same day). The efficiency calculations include the work done by the gas injected into each port. (For the quantity of gas normally injected, the calculated efficiency would increase by up to one point if the work done by the injected gas was ignored.)

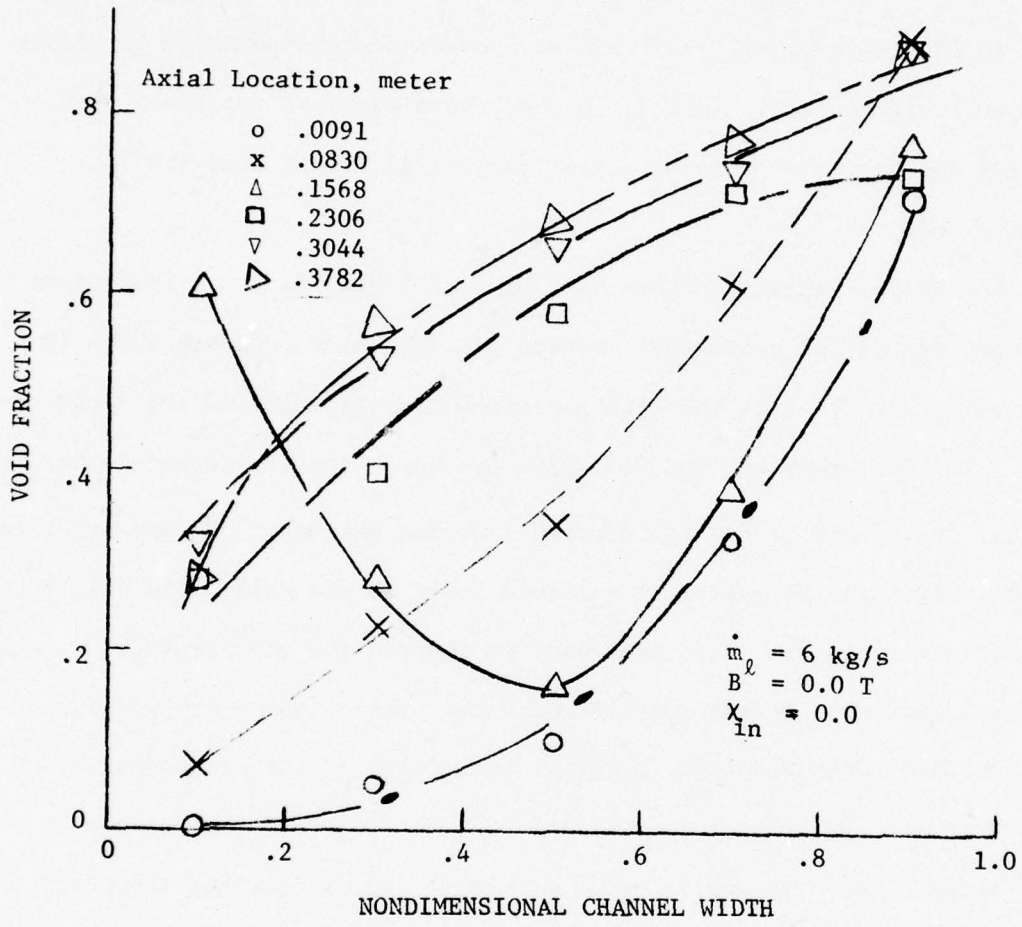

Figure III.29. Void Fraction Profiles With Gas Injection Along The Right Wall, B=0

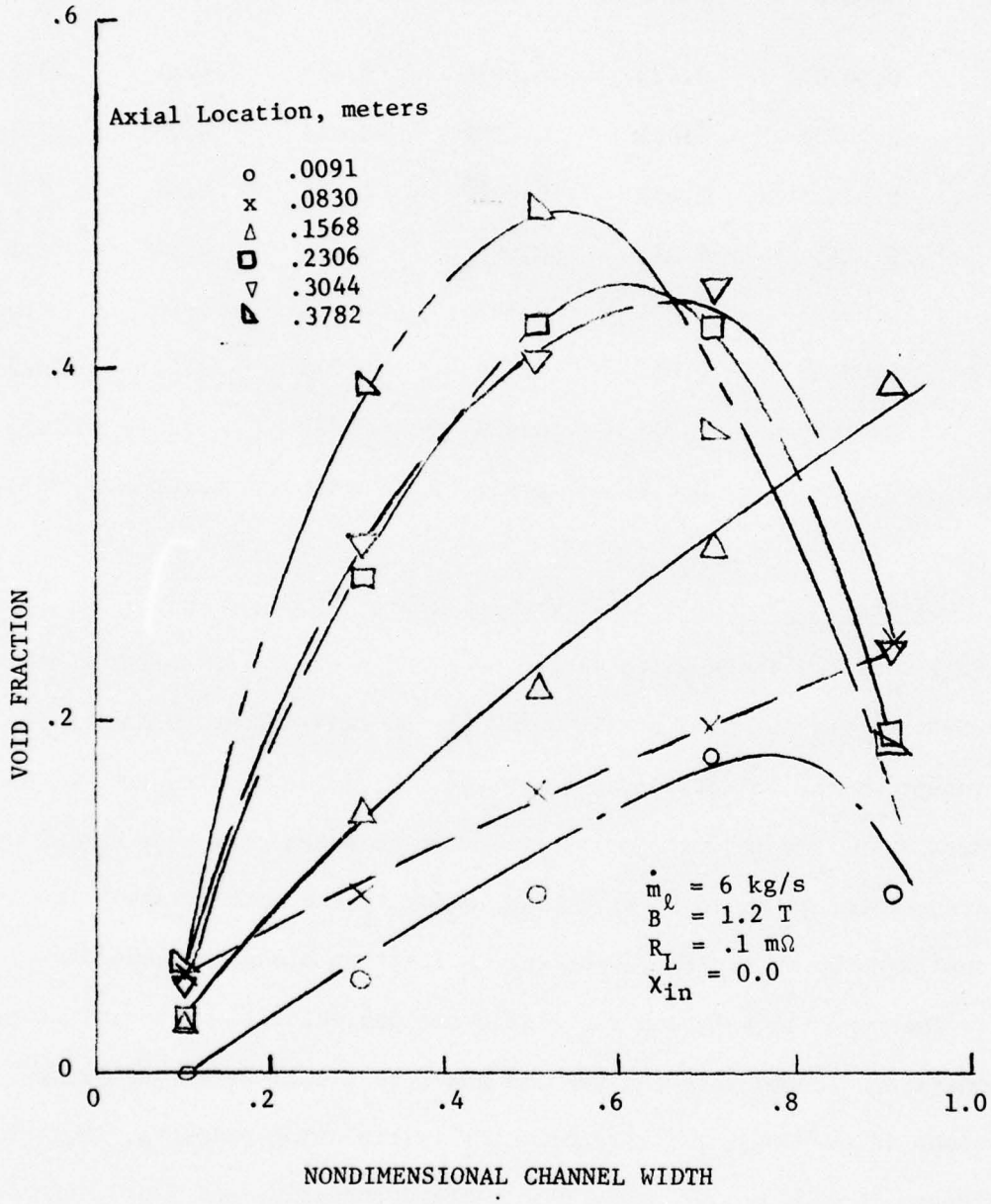

Figure III.30. Void Fraction Profiles With Gas Injection Along The Right Wall, B=1.2 T

Table III.2. Effect of Wall Gas Injection on Performance, B=1.16T

$\dot{m}_\ell$ [kg/s]	χ (inlet)	$\dot{m}_{gi}$ [g/s/inj]	R_L [mΩ]	V_L [V]	Δp [bars]	η [%]
4.84	0.00754	0.423	0.0974	0.414	4.51	25.7
4.84	0.00751	0.011	0.0982	0.416	4.48	27.3
4.55	0.0142	0.455	0.0968	0.401	4.66	17.2
4.55	0.0145	0.011	0.0980	0.413	4.54	18.5
6.05	0.00603	0.581	0.421	0.776	2.16	34.8
6.04	0.00602	0.011	0.419	0.775	2.17	36.7
6.06	0.0108	0.555	0.419	0.882	2.24	29.1
6.05	0.0109	0.010	0.417	0.878	2.21	30.3

III.3 Diverging Channel Without Gas Injectors

Following the tests which showed no gain in generator performance as the amount of gas injected at the walls was increased, but in fact a slight improvement as the injection was decreased, it was decided to remove the injectors. The gas injector ports protruded from the otherwise smooth insulating wall, as shown in Fig. II.3, reducing the local channel cross-sectional area by up to 18% (depending on location along the generator axis). The ports thus forced the liquid and gas velocities to vary along the generator, if the injected gas did not form a wall layer, creating variations in the local load factor, extra circulating currents, increased turbulence, changes in two-phase flow pattern and slip, and thus increased losses. (The injected gas layer should ideally provide a smooth surface.) Accordingly the ports were removed and all holes filled with epoxy to yield a variable-area channel with smooth walls.

One method used to obtain an idea of the possible effects of the area changes was to modify the computer code described previously[2] to include the area changes due to the ports but not the change in gas flow rate along the generator. Note that this code is mechanically one-dimensional and does not include variations in parameters across the generator height, so that it cannot be expected to yield accurate results for this true three-dimensional problem. Qualitative behavior may be ascertained, however.

The detailed code was run for one set of parameters with and without the injector ports. The liquid and gas velocities for both cases are shown in Fig. III.31, the slip ratios in Fig. III.32, the pressures in Fig. III.33, and the tabulated results in Table III.3. Without the ports the slip is less and the efficiency higher. With the ports

Table III.3. Calculated Generator Performances With and Without Gas Injector Ports, $\dot{m}_\ell$ = 6 kg/s, χ = 0.005, B = 1.2 T, R_L = 0.125 mΩ, C_d' = 100 m^{-1}

	With Gas Injectors (zero gas flow)	Without Gas Injectors
Efficiency, %	54.0	58.2
Power output, watts	4070	3620
Load voltage, volts	0.702	0.685
Load current, amps	5800	5280
Electrical efficiency	0.82	0.83
Average induced voltage, volts	0.774	0.748
Average load factor	0.906	0.916
Pressure difference, Pa x 10^{-5} (psi)	4.91 (71.2)	4.34 (62.9)

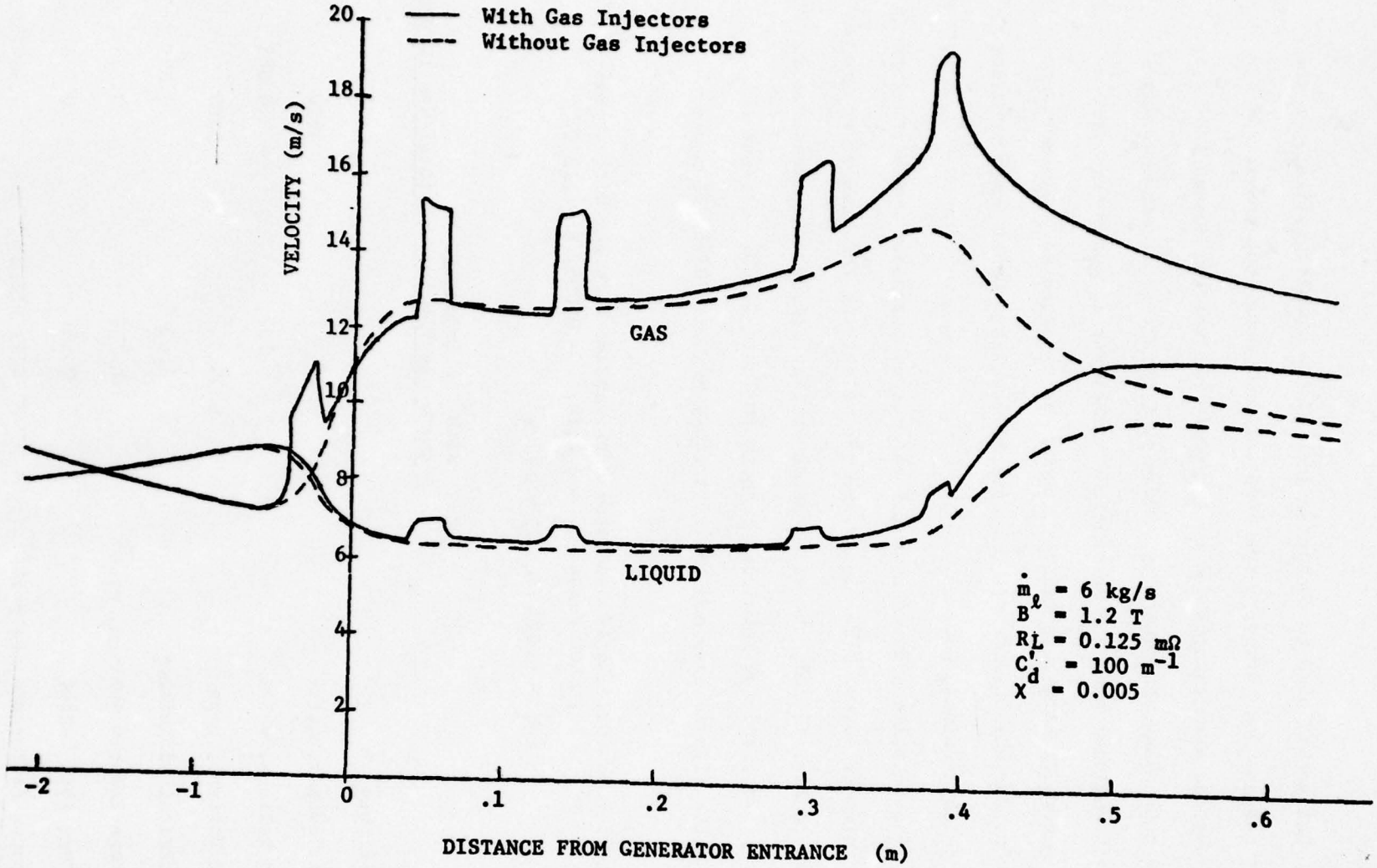

Figure III.31. Calculated Gas And Liquid Velocities Along Generator With And Without Gas Injectors

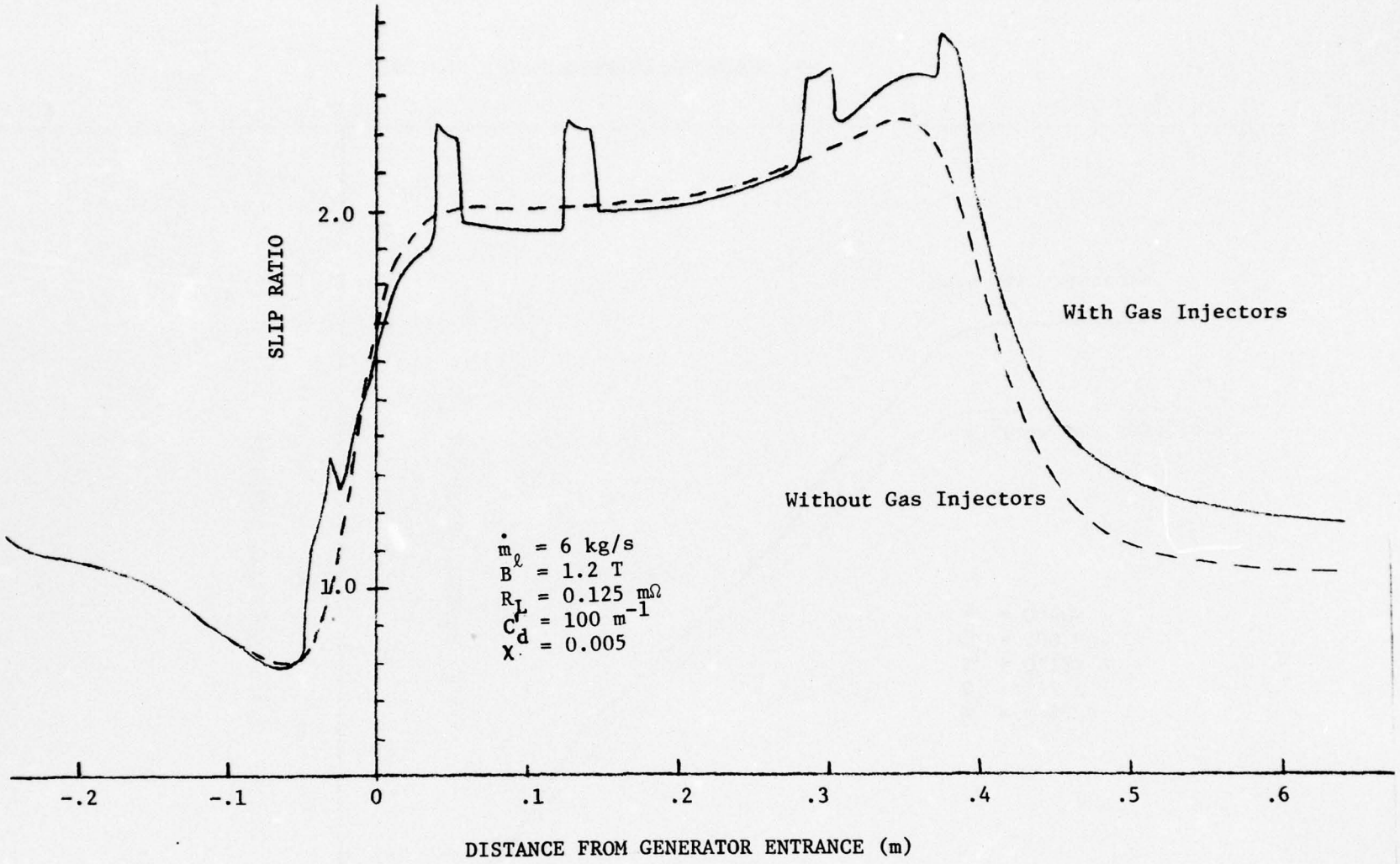

Figure III.32. Calculated Slip Ratio Along Generator With And Without Gas Injectors

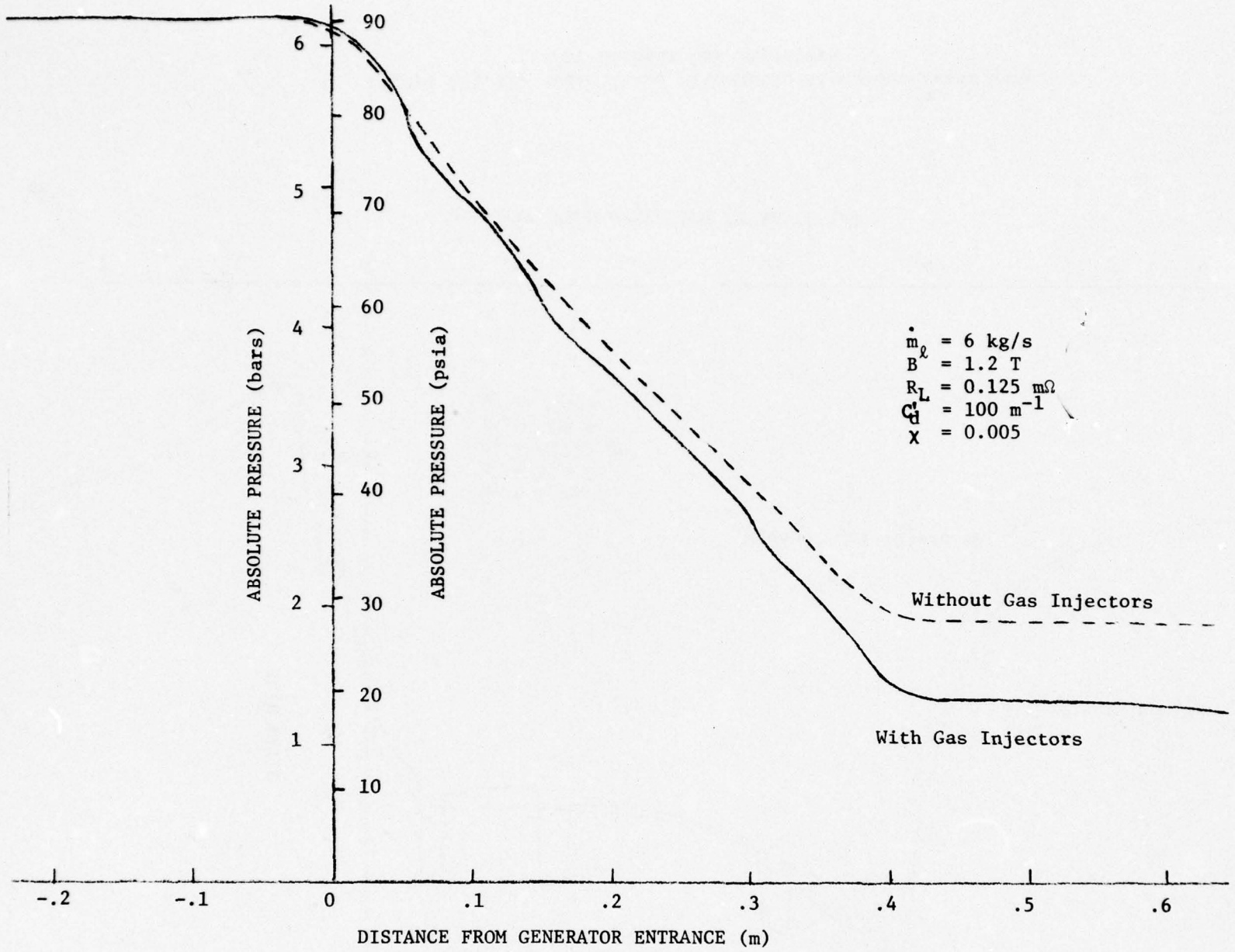

Figure III.33. Calculated Pressure Along Generator With and Without Gas Injectors

the terminal voltage and output power are higher due to the increased liquid velocity. With the ports the code is probably optimistic or actual performance will be worse than calculated because of variations over the channel cross section. If the gas injectors worked as desired the gas would tend to minimize the area changes as well as friction and shunt losses, and performance might be better with injection.

Tests of the variable-area channel without gas injectors were made for $\dot{m}_\ell$ = 6 kg/s; B = 1.2 T; χ = 0, 0.005, and 0.01; and R_L = ∞, 0.25 mΩ, and 0.14 mΩ. The generator isentropic efficiency is shown in Fig. III.34 as a function of average void fraction. Note the dramatic improvement over the data with injection. For R_L = 0.25 mΩ the efficiency increased by more than ten points at high average void fraction and about seven points at zero average void fraction. For R_L = 0.14 mΩ the increases were more than ten points.

The performance of this generator for R_L = 0.25 mΩ is compared with the previous ANL generators in Fig. III.5. Note the significant improvement in performance, and in particular the fact that performance did not decrease as much at higher average void fractions. Of course, this particular comparison is of limited value as discussed in Section III.1.1.

The load voltages and open-circuit voltages are compared with the calculated values (without the injection ports considered) and the data with injection in Figs. III.11 and III.12. Note the substantial increase compared to the data with gas injection in most cases in spite of the higher voltage predicted with the ports by the detailed computer code, Table III.3.

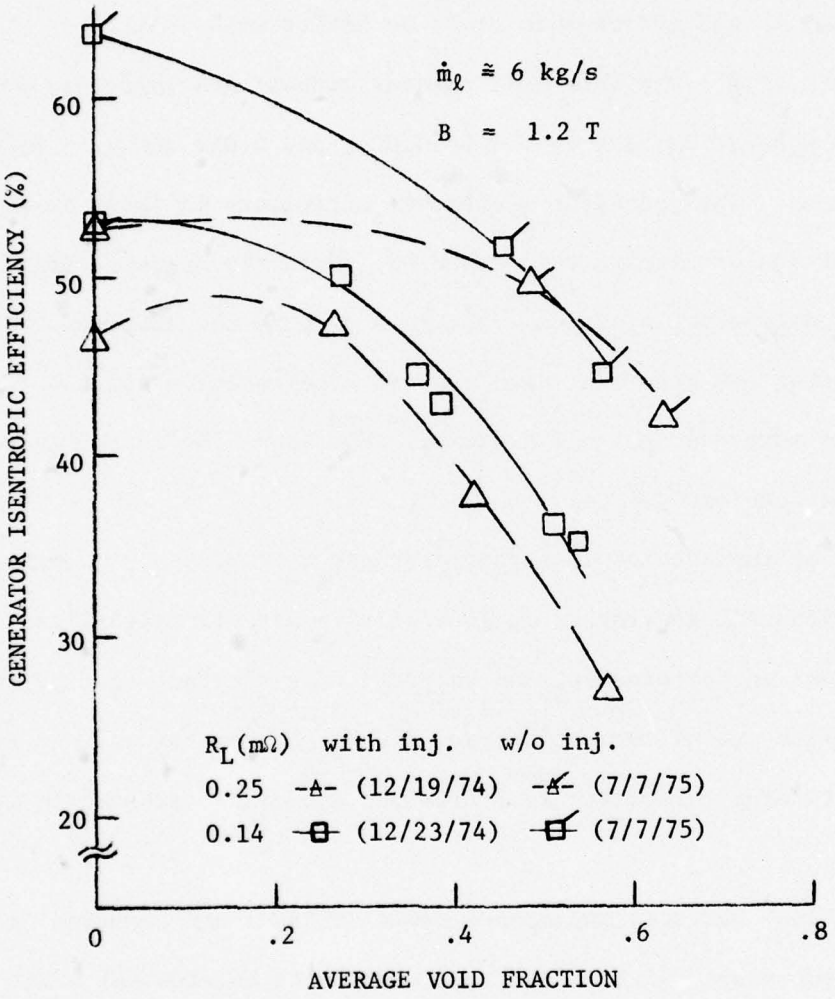

Figure III.34. Generator Isentropic Efficiency vs. Average Void Fraction With and Without Gas Injectors

The liquid and gas velocities, and the slip ratio along the generator for R_L = 0.14 mΩ are shown in Figs. III.35 and III.36, respectively. Note that in contrast to the data with injection, Figs. III.1 and III.15, the liquid velocity increases and the slip decreases near the exit from the generator. The slip ratios are significantly lower than with gas injection for the same parameters, and this is probably the main source for the increased efficiency. (See the significantly lower calculated slip loss for this case, Fig. III.6.) A cause for the lower slip ratios might be decreased turbulence (see Fujii-e et al. for a discussion of turbulence and slip[7]).

In the last third of the generator the slip ratio decreased, Fig. III.36, while with gas injection it increased, Fig. III.15. The previous increase may have been due to a transition to semi-annular flow and the resulting decoupling between the phases, Section III.1.2. Such a transition appears not to occur here, and the reduced pressure gradient near the end of the generator, Fig. III.37, results in a decreased slip ratio since the flow is still relatively homogeneous.

The pressure distribution along the generator, Fig. III.37, is similar to that with injection, Fig. III.20, except that the pressure gradient at high quality in the center of the generator [illegible] only twice instead of three times that in the first third. This more-uniform pressure gradient indicates better generator operation and should aid in achieving higher efficiency.

The local load factor F is shown in Fig. III.38. The average F at $\chi = 0$ is just under 1.0 and agrees very well with the predicted value, while with gas injection it was much lower, see Fig. III.17. At high

qualities F is much lower and the values are similar to those with injection except for the sharp drop near the generator exit. In this respect the data with injection is better.

The void fraction along the generator shows a steady rise, Fig. III.39, as expected. This did not occur with injection, Fig. III.22, where α remained almost constant. The difference is due to the lower slip ratios as this allows the generator to operate as designed. The exit void fraction reached 0.69, while previously it never exceeded 0.6.

No voltage probe or fluctuation measurements were made without injectors. The probes were removed to minimize leakage problems. The fluctuations may be reduced for this case because of the lower turbulence level and the lack of a transition to semi-annular flow.

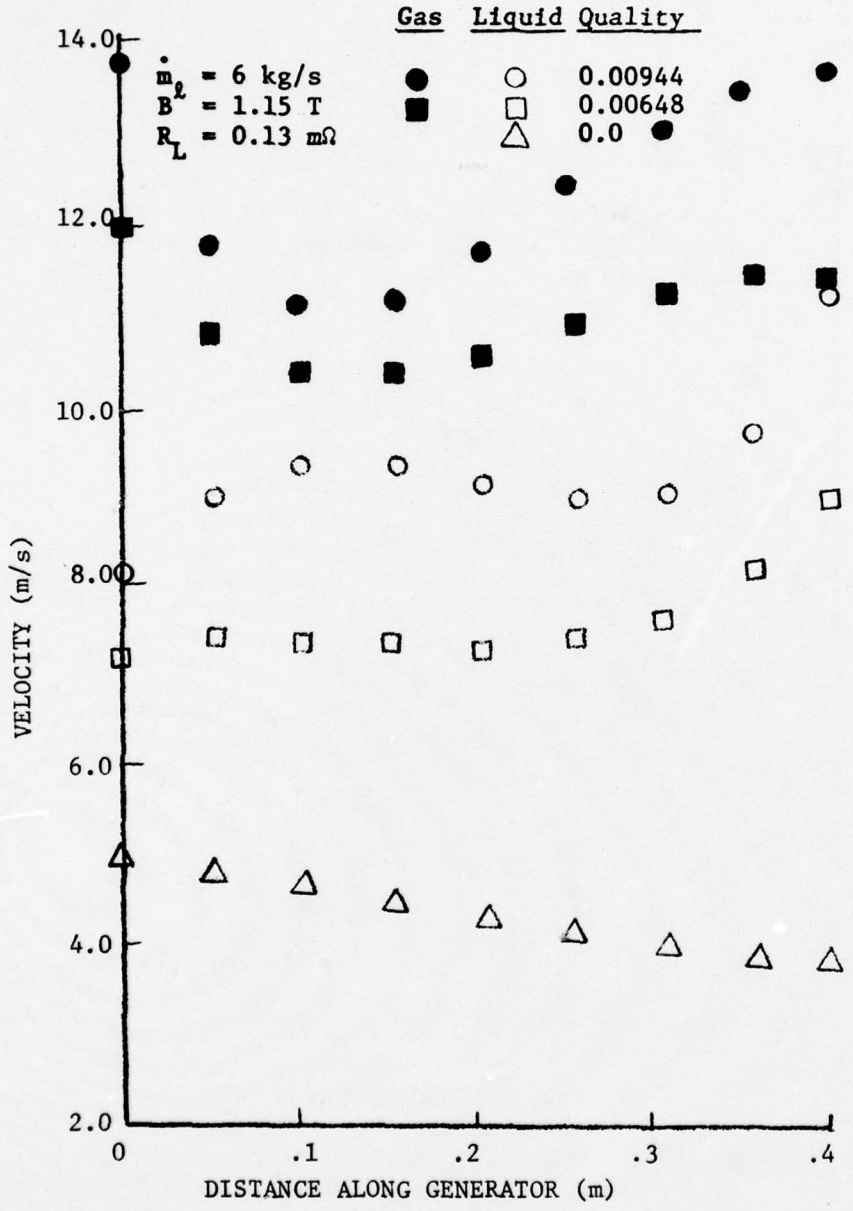

Figure III.35. Gas and Liquid Velocities Along Generator, Without Gas Injectors, R_L = 0.13 mΩ

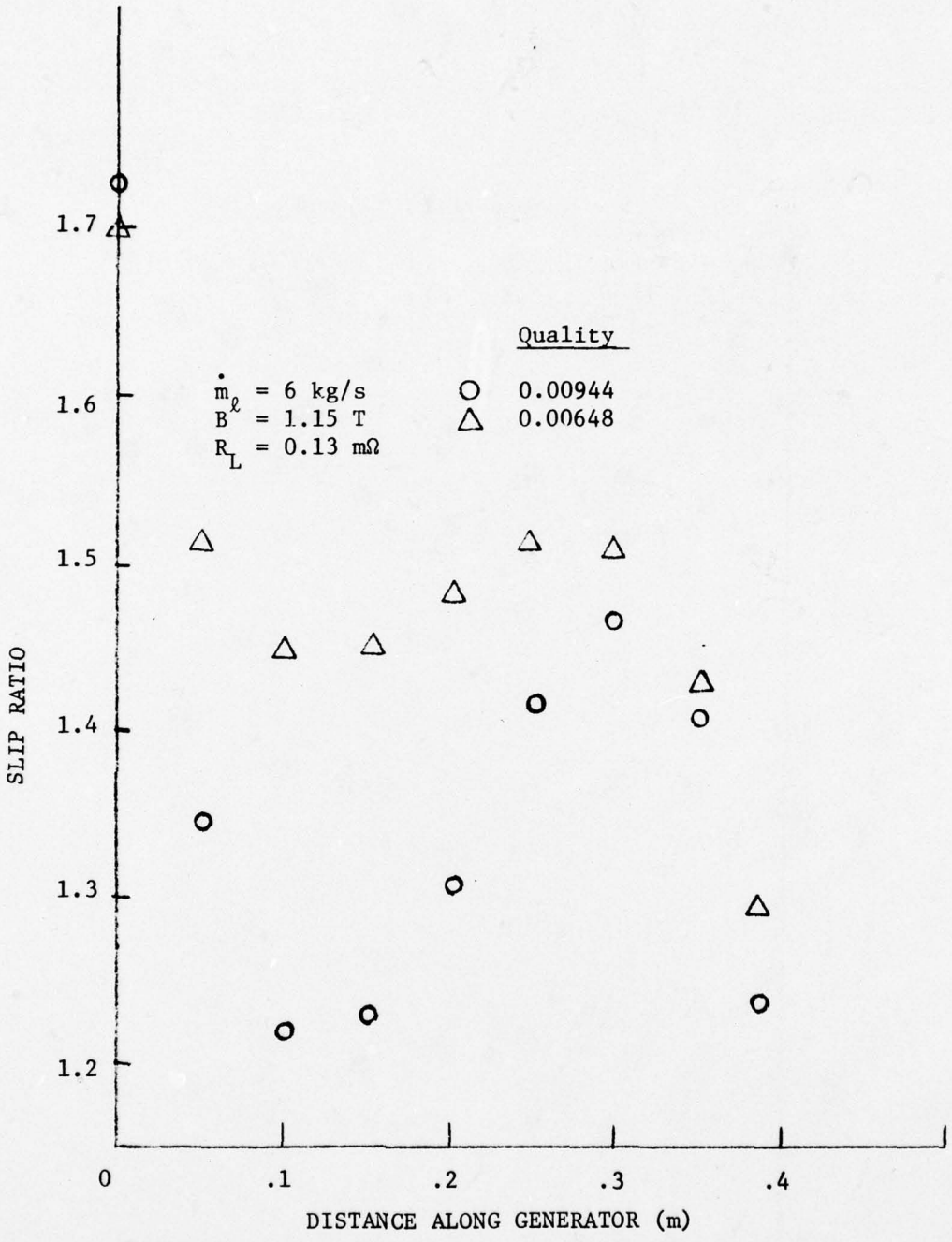

Figure III.36. Slip Ratio Along Generator Without Gas Injectors, R_L = 0.13 mΩ

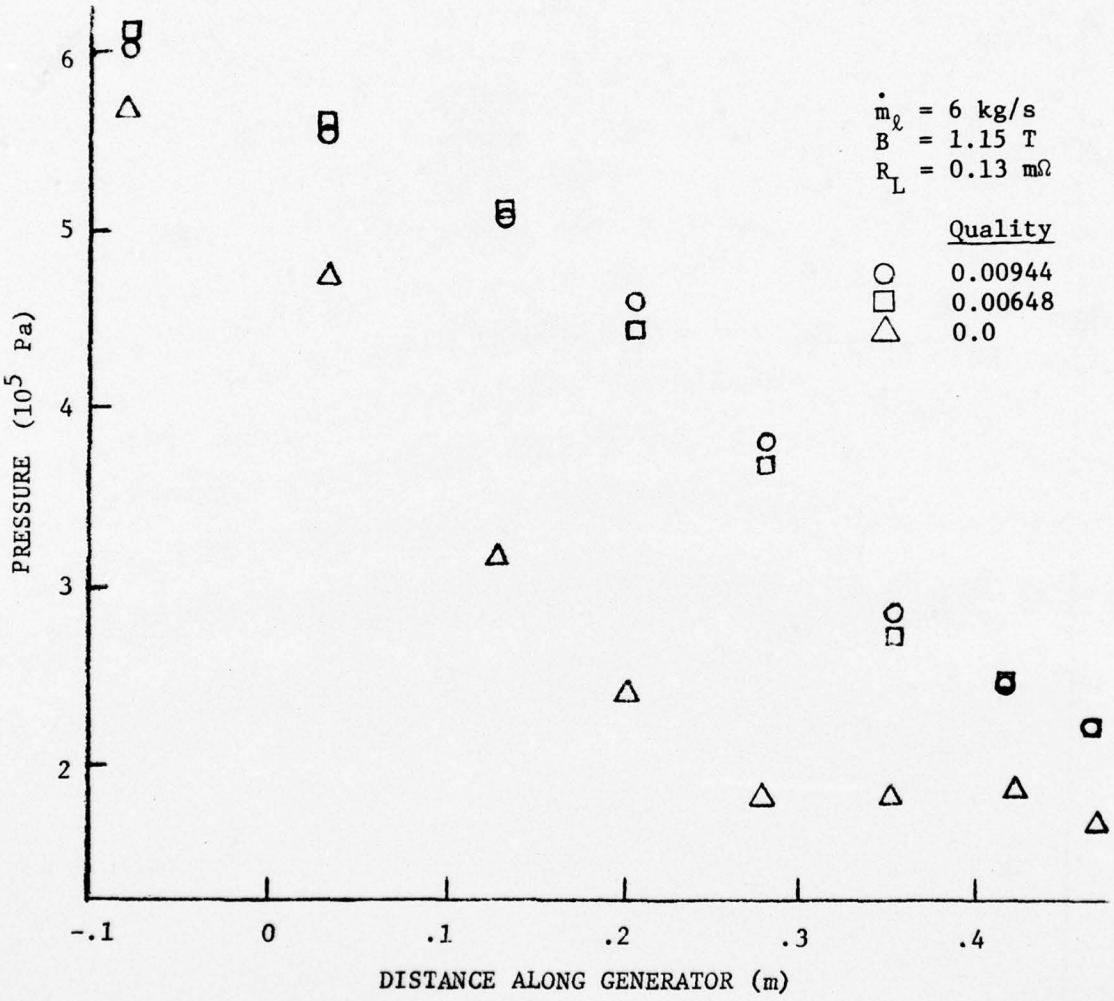

Figure III.37. Pressure Along Generator Without Gas Injectors, R_L = 0.13 mΩ

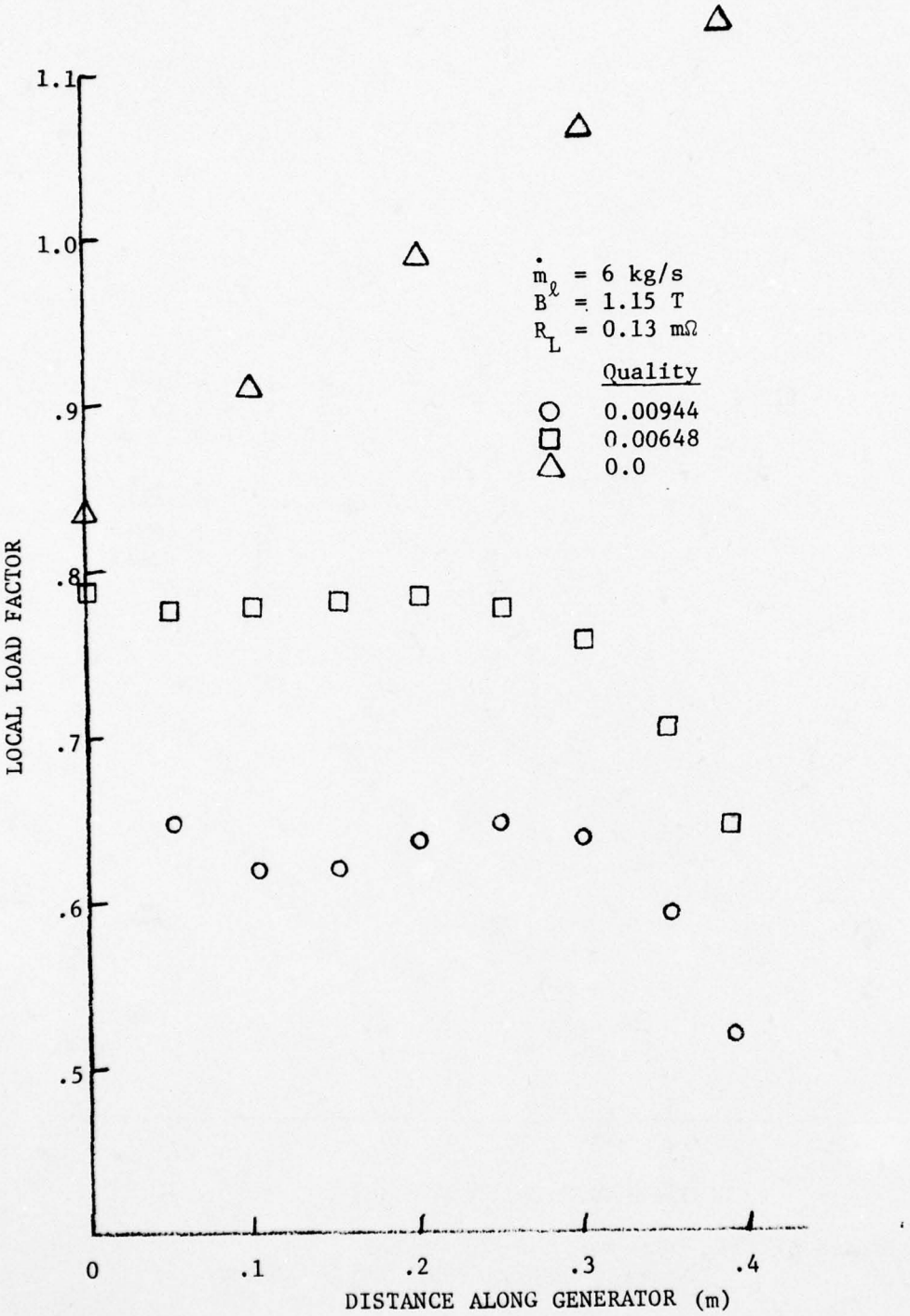

Figure III.38. Local Load Factor Along Generator Without Gas Injectors, R_L = 0.13 mΩ

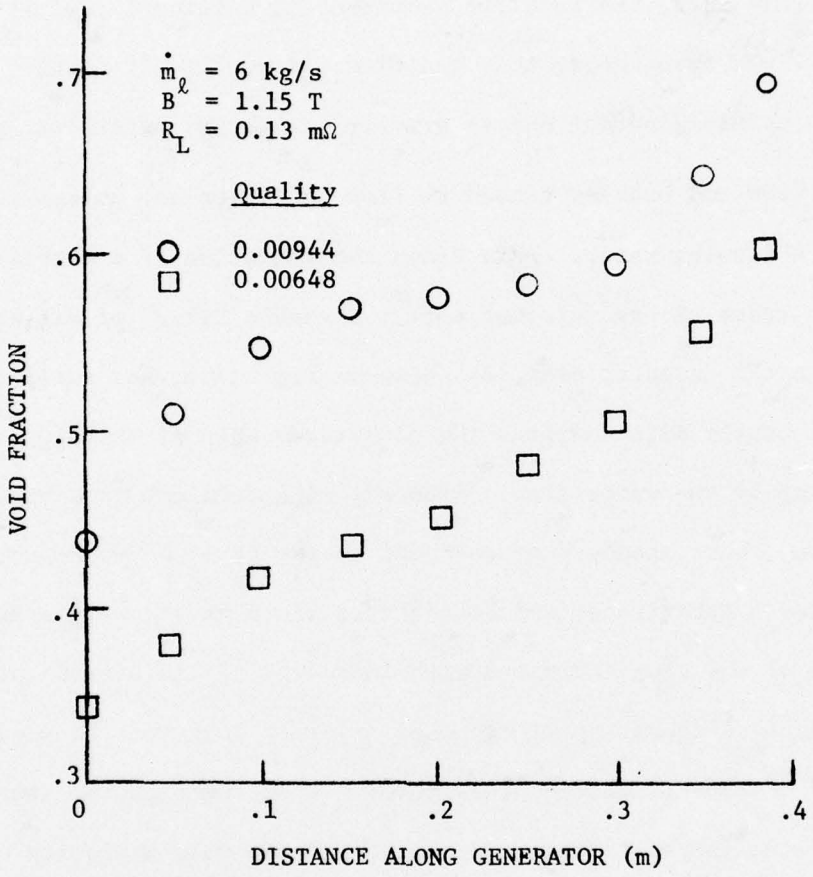

Figure III.39. Void Fraction Distribution Along Generator Without Gas Injectors, R_L = 0.13 mΩ

IV. AIR-WATER EXPERIMENTS

Gas was injected through an injector port along the wall of the water flow using the facility described in Section II.2. If the channel was oriented so that the flow was vertically down, then the pressure gradient due to gravity (weight of water) was positive along the flow and bubbles tended to flow up (upstream) unless carried down by the flowing water. This aided the formation of a stable gas layer downstream of the injector port. A stable "slug" of air was attached to the injector port, as shown in Fig. IV.1, and small bubbles were continuously detached from the downstream edge of the slug and carried away by the water flow. (The air slug does not show up clearly in the photo, but extends from the port to the first screw downstream. The slug has a clearly-defined boundary as shown by the wavy edge.) The length of the slug increased with increased air injection until the slug would suddenly spill over the injector port and the whole slug would move vertically up (upstream). The length of the stable slug increased with increased water velocity, but the water velocity was limited to a maximum of about 1 m/s by the capacity of the water supply.

If the channel was oriented so that the flow was vertically up, then the pressure gradient due to gravity was negative along the flow and the injected gas behavior was markedly different. The flow was very turbulent beginning at the injector port with relatively large gas bubbles breaking off. Water droplets even occasionally sprayed inside the injection slit, so that the entire wall was wetted. The main stream

of two-phase flow broke away from the wall about 0.05 m downstream of the slit, compared with about 0.1 m for the air slug in the previous case. There were many recirculating regions in the channel and many relatively-small bubbles due to the high turbulence level. The void fraction was about 0.3 based on displaced water level at zero water velocity. The flow pattern for this case, Fig. IV.2, is clearer. Note that the boundary between the two-phase region and the water is highly turbulent. The view from behind the injector port for this case, Fig. IV.3, clearly shows the breakup of the gas layer. The breakup could be due to an interfacial flow instability that generates turbulence and/or a surface-tension-related instability. The latter is suggested by the regularity of the bubble pattern.

These qualitative tests indicate that a stable gas layer may not be obtained with a negative pressure gradient along the flow. Since the pressure gradient is negative in the MHD generator, gas injection may not be effective, although further study is needed. This point is discussed in Sections II.2 and V.1.

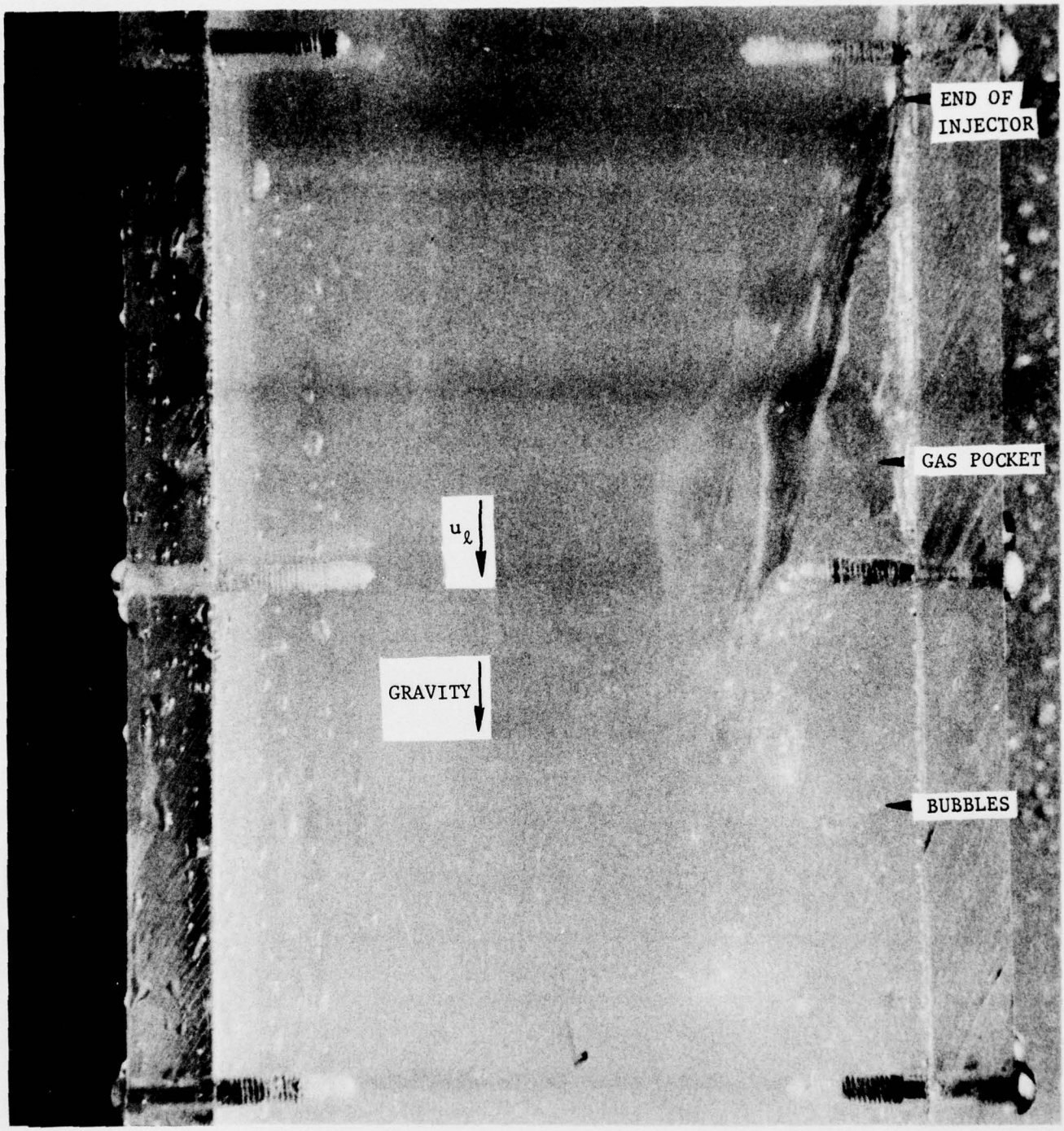

Figure IV.1. Air-Water Flow Vertically Down

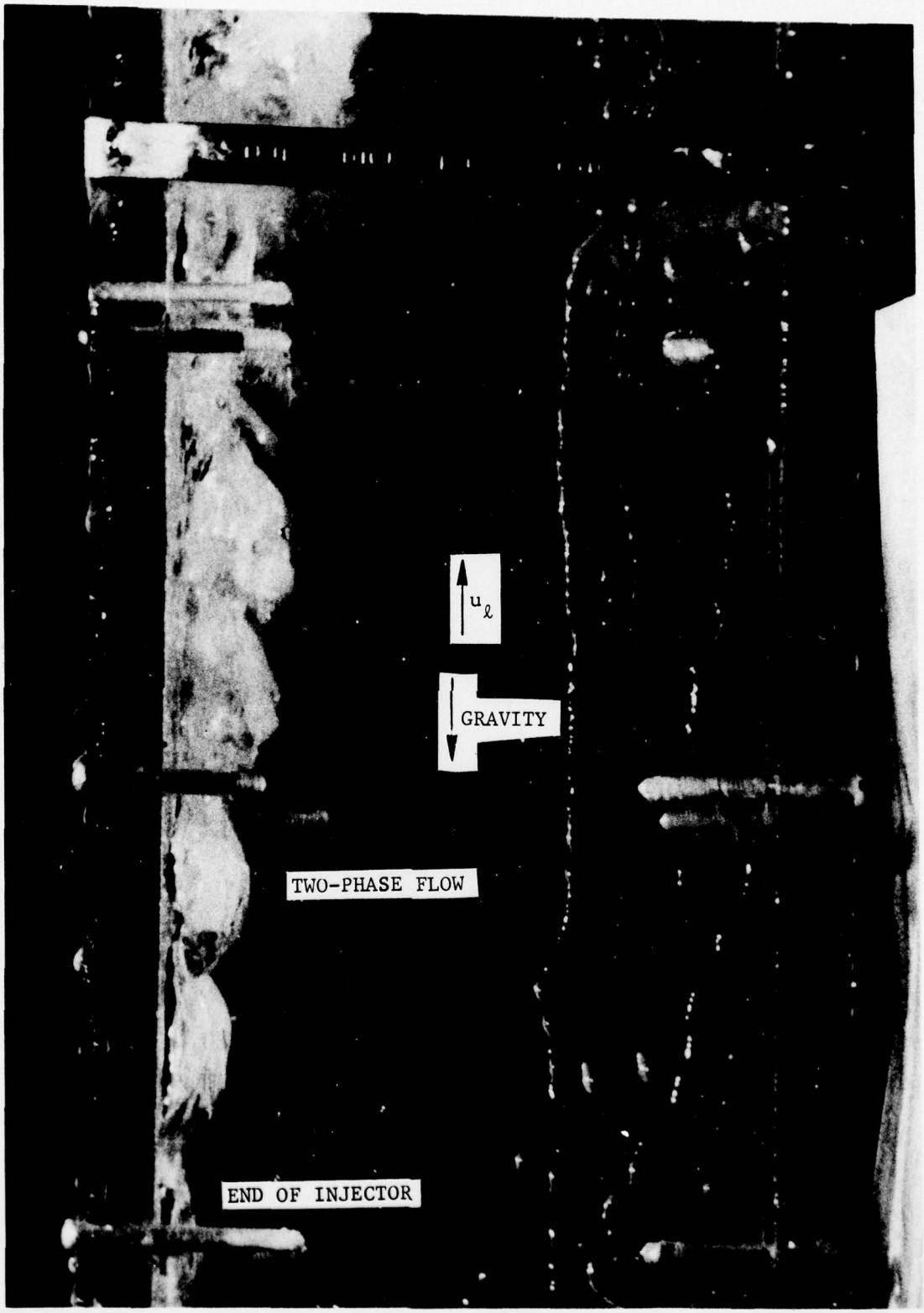

Figure IV.2. Air-Water Flow Vertically Up

Figure IV.3. Air-Water Flow Vertically Up,
View From Behind Injector Port

V. CONCLUSIONS AND FUTURE WORK

The experiments with the second diverging-channel generator without gas injection ports, the most recent tests, have yielded the best performance to date. This is an encouraging result, and indicates that the program is headed in the right direction. The desired next steps in the liquid-metal MHD generator program are described below.

V.1 Gas Injection

Gas injection was added to the constant-area channel to improve a lower-than-expected performance that was believe due to losses in a shunt boundary layer. The effect is expected to be largest for these small wall-dominated experimental generators. The performance for that case was apparently improved,[3] but gas injection with this diverging channel yielded a lower performance than without gas injection. The ports projected out into the flow, blocking up to 18% of the channel flow area, and possibly caused increased turbulence and higher slip if the injected gas did not form a wall layer. Based on the air-water experiments performed after the generator tests, the injected gas layer is expected to be unstable if the pressure decreases along the flow, as occurs in a generator. This agrees with the previously-observed generator data with and without the magnetic field. (Note that the flow was vertically down in the first nitrogen-water injector tests reported in Reference 3. This corresponds to a stable gas layer, as described in Section IV.)

The cause of this difference in gas injection effect for the two channels is not known, but suspicion is directed at the difficulties with, and changes in, the liquid flow-rate measurement. An EM (electromagnetic) flowmeter was used for all tests with the first diverging-channel generator, all tests with the constant-area channel without gas injection, and initial tests with the constant-area channel with gas injection up to January 18, 1974. However, the accuracy of the EM flowmeter at the higher flow rates was questioned, and discrepancies with a venturi flowmeter installed to check the EM flowmeter were observed. Later runs of the constant-area channel with gas injection used the venturi flowmeter. The observed discrepancies and the use of different flowmeters throws suspicion onto the comparison between the constant-area-channel data obtained with and without gas injection. With the diverging-channel tests, a turbine flowmeter with improved accuracy and repeatability was used, and every effort was made to keep the measurements consistent. Other factors in the difference between the two generators may be the change from three to five pairs of injector ports, and the change from a straight to a diverging channel.

The effectiveness of gas injection needs further study before injectors are routinely included on future generators. For example, the use of nonwettable walls or a repulsive force to "hold" the liquid away from the walls might improve the performance of the gas injectors. Alternative methods, such as gas injection through a porous wall, may be evaluated. Another possibility is the use of surface-active agents, as discussed in Section V.4. Note that injection may perform better

with larger generators where the injector ports block only a very small fraction of the channel cross-sectional area. However, for larger generators the relative shunt boundary layer thickness may be small.

V.2 Higher Velocities and Pressures

The motivations for tests at higher liquid velocities are to reduce the slip loss due to the relative phase velocities, as recent experimental research has demonstrated that this loss can be decreased by increasing the liquid velocity,[3] and to test the generator at velocities typical of practical generators. In the experiments to date, the liquid velocity has been limited to about 12 m/s. The modified facility, as described below, will allow generator operation at higher liquid velocities or flow rates and higher pressures. After completion of the modifications, the existing diverging channel without gas injector ports will be tested at liquid flow rates up to about 10.9 kg/s (200 gpm), versus the current limit of about 6 kg/s (110 gpm). This generator was designed for lower velocities and has an operating pressure range up to about 7.2×10^5 Pa absolute (90 psig), so that operation at higher velocities will require a reduced magnetic field strength.

A new generator will be built to utilize the full loop capability of 10.9 kg/s and 1.48×10^6 Pa absolute (200 psig). This will allow high velocities with high field strengths, and variation of the generator pressure range with a maximum generator exit pressure of 1.14×10^6 Pa absolute (150 psig). This generator will probably have a different taper to fit the different design pressure ratio. Also, the maximum void fraction in the generator should be increased - this will be aided by a reduced velocity slip ratio.

V.2.1 Revised Facility

The maximum liquid flow rate will be increased from 6 kg/s to 10.9 kg/s (110 gpm to 200 gpm). As increasing the flow rate increases the pressure difference across the generator, the available generator inlet pressure will be increased from about 7.2×10^5 Pa to 1.48×10^6 Pa absolute (90 to 200 psig).

The present loop is constructed primarily of two-inch pipe and has several two-inch globe valves that cause severe flow restrictions. In addition the pressure tanks do not have a high-enough pressure rating for some of the proposed tests. Thus, the loop must be completely dismantled and rebuilt, as shown in Fig. V.1 for the NaK flow circuit. The major changes in the NaK circuit are:

1. Add two new canned-rotor NaK pumps in series with the existing pump. The three pumps will produce a gross pressure difference of 1.57×10^6 Pa (228 psi) at 10.9 kg/s (200 gpm). For experiments where the total pump capacity is not required, one or two pumps may be bypassed.

2. Replace the existing separation and supply tanks with a single, larger tank with a rated pressure of 1.31×10^6 Pa absolute (175 psig). It has internal baffles enabling it to separate twice the NaK and nitrogen flow rate of the old tanks.

3. Replace the calibration tank with a larger one of 210 kg NaK capacity and a rated pressure of 2.14×10^6 Pa absolute (295 psig).

4. Replace the 150 psi NaK filter housing with a 300 psi housing.

5. Replace the air-cooled heat exchanger with two water-cooled heat exchangers connected in parallel. This eliminates the pressure loss of the previous heat exchanger and provides sufficient cooling capacity for year-round operation.

AD-A035 245 ARGONNE NATIONAL LAB ILL ENGINEERING DIV F/G 10/2
EXPERIMENTAL TWO-PHASE LIQUID-METAL MAGNETOHYDRODYNAMIC GENERAT--ETC(U)
NOV 76 M PETRICK, G FABRIS, R COLE, R HANTMAN NAONR-16-76
UNCLASSIFIED ANL/ENG-76-04 NL

2 OF 2
ADA035245

END
DATE FILMED
3-77

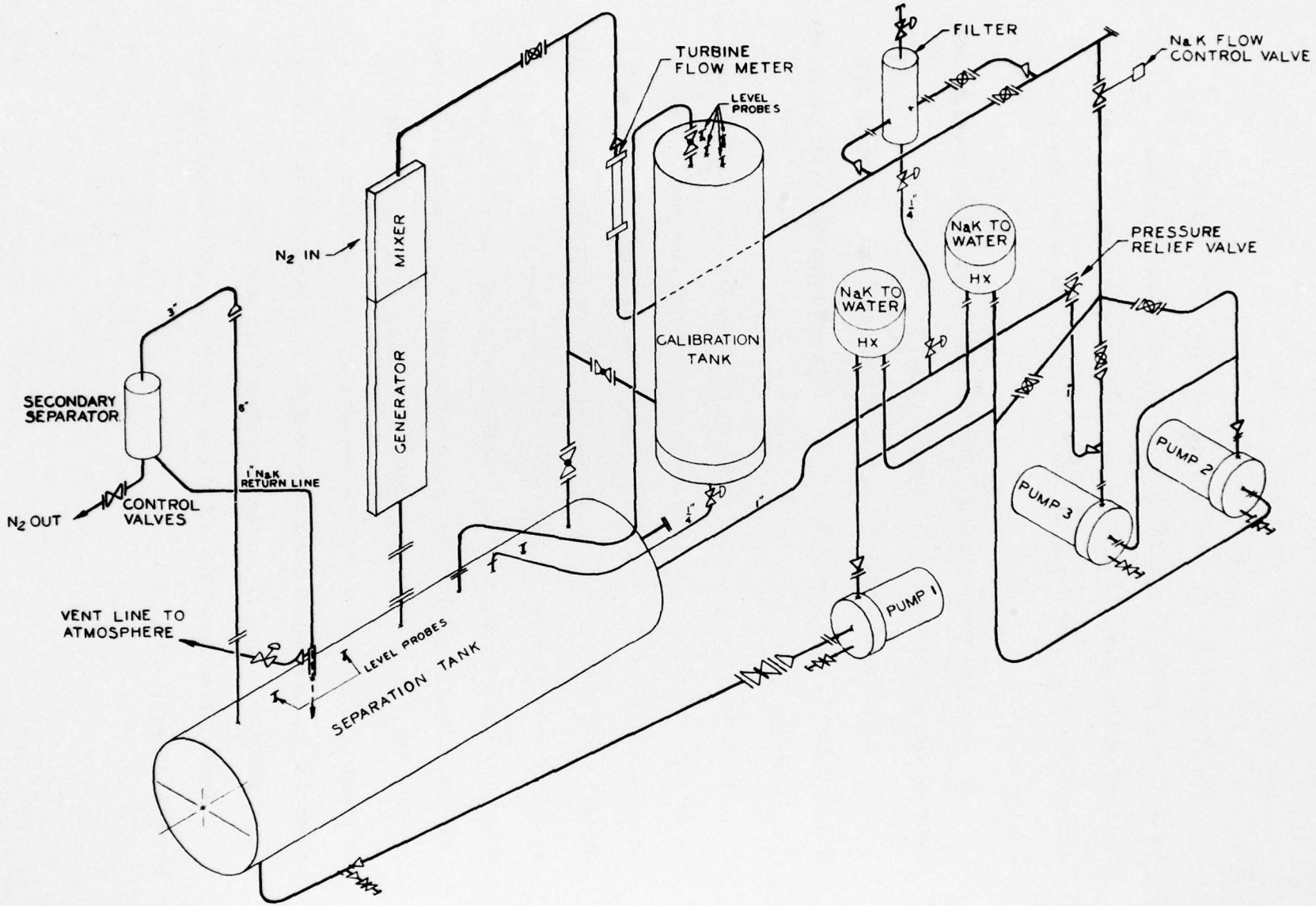

Figure V.1. NaK-Nitrogen Flow Loop

6. Most of the two-inch piping is eliminated, and NaK flow control is provided by a three-inch air-operated valve rather than a two-inch manual globe valve. All non-control valves are ball valves, except for a four-inch Y-pattern globe valve in the inlet line to the first pump.

7. Most new components are carbon steel as stainless steel is not required for a room-temperature NaK facility.

8. All kerosene cooling will be eliminated, and the magnet and load resistor will be cooled by water. This prevents the possibility of a combined NaK and kerosene fire.

The nitrogen side of the facility requires future minor modifications. The nitrogen heater is not adequate for the higher flow rates, so that extra heated pipe will probably be added. The nitrogen purifier (NaK bubbler) tank requires only a hydrostatic test to increase its pressure rating. Some pipe sections and valves will be replaced with pipe of a higher pressure rating, mostly two-inch pipe and valves will be used, and a number of bends and fittings will be decreased. An electrically-operated valve to shut off the nitrogen supply in case of an emergency and a new pressure relief valve will be installed. The flowmeters and check valves for the gas injection system will be replaced by units with a higher pressure rating if further injector tests are made.

The modified loop will allow two modes of operation that were not possible before. These are:

1. Operation at up to 10.9 kg/s (200 gpm) NaK flow with a corresponding increase in the nitrogen flow to determine the effect of liquid velocity on slip and generator efficiency, as mentioned.

2. Variable back pressure at the generator exit, up to 1.14 x 10^6 Pa absolute (150 psig) at reduced flow rates, to determine the effect of back pressure on generator performance. In this mode only one or two pumps may be used to avoid excessive pressure.

Several safety features are incorporated into the modifications. The piping is designed for 2.00 x 10^6 Pa absolute (275 psig) and the separation/storage tank for 1.31 x 10^6 Pa absolute (175 psig). Pressure switches will stop or prevent from starting one, two, or all three pumps if pre-set pressures in the separation tank or high-pressure piping are exceeded. The separation and nitrogen purification tanks will be protected by safety valves, as before, but with higher pressure ratings. Emergency switches to turn off the NaK pumps and the nitrogen supply will be placed on the main control panel and adjacent to two doors. A future remote valve for the cooling-water supply has been provided for in the control panel.

V.3 Improved Diagnostics

Improved diagnostics are needed to obtain a better understanding of two-phase flows in a magnetic field. The data to be measured include direct local values of liquid and gas velocities, void fractions, bubble diameters, pressures, and temperatures. These data will be used to develop and evaluate improved analytical models for two-phase flows.

Thus, a program to develop such measurements should be initiated. First tests should use the air-water facility before incorporation into the NaK-nitrogen loop.

V.4 Surface-Active Agents

The slip loss due to the relative phase velocities is presently one of the major loss mechanisms in two-phase liquid-metal MHD generators, especially at the high void fractions required for efficient cycle operation. One method of reducing this loss is to produce a more-stable foam flow by means of surface-active agents. The potential gains in generator and cycle performances make this approach very attractive. Thus, a program to evaluate surface-active agents will be developed. The major points are:

1. Locate suitable agents for the liquid metals of practical interest.
2. Determine the techniques required for adequate separation of the phases after the generator.
3. Perform tests in an MHD generator.

V.5 Imperfect Compensation

Most analyses of the two-phase MHD generator have assumed perfect compensation, i.e. the generator current is returned through the air gap in the magnetic circuit in such a fashion that the applied magnetic field

is not changed by the generator current. This may not be true in practice because of end currents, non-uniform current distributions in the generator and/or compensating conductors, and compensating conductors that are longer than the electrodes as in the present generator. The simple analysis used in Section III.1.2 showed the existence of a potential effect that could explain some of the experimental results, such as the non-constant pressure gradient along the generator. Thus the development of an analytical model for the generator with imperfect compensation has been initiated. Future plans include experimental verification of the model.

V.6 Analytical Models for the Two-Phase Flow in the Generator

Further analytical studies on the two-phase flow in the MHD generator will be carried out in parallel with the above efforts. The experimental data, especially that from the improved diagnostics as they become available, will be used in developing and evaluating these models. The primary goals are a better understanding of and model for the two-phase flow at high void fractions in a practical generator. The conditions for transitions between bubbly, churn-turbulent, slug, and annular flows at high void fractions may be explored. Of particular importance are the effects on generator performance of velocity, void fraction, and conductivity distributions across the channel, i.e. parallel to either the applied magnetic field or the current. These have not been included in any model to date except for a simple boundary-layer analysis.[3]

V.7 Annular Generator Geometry

The annular geometry for an MHD generator appears attractive because the fluid flows in the axial direction between two concentric cylinders which serve as the electrodes. Thus there is no need for insulating walls to separate the electrodes, and the accompanying viscous boundary layers and electrical shorting effects are eliminated. In addition, the cylindrical channel is very attractive for containg the required pressures. The circumferentially-directed magnetic field is entirely contained within the working volume of the generator, and is easily produced by a superconducting or ordinary torroidal winding without magnetic iron. Because of these advantages the annular geometry warrants consideration for both liquid-metal and plasma generators. However, there are also several disadvantages. The most important are the radial dependence of the electromagnetic force density and its effect on the velocity profile, the inability to compensate this geometry for the magnetic field generated by the induced current, the inherent low-voltage high-current channel dimensions, and the practical problem of closing the magnet winding thru the end regions of the annular generator duct.

An analytical study of the annular generator geometry has been initiated using separate models to observe the voltage limits, the velocity profile effects, and the compensation problem. These results will be included in the next annual report.

REFERENCES

1. L. C. Pittenger, et al., "Experimental Two-Phase Liquid-Metal MHD Generator Program", Report No. ANL/ETD-72-07, Argonne National Laboratory, Argonne, IL, June 1972.

2. W. E. Amend, et al., "Experimental Two-Phase Liquid-Metal Magnetohydrodynamic Generator Program", ANL/ENG 73-02, Argonne National Laboratory, Argonne, IL, June 1973.

3. M. Petrick, et al., "Experimental Two-Phase Liquid-Metal Magnetohydrodynamic Generator Program", ANL/ENG-75-02, Argonne National Laboratory, Argonne, IL, January 1975.

4. M. Petrick, W. E. Amend, E. S. Pierson, and C. Hsu, "Investigation of Liquid-Metal MHD Power Systems", Report No. ANL/ETD-70-12, Argonne National Laboratory, Argonne, IL, December 1970.

5. H. Branover, "On Some Important Effects in Laboratory MHD Flows in Rectangular Ducts in Transverse Magnetic Fields", 15th Symposium on the Engineering Aspects of Magnetohydrodynamics, April 8-10, 1975, Tullahoma, Tennessee.

6. J. A. Shercliff, A Textbook of Magnetohydrodynamics, Section 4.14, Pergamon Press, Oxford, 1965.

7. Y. Fujii-e, et al., "Experimental Study of Two Phase Induction Power Generation Using NaK-N_2 Mixture", Proceedings of the Sixth International Conference on Magnetohydrodynamic Electrical Power Generation, Washington, D.C., June 1975, p. 247-263.

SECURITY CLASSIFICATION OF THIS PAGE (When Data Entered)

REPORT DOCUMENTATION PAGE

READ INSTRUCTIONS BEFORE COMPLETING FORM

1. REPORT NUMBER: ANL/ENG-76-04	2. GOVT ACCESSION NO.
3. RECIPIENT'S CATALOG NUMBER	
4. TITLE (and Subtitle): EXPERIMENTAL TWO-PHASE LIQUID-METAL MAGNETOHYDRODYNAMIC GENERATOR PROGRAM.	5. TYPE OF REPORT & PERIOD COVERED: Annual Report, Aug. 1974 to Jul. 1975.
	6. PERFORMING ORG. REPORT NUMBER: ANL/ENG-76-04
7. AUTHOR(s): M. Petrick, G. Fabris, R. Cole, R. Hantman, E. Pierson & T. Coultas	8. CONTRACT OR GRANT NUMBER(s): NAonr-16-76
9. PERFORMING ORGANIZATION NAME AND ADDRESS: Argonne National Laboratory, 9700 South Cass Avenue, Argonne, Illinois 60439	10. PROGRAM ELEMENT, PROJECT, TASK AREA & WORK UNIT NUMBERS: NR099-404
11. CONTROLLING OFFICE NAME AND ADDRESS: Office of Naval Research (Code 473), Department of the Navy, Arlington, Virginia 22217	12. REPORT DATE: Nov. 1976 13. NUMBER OF PAGES: 102
14. MONITORING AGENCY NAME & ADDRESS (if different from Controlling Office): Same as 11	15. SECURITY CLASS. (of this report): Unclassified 15a. DECLASSIFICATION/DOWNGRADING SCHEDULE

16. DISTRIBUTION STATEMENT (of this Report)

Approved for public release; distribution unlimited

17. DISTRIBUTION STATEMENT (of the abstract entered in Block 20, if different from Report)

18. SUPPLEMENTARY NOTES

19. KEY WORDS (Continue on reverse side if necessary and identify by block number)

bubble parameter	generator efficiency	pressure gradient	two-phase
boundary layer	liquid metals	quality	viscous drag
conductivity	load voltage	slip	void fraction
gas injection	magnetohydrodynamics	shunt resistance	

20. ABSTRACT (Continue on reverse side if necessary and identify by block number)

A new diverging-channel liquid-metal MHD generator with gas injection along the insulating walls was built and placed in operation in late 1974. This generator yielded nearly-constant liquid velocity along the channel for near-design conditions, as desired for best performance. Extensive measurements of the generator terminal and internal parameters were made over a range of gas and liquid flow rates, magnetic field strengths, and load resistance values. Data is given for generator efficiency and load voltages, and the variations

DD FORM 1 JAN 73 1473 EDITION OF 1 NOV 65 IS OBSOLETE
S/N 0102-014-6601

SECURITY CLASSIFICATION OF THIS PAGE (When Data Entered)

410027

20.

along the channel of liquid and gas velocities, pressure, local load factor, void fraction, and slip ratio. Comparisons are made with theoretical predictions.

Tests made to evaluate the effectiveness of the gas injection indicated that the generator performance improved slightly as the amount of gas injected was decreased, and that the injected gas was not forming the desired pure-gas wall layer. Following this, air-water tests indicated that this was to be expected, and a one-dimensional computer model indicated that performance should be better without the partial flow obstruction of the gas injection ports. The gas injection ports were removed, and substantial improvement was obtained in generator performance - by far the best to date. Data comparable to that for gas injection is presented for this case.

The future directions of the program, including the role of gas injection, and the modifications to the NaK-nitrogen facility are described.